Microwave Transmission Line Discontinuity Analysis: A Foundation for a Fast Microwave Computer Aided Design Program

A Thesis

Submitted to the College of Graduate Studies and Research

in Partial Fulfillment of the Requirements

for the Degree of

Master of Science

in the Department of Electrical Engineering

University of Saskatchewan

Saskatoon

by

David A. Cargill

Spring 2001

Permission To Use

In presenting this thesis in partial fulfillment of the requirements for a Postgraduate degree from the University of Saskatchewan, I agree that the Libraries of this University may make it freely available for inspection. I further agree that permission for copying of this thesis in any manner, in whole or in part, for scholarly purposes may be granted by the professor or professors who supervised my thesis work or, in their absence, by the Head of the Department or the Dean of the College in which my thesis work was done. It is understood that any copying of publication or use of this thesis or parts thereof for financial gains shall not be allowed without my written permission. It is also understood that due recognition shall be given to me and to the University of Saskatchewan in any scholarly use which may be made of any material in my thesis.

Request for permission to copy or to make use of material in this thesis in whole or part should be addressed to:

Head of the Department of Electrical Engineering
University of Saskatchewan
57 Campus Drive
Saskatoon, Saskatchewan, Canada
S7N 5A9

Abstract

Modern communication systems, in particular those using wireless technology, usually employ a large number of microwave circuits operating at microwave frequencies (0.3 to 30 GHz). Analog cellular phones, for example, contain two microwave filters that operate in the 800 MHz frequency range. Traditionally, microwave circuits were designed using empirical equations to model the circuit elements and the resulting circuits would require hand tuning. However, with the growing demand for wireless communication, accurate design of microwave circuits that no longer require hand tuning became a necessity. Today, advanced numerical methods provide accurate complete electromagnetic, or full-wave, solutions to complicated electromagnetic field theory problems. These methods are available due to the increase of computing power available at low cost and to the extensive research on numerical methods for the design of microwave circuits. However, many of these advanced numerical methods still require significant computational power, so even with today's powerful desktop computers, analysis can still take several hours to complete. Consequently, these methods are not suited for use during the iterative design process.

Since computer aided design (CAD) of microwave integrated circuits relies on accurate characterization of discontinuities, analyzing them is a logical first step towards the generation of a microwave computer aided design program. The objective of this research is to develop a set of routines to accurately, quickly and efficiently analyze steps, right angle bends and T-junctions, which are the fundamental building blocks for microwave circuits. The routines are developed to handle both rectangular waveguide H-plane and microstrip discontinuities. The discontinuity analysis method described in this thesis extensively utilizes the mode matching method, which is a numerical method that efficiently and accurately characterizes discontinuities in structures with well defined boundary conditions. The results obtained are verified with published results. As an example of how the method is used for a practical real world problem, a rectangular waveguide H-plane diplexer is designed and analyzed.

Acknowledgements

The author is indebted to Dr. Protap Pramanick for his supervision and constant encouragement during the course of this work. The author would also like to thank Dr. David Klymyshyn for his assistance and Jacquie Matthies for her assistance and support. Thanks are due to the Department of Electrical Engineering, University of Saskatchewan, Saskatoon for providing the facilities to pursue this research.

The author would like to acknowledge the Natural Sciences and Engineering Research Council (NSERC) for providing financial assistance for this research.

The author would like to acknowledge IBM Canada Ltd. for allowing me the time to pursue my thesis, with special thanks to the managers who allowed me to undertake this opportunity: Emeline Tjan, Connie Kung, Michael White, Peter Hunt and Kelly Arrey.

The author is indebted to many friends for invaluable suggestions and advice. Particular thanks are due to Raju "Bala" Balasubramanian and Anita Dave.

Dedication

This thesis is dedicated to the memory of the author's mother, Dianne L. Cargill, who passed away after a courageous struggle with breast cancer on March 17th, 1995. This thesis is also dedicated to the author's father, David D. Cargill, for his love, care, patience, dedication and constant support.

Table of Contents

List of Figures

List of Tables

List of Symbols and Acronyms

CAD	Computer Aided Design
TEM	Transverse Electromagnetic
TE	Transverse Electric
TE_{mn}	Transverse Electric field for mode m,n
TM	Transverse Magnetic
TM_{mn}	Transverse Magnetic field for mode m,n
a	broad dimension of rectangular waveguide
b	narrow dimension of rectangular waveguide
ε	permittivity
ε_o	permittivity of free space (8.8554×10^{-12} F/m)
ε_r	dielectric constant or relative permittivity
ε_{eff}	effective dielectric constant
μ	permeability
μ_o	permeability of free space ($4\pi \times 10^{-7}$ H/m)
β	propagation constant
β_{mn}	propagation constant for mode m,n
c	velocity of light
f	operating frequency
f_{cmn}	waveguide cutoff frequency
k_{cmn}	cutoff wave number
k_o	wave number for free space
H	magnetic field
E	electric field
ω	angular frequency
j	imaginary number ($\sqrt{-1}$)
A_{mn}	amplitude mode constant
W	width of a microstrip conductor
W_{eff}	effective width of a microstrip conductor
h	height of a microstrip dielectric
t	thickness of a microstrip conductor
λ	wavelength
λ_g	guided wavelength
λ_o	free space wavelength
λ_{cmn}	cutoff wavelength

Z_o	characteristic impedance
Z_{TEmn}	waveguide impedance for TE modes m,n
Y_{TEmn}	waveguide admittance for TE modes m,n
Z	waveguide impedance matrix (a diagonal matrix)
Y	waveguide admittance matrix (a diagonal matrix)
V_n^+	incident voltage wave at port n
V_n^-	reflected voltage wave at port n
$[S]$	scattering matrix
$[S]^t$	transpose of scattering matrix
$[S]^*$	conjugate of scattering matrix
$[S]^{-1}$	inverse of scattering matrix
S_{ij}	scattering parameter
$[S_{ij}]$	multi-mode scattering matrix
$[U]$	unitary or identity matrix
$[0]$	zero matrix
$[TL]$	transmission line matrix (a diagonal matrix)
L_i	length of a transmission line
Γ_L	reflection coefficient for a terminated load
Γ_{in}	reflection coefficient looking into a one-port network
η	impedance of free space
δ_{ij}	Kronecker delta function
$\phi_{in}(x)$	modal function for mode i of region n
H	coupling matrix
h_x	step discontinuity offset
N	number of modes on the larger side of a step discontinuity
M	number of modes on the smaller side of a step discontinuity
MIC	Microwave Integrated Circuit
FEM	Finite Element Method
MoM	Method of Moments
MoL	Method of Lines
TLM	Transmission Line Modeling Method or Transmission Line Matrix Method
FDTD	Finite Difference Time Domain
FDM	Finite Difference Method
BEM	Boundary Element Method
IL	Insertion Loss
RL	Return Loss

Chapter 1. Introduction

The term microwave refers to electromagnetic waves with a frequency ranging between 0.3 and 30 GHz, which corresponds to a wavelength ranging from 100 to 1 cm. These properties provide allow wide bandwidth for communication links and allow microwaves to travel by line-of-sight through the ionosphere without bending, which have led to their widespread use in modern communication systems. Although the foundations for electromagnetic theory were laid down by James Clerk Maxwell in 1873 [1], the growing demand for wireless communication has led to extensive research in microwave engineering during the last fifty years.

Since the dimensions of microwave circuit elements are close to the operating wavelength for the circuit, the conventional circuit theories, such as Kirchhoff's Laws, used in electrical engineering cannot be directly used to solve microwave network problems. Instead, Maxwell's equations are used to solve problems in electromagnetic field theory. Traditionally, these problems were solved with empirical equations and the manufactured components were hand tuned. Today, with the availability of powerful computers and the development of microwave computer aided design (CAD) programs, complete and accurate solutions to complex electromagnetic field theory problems can be found and the resulting manufactured components do not require hand tuning.

1.1 Rectangular Waveguides

Transmission lines and waveguides are fundamental components of microwave engineering and are used to distribute microwave power from one point to another. While waveguides can be of an arbitrary shape, the most commonly used are those with a rectangular cross-section. The propagation of electromagnetic waves can be categorized as either Transverse Electromagnetic (TEM) or non-TEM. TEM waves can exist in free space and when two or more conductors exist, and in a TEM wave both the electric and magnetic fields are transverse to the direction of propagation. In non-TEM waves either the electric field or magnetic field are present in the direction of propagation, but not both. Transverse Electric (TE) waves have a magnetic field component in the direction of propagation. Transverse Magnetic (TM) waves have an electric field component in the direction of propagation. Only TE and TM waves can propagate in hollow rectangular waveguides since

there is only one conductor. A rectangular waveguide with width a and height b, where by convention $a > b$, permittivity ε, permeability μ, is illustrated in Figure 1.1.

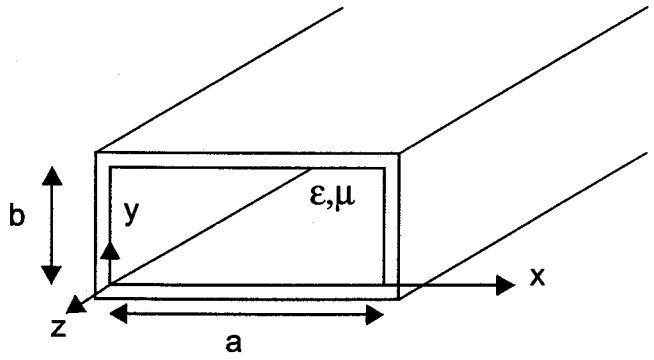

Figure 1.1. Rectangular Waveguide

The TE and TM waves propagate through the waveguide by multiple reflections from the metallic walls. Assuming a lossless system, perfectly conducting walls exist at $x = 0, x = a, y = 0$ and $y = b$. The waveguide may be filled with a material of dielectric constant ε_r although in practice the waveguide is usually air-filled ($\varepsilon_r = 1$).

1.1.1 Mode Nomenclature

In an air-filled lossless waveguide there are an infinite number of solutions for both TE and TM waves. These waves, or modes, are identified by using two integer subscripts m and n, and the waves are labelled as TE_{mn} or TM_{mn}. The subscript m indicates the number of half-wave variations of the electric field or the magnetic field along the wide dimension of the waveguide (a). The subscript n indicates the number of half-wave variations of the electric field or the magnetic field along the narrow dimension of the waveguide (b). Each mode has a cutoff frequency f_{cmn} given by

$$f_{cmn} = \frac{c}{2\pi}\sqrt{\left(\frac{m\pi}{a}\right)^2 + \left(\frac{n\pi}{b}\right)^2}, \tag{1.1}$$

where c is the velocity of light in free space ($c = 1/(\sqrt{\varepsilon_o \mu_o})$) and, ε_o and μ_o are the permittivity and permeability of free space. Below this cutoff frequency, which is a function of the geometry of the waveguide, the mode is evanescent and does not propagate.

The propagation of the waves in the z direction is governed by the function $e^{\pm j\beta_{mn}z}$. The propagation constant β_{mn} is defined by

$$\beta_{mn} = \sqrt{k_o^2 - k_{cmn}^2}, \tag{1.2}$$

where k_o is the wave number for free space and k_{cmn} is the cutoff wave number. The wave number is also known as the phase constant since it gives the change in phase per unit length. The wave number parameters are defined as

$$k_o = \omega\sqrt{\mu_o\varepsilon_o} = 2\pi f\sqrt{\mu_o\varepsilon_o} = \frac{2\pi f}{c} = \frac{2\pi}{\lambda_o} \text{ and} \tag{1.3}$$

$$k_{cmn} = 2\pi f_{cmn}\sqrt{\mu_o\varepsilon_o} = \sqrt{\left(\frac{m\pi}{a}\right)^2 + \left(\frac{n\pi}{b}\right)^2}, \tag{1.4}$$

where f is the operating frequency, ω is the angular frequency and λ_o is the free space wavelength ($\lambda_o = c/f$). The guide wavelength is defined as the distance between two equal phase planes along the waveguide, and is equal to

$$\lambda_g = \frac{2\pi}{\beta_{mn}} = \frac{\lambda_o}{\sqrt{1 - \left(\frac{\lambda_o}{\lambda_{cmn}}\right)^2}}, \tag{1.5}$$

where the cutoff wavelength is given by

$$\lambda_{cmn} = \frac{2\pi}{k_{cmn}}. \tag{1.6}$$

It is interesting to note the behaviour of the guide wavelength relative to the free space wavelength:

- When the operating frequency is higher than the cutoff frequency the free space wavelength is smaller than the cutoff wavelength. Thus the denominator of equation (1.5) approaches unity and λ_g approaches λ_o, but is always larger than λ_o.
- When the operating frequency is equal to the cutoff frequency the free space wavelength is equal to the cutoff wavelength. Thus the denominator of equation (1.5) approaches zero and λ_g approaches infinity.
- When the operating frequency is less than the cutoff frequency the free space wavelength is larger than the cutoff wavelength. Thus the denominator of equation (1.5) is imaginary so λ_g is imaginary (an evanescent mode).

The actual electric and magnetic fields are determined by solving Maxwell's equations within the waveguide. For a linear, source-free air-filled waveguide with an electromagnetic field having time dependence $e^{j\omega t}$, Maxwell's equations are [2]:

$$\nabla \times \bar{H} = j\omega\varepsilon_o\bar{E}, \tag{1.7}$$

$$\nabla \times \bar{E} = -j\omega\mu_o\bar{H}, \tag{1.8}$$

$$\nabla \cdot \bar{E} = 0, \tag{1.9}$$

$$\nabla \cdot \overline{H} = 0, \tag{1.10}$$

where $\overline{H}$ is the magnetic field vector, $\overline{E}$ is the electric field vector, and j is the imaginary number. Since sources are not considered, Maxwell's equations can be simplified through the use of a vector identity to the Helmholtz equation [3]:

$$\nabla^2\overline{H} + k_o^2\overline{H} = 0 \quad \text{or} \quad \nabla^2\overline{E} + k_o^2\overline{E} = 0. \tag{1.11}$$

Using the boundary condition that the electric field tangential to the waveguide walls must be zero, the following field components are derived for TE modes ($E_z = 0$) using the co-ordinate system shown in Figure 1.1 [3]:

$$H_z(x, y, z) = A_{mn}\cos\left(\frac{m\pi x}{a}\right)\cos\left(\frac{n\pi y}{b}\right)e^{-j\beta_{mn}z}, \tag{1.12}$$

$$E_x(x, y, z) = \frac{j\omega\mu_o n\pi}{k_{cmn}^2 b}A_{mn}\cos\left(\frac{m\pi x}{a}\right)\sin\left(\frac{n\pi y}{b}\right)e^{-j\beta_{mn}z}, \tag{1.13}$$

$$E_y(x, y, z) = \frac{-j\omega\mu_o m\pi}{k_{cmn}^2 a}A_{mn}\sin\left(\frac{m\pi x}{a}\right)\cos\left(\frac{n\pi y}{b}\right)e^{-j\beta_{mn}z}, \tag{1.14}$$

$$H_x(x, y, z) = \frac{j\beta_{mn} m\pi}{k_{cmn}^2 a}A_{mn}\sin\left(\frac{m\pi x}{a}\right)\cos\left(\frac{n\pi y}{b}\right)e^{-j\beta_{mn}z} = -\frac{E_y(x, y, z)}{Z_{TEmn}}, \tag{1.15}$$

$$H_y(x, y, z) = \frac{j\beta_{mn} n\pi}{k_{cmn}^2 b}A_{mn}\cos\left(\frac{m\pi x}{a}\right)\sin\left(\frac{n\pi y}{b}\right)e^{-j\beta_{mn}z} = \frac{E_x(x, y, z)}{Z_{TEmn}}, \tag{1.16}$$

where A_{mn} is the amplitude mode constant. Similar equations are derived for TM modes ($H_z = 0$).

1.1.2 Dominant Mode

The TE_{10} mode is called the dominant mode of a rectangular waveguide because it has the lowest cutoff frequency, provided $a > b$. The cutoff frequency for TE_{10} is $f_{c10} = c/(2a)$. The field components for the dominant mode are found by substituting m=1 and n=0 into equations (1.12) to (1.16) resulting in the following equations

$$H_z(x, y, z) = A_{10}\cos\left(\frac{\pi x}{a}\right)e^{-j\beta_{10}z}, \tag{1.17}$$

$$E_y(x, y, z) = \frac{-j\omega\mu_o\pi}{k_{c10}^2 a}A_{10}\sin\left(\frac{\pi x}{a}\right)e^{-j\beta_{10}z}, \tag{1.18}$$

$$H_x(x, y, z) = \frac{j\beta_{10}\pi}{k_{c10}^2 a}A_{10}\sin\left(\frac{\pi x}{a}\right)e^{-j\beta_{10}z} = -\frac{E_y(x, y, z)}{Z_{TEmn}}, \tag{1.19}$$

and $H_x = E_y = 0$.

The dominant mode for a waveguide has the following characteristics [4]:

- It has the longest operating wavelength.
- It has the greatest energy transfer efficiency.
- It has the simplest field configuration.
- It is the easiest mode to induce (or extract) in a waveguide.

1.1.3 Waveguide Impedance and Admittance

The wave impedance in a waveguide is defined as

$$Z_w = \frac{E_t}{H_t} \tag{1.20}$$

where the subscript "t" is used to denote the components of the field transverse (perpendicular) to the direction of propagation. The waveguide impedance for TE modes is defined as

$$Z_{TEmn} = \frac{k_o \eta}{\beta_{mn}} = \frac{\omega \mu_o}{\beta_{mn}} = \frac{\eta \lambda_g}{\lambda_o} = \frac{\eta}{\sqrt{1 - \left(\frac{\lambda_o}{\lambda_{cmn}}\right)^2}}, \tag{1.21}$$

where η, the impedance of free space, is given by

$$\eta = \sqrt{\frac{\mu_o}{\varepsilon_o}} \approx 120\pi\ \Omega \approx 377\Omega. \tag{1.22}$$

The behaviour of the waveguide impedance for TE modes is similar to the guide wavelength behaviour described on page 3:

- When the operating frequency is higher than the cutoff frequency, Z_{TEmn} approaches 377Ω, but is always larger than 377Ω.
- When the operating frequency is equal to the cutoff frequency, Z_{TEmn} approaches infinity.
- When the operating frequency is less than the cutoff frequency, Z_{TEmn} is imaginary (an evanescent mode).

For TE modes in a waveguide, the wave impedance is constant for any mode irrespective of the position in the cross-section of the waveguide at which E_t and H_t are taken.

When multiple modes are considered, the waveguide impedance is frequently represented as a matrix. For example, the waveguide impedance matrix for the modes TE_{m0} that is used throughout this thesis is

$$Z = \begin{bmatrix} Z_{TE10} & 0 & \cdots & 0 \\ 0 & Z_{TE20} & \cdots & 0 \\ \vdots & \vdots & \cdots & \vdots \\ 0 & 0 & \cdots & Z_{TEn0} \end{bmatrix}. \tag{1.23}$$

The waveguide admittance is similarly defined with

$$Y_{TEmn} = \frac{1}{Z_{TEmn}} \text{ and } Y = Z^{-1}. \tag{1.24}$$

1.2 Planar Transmission Lines

One of the principal requirements for a transmission line to be suitable for use in a microwave integrated circuit (MIC) is that the line should be "planar" in configuration. When the impedance of a transmission line can be controlled by the dimensions in a single plane (for example, by changing the width of the transmission line), the circuit can be fabricated by photolithographic processes. As seen in Figure 1.2 various forms of planar transmission lines have been developed.

While the geometries of these planar transmission lines are similar, their electrical characteristics differ so they tend to be used for different applications and frequency ranges. Stripline and microstrip are the most popular. Coplanar strips and slot-line are used exclusively for monolithic circuits. In this thesis the focus is on microstrip and rectangular waveguides, although the discontinuity analysis method can be applied to other transmission lines.

1.3 Microstrip

Microstrip is the most popular planar transmission line that is used extensively in printed microwave circuits and microwave integrated circuits. Figure 1.3 (a) shows the geometry of a microstrip line: a conductor of width W and thickness t on a dielectric of height h with permittivity ε_r that is attached to a ground plane.

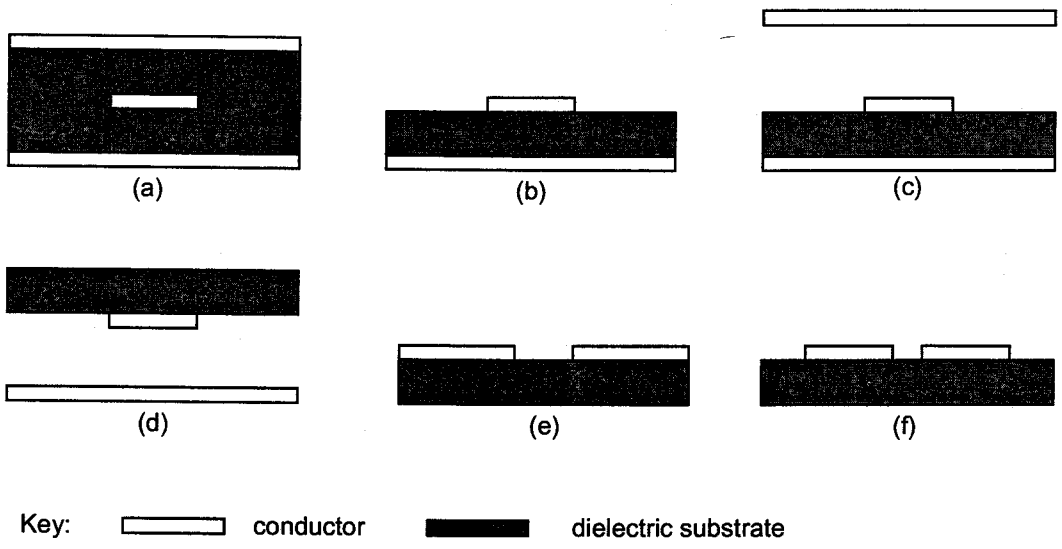

Figure 1.2. Cross-sectional Views of Planar Transmission Lines: (a) stripline; (b) microstrip; (c) shielded microstrip; (d) inverted microstrip; (e) slot-line; (f) coplanar strips

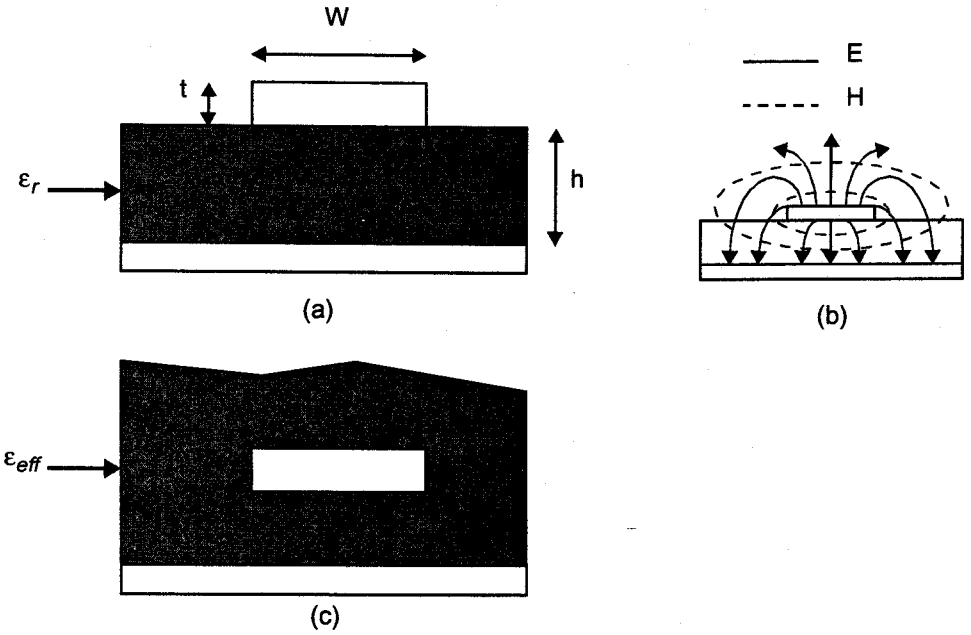

Figure 1.3. Microstrip Transmission Line: (a) geometry; (b) electric and magnetic field lines; (c) effective dielectric for a microstrip line

Since some of the electromagnetic fields are in the air above the dielectric region, as seen in Figure 1.3 (b), microstrip cannot support a pure TEM wave. However, when the dielectric substrate is very thin relative to the wavelength ($h \ll \lambda$), as it is in most practical

applications, the fields may be treated as quasi-TEM or quasi-static. The effective dielectric constant of microstrip, which satisfies the relation $1 < \varepsilon_{eff} < \varepsilon_r$, represents a dielectric constant of a homogenous region that replaces the air and dielectric regions of the original microstrip as seen in Figure 1.3 (c), and is given approximately by [5, 6]

$$\varepsilon_{eff} = \frac{\varepsilon_r + 1}{2} + \frac{\varepsilon_r - 1}{2}\left(\frac{1}{\sqrt{1 + \frac{12h}{W}}}\right). \tag{1.25}$$

The characteristic impedance of microstrip is given by [5, 6]

$$Z_o = \frac{1}{\sqrt{\varepsilon_{eff}}}\left(\frac{120\pi}{\frac{W}{h} + 1.98\left(\frac{W}{h}\right)^{0.172}}\right). \tag{1.26}$$

The propagation constant of microstrip is defined as

$$\beta = k_o\sqrt{\varepsilon_{eff}}, \tag{1.27}$$

where k_o has the same definition as shown in equation (1.3). The guided wavelength for microstrip is defined as

$$\lambda_g = \frac{2\pi}{\beta}. \tag{1.28}$$

1.3.1 Dispersion

The effective dielectric constant and characteristic impedance, equations (1.25) and (1.26), do not account for dispersion, a behaviour where the frequency and wavelength are not inversely proportional. The dispersive nature of microstrip is taken into account by considering the effective dielectric constant and characteristic impedance to vary with frequency [7, 8]:

$$\varepsilon_{eff}(f) = \varepsilon_r - \frac{\varepsilon_r - \varepsilon_{eff}}{1 + \frac{\varepsilon_{eff}}{\varepsilon_r}\left(\frac{f}{f_p}\right)^2}, \text{ where } f_p = \frac{Z_o}{2\mu_o h} \text{ and} \tag{1.29}$$

$$Z_o(f) = Z_o\sqrt{\frac{2(1-q)}{\varepsilon_{eff}(f) - \sqrt{(\varepsilon_{eff}(f))^2 - 4q(1-q)\varepsilon_r}}}, \text{ where } q = \frac{\varepsilon_{eff} - 1}{\varepsilon_r - 1}. \tag{1.30}$$

1.3.2 Microstrip Planar Waveguide Model

The equivalent planar waveguide model for microstrip lines [5, 6] is well known for accurate modeling of microstrip lines with dispersion considered. The equivalent planar waveguide model for a microstrip line is shown in Figure 1.4, where the microstrip line is equivalent to a rectangular waveguide with magnetic side-walls that has effective dielectric constant ε_{eff}, effective width W_{eff}, and height h.

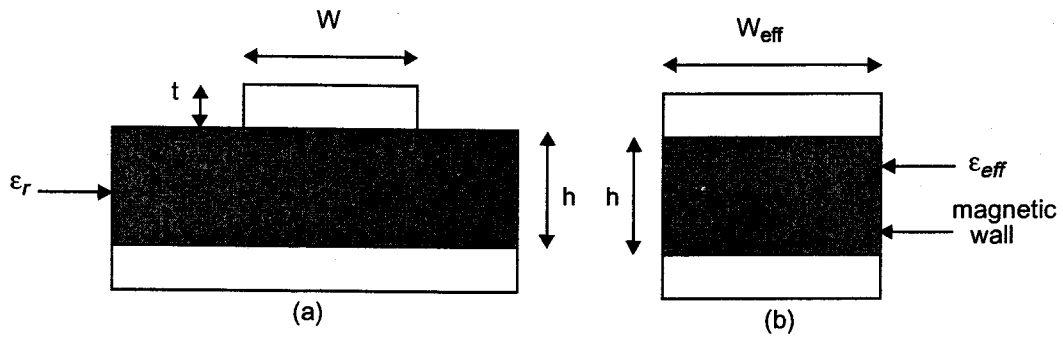

Figure 1.4. Microstrip Planar Waveguide Model: (a) microstrip line; (b) equivalent planar waveguide model

The side-walls of the waveguide are assumed to be perfect magnetic conductors and the effective width is given by the following [7, 8], which accounts for dispersion

$$W_{eff}(f) = \frac{120\pi h}{Z_o(f)\sqrt{\varepsilon_{eff}(f)}} = \frac{h\sqrt{\varepsilon_{eff}}\left(\frac{W}{h} + 1.98\left(\frac{W}{h}\right)^{0.172}\right)}{\sqrt{\varepsilon_{eff}(f) - \sqrt{(\varepsilon_{eff}(f))^2 - 4q(1-q)\varepsilon_r}}}, \qquad (1.31)$$

where, as in equation (1.30), $q = \frac{\varepsilon_{eff} - 1}{\varepsilon_r - 1}$.

By using the equivalent planar waveguide model, the analysis of a microstrip structure is very similar to the analysis of a rectangular waveguide with the exception of the boundary condition. A rectangular waveguide has electric walls (the tangential components of the electric field are zero), while the microstrip planar waveguide model has magnetic walls (the tangential components of the magnetic field are zero and the normal component is a maximum). However, the most significant difference in the characteristic of these two waveguides is that the microstrip planar waveguide model is capable of supporting a quasi-TEM mode, TE_{00}, in addition to TE_{m0} modes.

With the planar waveguide model, the microstrip propagation constant is represented as a function of the mode number with

$$\beta_{mn} = \beta_{m0} = \beta_m = \sqrt{k_o^2\varepsilon_{eff}(f) - \left(\frac{m\pi}{W_{eff}(f)}\right)^2}, \qquad (1.32)$$

which simplifies to equation (1.27) for the fundamental mode, TE_{00}. Similarly, the microstrip impedance is also represented as a function of the mode number by using equation (1.21).

1.4 Research Objectives

Rapid developments in computer processing speeds and technology, such as multiprocessors, have resulted in rapid innovation in technical software. In the area of microwave CAD there is a booming market for design, analysis and optimization tools. Traditionally, microwave circuits were designed using empirical equations to model the circuit elements and the resulting circuits would require hand tuning. With the ever increasing demand for accurate design of microwave circuits that no longer require hand tuning, accurate and complete electromagnetic, or full-wave, solutions became a necessity. Today, advanced numerical methods provide accurate solutions for complicated electromagnetic field theory problems, due in part to the increase of computing power available at a low enough cost and to the extensive research on numerical methods for the design of microwave circuits.

Many of these advanced numerical methods still require significant computational power, such as the Finite Element Method (FEM), which provides a full-wave solution to the problem. So even with today's powerful desktop computers, with dual processors, analysis can still take several hours to complete. With these large analysis times full-wave solutions are typically only used to validate a completed design and not during the iterative design process.

Developing a complete microwave CAD program that can quickly analyze a microwave circuit is beyond the scope of this thesis. Since CAD of microwave circuits relies on accurate characterization of discontinuities, analyzing them is a logical first step towards the generation of a microwave CAD program. Consequently, the objective of this research is to develop a set of routines that can be used as a foundation for a microwave CAD program that can provide an accurate solution, quickly and efficiently. Specifically routines to analyze steps, right angle bends and T-junctions for both rectangular waveguide H-plane and microstrip planar transmission lines are developed in this thesis that provide an accurate solution, quickly and efficiently. The numerical method that is used to analyze these discontinuities is the mode matching method, since it efficiently and accurately characterizes discontinuities in structures with well defined boundary conditions.

1.5 Thesis Organization

This thesis is divided into seven chapters. Chapter 2 presents the background and literature review of the related research. Discontinuities and the general concept of scattering parameters are also introduced in this chapter. Chapter 3 presents the mode

matching method for the characterization of rectangular waveguide H-plane and microstrip step junctions. Chapter 4 describes the discontinuity analysis method that is implemented as a set of Fortran routines for the computer aided analysis of rectangular waveguide H-plane and microstrip step junctions, right angle bends and T-junctions. Chapter 5 furnishes the results obtained from the discontinuity analysis method described in this thesis and its comparison with other methods. Chapter 6 provides a practical application on how the method is used for a real world problem, the design and analysis of a rectangular waveguide H-plane diplexer. Finally, chapter 7 contains the conclusions of the research.

Chapter 2. Literature Review and Background

This chapter will provide an introduction to the literature review and background of the related research for microstrip and rectangular waveguide H-plane bends and T-junctions, and microwave computer aided design (CAD). The general concept of scattering parameters and electrical and physical ports are also introduced in this chapter.

2.1 Transmission Line Bends and T-junctions

Transmission line bends and T-junctions are an indispensable component for numerous microwave circuits including diplexers, filters, power dividers and couplers. An excellent review of the characterization of planar transmission line discontinuities is available in reference [9]. To satisfy the need for practical design, many methods have been used to analyze these types of discontinuities including experimental results [10], full-wave analysis [11], Green's Function [12], and equivalent reactances [13, 14, 15]. There are limitations with each of these methods: experimental measurements cannot be easily generalized for CAD; full-wave analysis is computationally intensive; Green's Function is limited to a regular geometry; and the equivalent reactances are limited to low frequencies. So an attempt is made to find a general method that can be used in the CAD of microwave circuits.

2.2 Microwave Computer Aided Design

Microwave computer aided design was founded approximately thirty years ago to meet the need for faster and more accurate design of microwave circuits and initially these microwave CAD programs ran on supercomputers [16]. For fifteen years the microwave CAD market has been dominated by two products that can quickly analyze a circuit with relatively good accuracy considering they do not use full-wave analysis: Harmonica from Compact Software (now Ansoft) and Touchstone from EEsof (which became HP and is now Agilent). These programs operate in a similar fashion to SPICE, the popular low frequency electric circuit simulator [17]. As competition to these microwave circuit simulators, specialized software programs became available to analyze specific microwave structures, such as filters. With the rapid advancements in computer speed and memory, microwave CAD programs became available on desktop computers. Eagleware developed SuperStar, which was the fastest microwave circuit simulator available, by using a two-port analysis technique

instead of the traditional nodal analysis method [18]. Source code even became available for the microwave CAD programs MCAP (Microwave Circuit Analysis Program) and Jadmic2 in some of the books on the subject [19, 20, 21]. The International Journal of RF and Microwave Computer-Aided Engineering and the Applied Computational Electromagnetics Society Journal have also been created to focus on microwave CAD.

With the increased computational power available at the desktop, numerical methods (described in Section 2.2.1) that were once theoretical can actually be implemented in an electromagnetic simulator [2, 22]. This has resulted in numerous microwave CAD programs being developed and Table 2.1 lists some that are available today [23].

Table 2.1. Microwave CAD Programs

Name	Numerical Method
Ansoft HFSS	Finite Element Method (FEM)
FullWave	Finite Element Method (FEM)
EmSight and Microwave Office	Method of Moments (MoM)
Sonnet	Method of Moments (MoM)
IE3D	Method of Moments (MoM)
Empower	Method of Lines (MoL)
Micro-Stripes	Transmission Line Modeling Method (TLM)
EMPIRE	Finite Difference Time Domain (FDTD)
XFDTD	Finite Difference Time Domain (FDTD)
Fidelity	Finite Difference Time Domain (FDTD)

With so many microwave CAD programs available to choose from, there have been various studies on comparing the accuracy and speed of these programs [23, 24, 25] and in comparing specific numerical methods [26]. However, no one numerical method is suitable for all problems, so one has to make a choice as to which method is best suited for the problem to be analyzed. With computer speeds now in the gigahertz range and the advances in parallel processing, the number of microwave CAD programs will continue to increase as "The pace of innovation in technical software shows no sign of slowing down." [27]

The use of microwave CAD programs has also transformed the microwave circuit design process. Figures 2.1 and 2.2 show the conventional microwave design procedure and the microwave CAD procedure, respectively [28, 29]. Of particular interest is the step to construct a laboratory model or prototype in the conventional procedure. If the model does

not meet the specifications it may have to be hand tuned or, in the worst case, all or part of the circuit may have to be redesigned and rebuilt. With the microwave CAD procedure, a prototype is not built until the circuit has been successfully analyzed by a microwave CAD program. This eliminates the expensive and time consuming process of iteratively prototyping, measuring and modifying an actual circuit. Some modifications may still be required with the microwave CAD procedure, however with accurate modeling and analysis it is hoped that these changes will be small, as the aim of microwave CAD is to minimize the post design modifications.

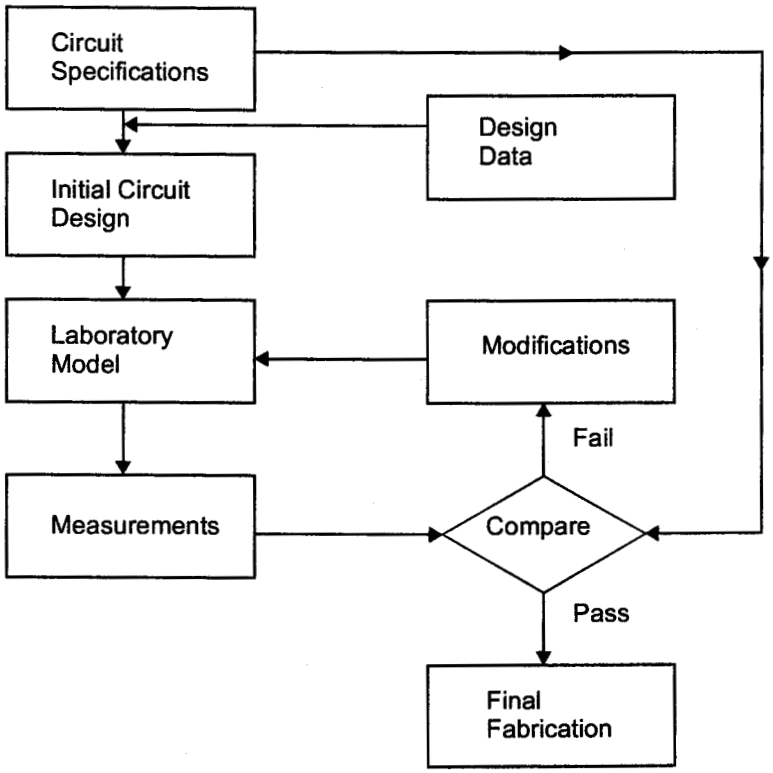

Figure 2.1. Conventional Procedure for Microwave Circuit Design

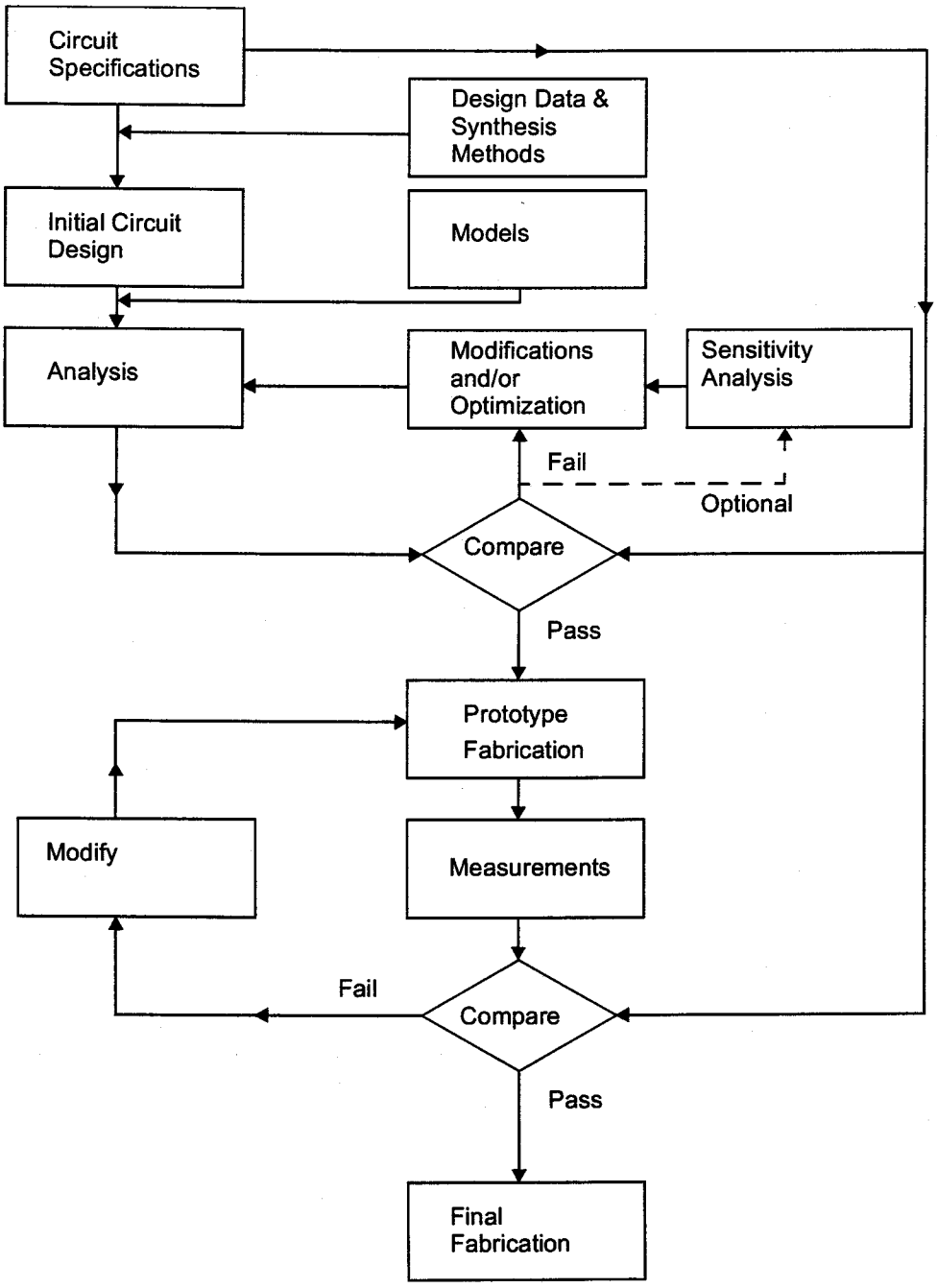

Figure 2.2. Microwave CAD Procedure

2.2.1 Numerical Methods

All of the microwave CAD programs listed in Table 2.1 are based on meshing the entire circuit being analyzed into a number of discrete cells, so for an acceptable accuracy a large number of discretizations is required. The number of discretizations determines the matrix

size in the numerical computation, which in turn determines the required memory and speed of the circuit analysis. As an example consider the simple two dimensional problem of a uniform rectangular line as shown in Figure 2.3.

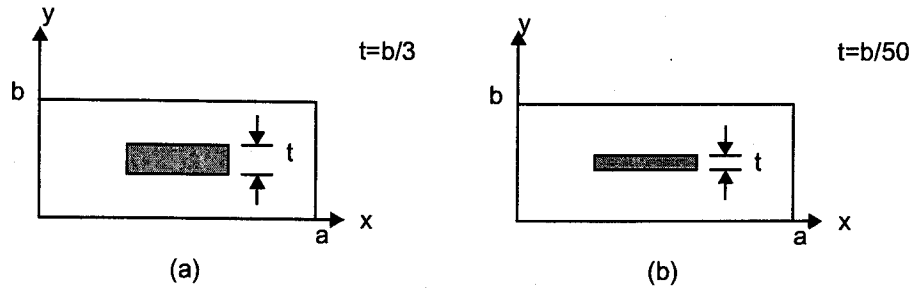

Figure 2.3. Effect of Line Thickness on Discretization

While the entire field problem for all modes can be solved analytically in closed form, it can also be solved using the finite element method (FEM). However, when solved analytically the analysis effort for both lines is the same. For the FEM the matrix size increases dramatically for the smaller line since the discretization of the circuit needs to be much finer.

In addition to the discretization issue, there are also some other issues for some of the packages [22, 23]:

- Method of moments (MoM) and method of lines (MoL) cannot solve three dimensional problems (they are referred to as 2.5 dimensional methods) and they cannot handle finite metallization thickness.
- Finite difference time domain (FDTD) and transmission line modeling method (TLM) require an inverse transformation to get the frequency response.
- FEM and Finite Difference Method (FDM) are the most versatile methods as they can handle any geometry, however precaution needs to be exercised when analyzing an open region problem in which the region is truncated to a finite size.

An alternative numerical method used in this thesis is the mode matching method (described in the next chapter), which has the advantage that it does not require meshing.

Due to the large time and memory requirements to solve an electromagnetic problem with the existing microwave CAD programs, there is continued research in developing faster numerical methods so that these tools can be used as an analysis engine in an iterative design environment [30]. The discontinuity analysis method, which is described in Chapter 4, is one possible solution for a microwave CAD program that could be used for both design and analysis. However, when a specific circuit is to be analyzed there may be advantages to using one numerical method over another, so one microwave CAD program will not be able to

efficiently handle all problems. A review of the most representative numerical methods is available in the first chapter of reference [22].

2.3 Microwave Transmission Line Discontinuities

Microwave transmission line discontinuities are the fundamental building blocks used in connecting microwave circuit elements together for both planar transmission lines and waveguides. The three main types of discontinuities are:

- step or step junction (the point at which there is a change in a dimension)
- bend (the point at which there is a change in direction of a transmission line)
- T-junction or Tee-junction (the intersection of three transmission lines)

As these discontinuities are used throughout microwave circuits, it is very important that they are characterized correctly so that the circuit being designed operates correctly. Traditionally, empirical equations were used to characterize these discontinuities. Today, with the advancements in computer technology more rigorous numerical methods have been developed to characterize these discontinuities. In this thesis the port reduction method is used to characterize these discontinuities.

2.3.1 Step Junction

Step junctions are used to connect waveguides or planar transmission lines of different dimensions together. It can be argued that step junctions are the building blocks for all other transmission line discontinuities; for example, a T-junction can be viewed as a combination of two step junctions. A step junction gives rise to a large number of higher order modes when a fundamental mode strikes it. A waveguide can have a step junction in the width of the waveguide, the height of the waveguide or in both dimensions at once. A planar transmission line can obviously only have a step junction in one dimension, the width of the conductor. Figure 2.4 shows the various structures for a step junction.

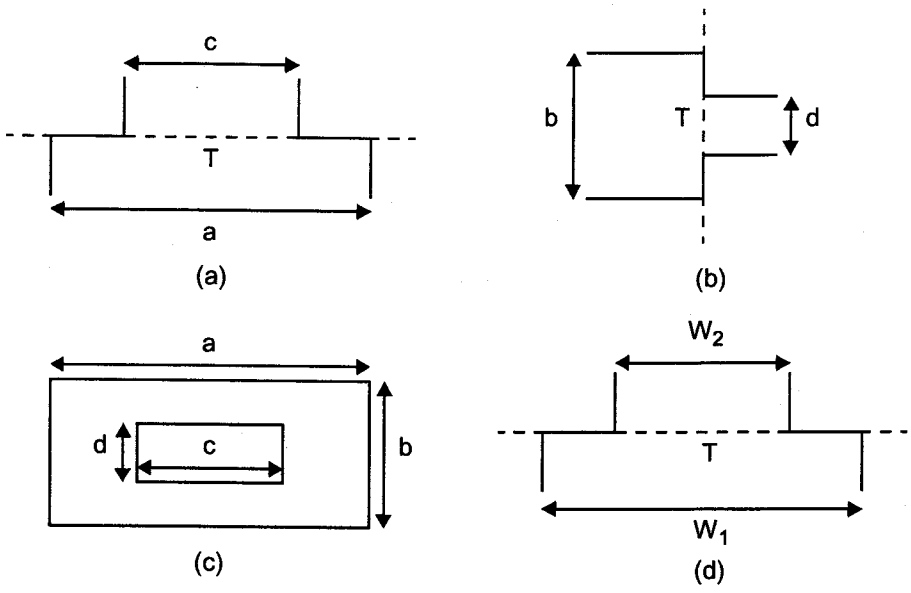

Figure 2.4. Step Junction: (a) rectangular waveguide change in width (top view); (b) rectangular waveguide change in height (side view); (c) rectangular waveguide change in width and height (end view); (d) microstrip change in width (top view)

The change in width for a rectangular waveguide is also known as an H-plane step because only the magnetic field is present in that dimension (recall that $E_x = 0$ for a TE_{10} mode). The resulting modes that are generated from the H-plane step are TE_{m0}. Similarly, a change in height is known as an E-plane step. The resulting modes that are generated from the E-plane step are TE_{1n}. In an EH-plane step, where both the width and height change, the resulting modes are TE_{mn} and TM_{mn}.

Step junctions can be further classified based on the symmetry of the step as seen in Figure 2.5.

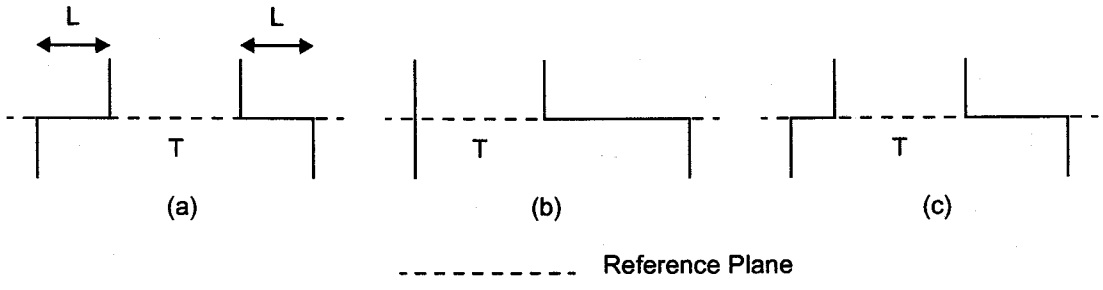

Figure 2.5. Step Junction Classification: (a) symmetric; (b) asymmetric; and (c) arbitrary

2.3.2 Bend

Bends are used to connect planar transmission lines or waveguides of different directions together. While the lines may be connected at an arbitrary angle, this thesis focuses on right angle bends as seen in Figure 2.6.

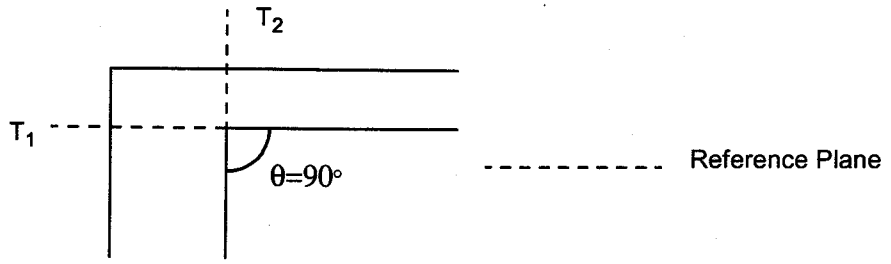

Figure 2.6. Bend

Bends may also be compensated to minimize the effects of the sharp discontinuity at the corner.

2.3.3 T-junction

T-junctions are used to connect three planar transmission lines or waveguides. While the lines may be connected at an arbitrary angle, which are referred to as Y-junctions, this thesis focuses on T-junctions as seen in Figure 2.7.

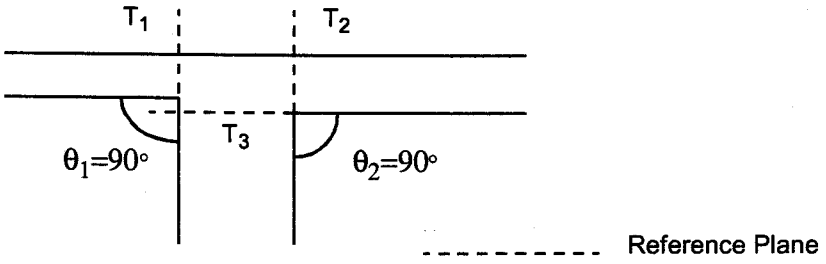

Figure 2.7. T-junction

T-junctions may also be compensated to minimize the effects of the sharp discontinuity at the junction.

2.4 Scattering Parameters

At lower frequencies, where the dimensions of the circuit are small relative to the wavelength, networks are typically characterized by voltages and currents, and the associated admittance and impedance. At microwave frequencies the measurement of voltage or current is exceedingly difficult for a number of reasons:

- it is very difficult to realize proper open and short circuit terminations at microwave frequencies because of the parasitic reactances associated with elements (open and short circuits are frequently used to determine admittance and impedance at lower frequencies)
- the dimensions of the circuit are not small relative to the wavelength
- in the case of a waveguide, the voltage is dependent on the position of the waveguide as the electric and magnetic fields vary across the waveguide
- admittance and impedance matrices do not exist for every linear, passive, and time-invariant network [29]
- the phase and magnitude of the voltage and current varies along a uniform lossless line [29]
- direct measurements usually involve the phase and magnitude of a wave.

A more convenient representation is given by the scattering matrix or S-matrix, whose elements are known as scattering parameters or S-parameters which are defined in terms of the incident and reflected waves. Consider the N-port network in Figure 2.8, where V_n^+ is the incident voltage wave at port n and V_n^- is the reflected voltage wave at port n.

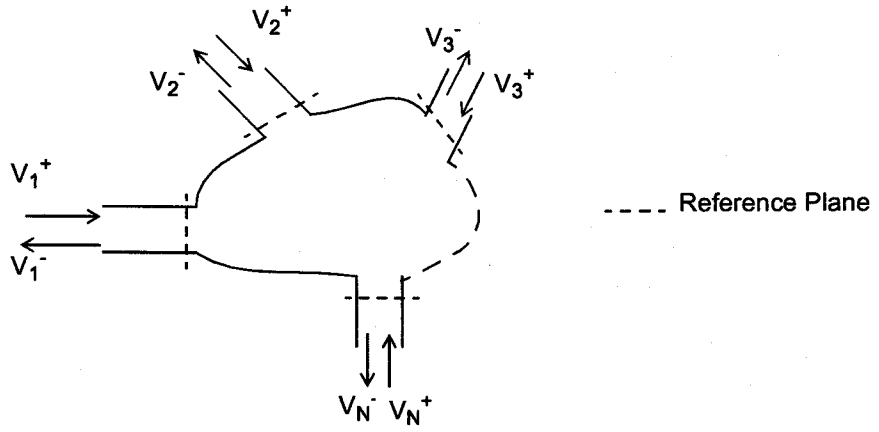

Figure 2.8. An Arbitrary N-port Network

When V_1^+ is incident on port 1 and all the other ports are terminated with matched loads, the reflected wave $V_1^- = S_{11}\, V_1^+$ is produced, where S_{11} is the reflection coefficient at port 1. In addition to the wave reflected at port 1, waves will be transmitted to other ports and will have an output proportional to the input wave. The reflected wave at port 2 is $V_2^- = S_{21}\, V_1^+$, where S_{21} is the transmission coefficient from port 2 to port 1. The order of the subscripts S_{ij} is opposite to the direction of the power transmission being consider (S_{21} is the power transmitted to port 2 from port 1). Thus a specific scattering parameter can be determined as

$$S_{ij} = \left.\frac{V_i^-}{V_j^+}\right|_{V_k^+ = 0,\ \text{for } j \neq k} \tag{2.33}$$

and the $[S]$ matrix is defined as

$$\begin{bmatrix} V_1^- \\ V_2^- \\ \vdots \\ V_N^- \end{bmatrix} = \begin{bmatrix} S_{11} & S_{12} & \cdots & S_{1N} \\ S_{21} & S_{22} & \cdots & S_{2N} \\ \vdots & \vdots & \cdots & \vdots \\ S_{N1} & S_{N2} & \cdots & S_{NN} \end{bmatrix} \begin{bmatrix} V_1^+ \\ V_2^+ \\ \vdots \\ V_N^+ \end{bmatrix} \tag{2.34}$$

or

$$[V^-] = [S][V^+]. \tag{2.35}$$

2.4.1 Physical and Electrical Ports

The number of physical terminal-pair ports in a network is equal to the number of physical ports in the network. For example, a two terminal-pair network, such as a transmission line, is said to be a physical two-port network. In a transmission line discontinuity a single incident mode can scatter into infinite number of modes or waves. Thus a two-port network can have several electrical ports, which is usually referred to as multi-mode scattering matrix. In this situation, each scattering parameter no longer remains a single value, but now becomes a matrix of its own, and the scattering matrix of the network is expressed as a matrix of matrices

$$[S] = \begin{bmatrix} [S_{11}] & [S_{12}] \\ [S_{21}] & [S_{22}] \end{bmatrix}. \tag{2.36}$$

In this form, the $[S_{ij}]$ matrices still represent the reflection and transmission coefficients for the physical two-port network. The elements of the $[S_{ij}]$ matrices represent the coupling between the electrical ports. The scattering matrix for a two-port network that has two modes is

$$[S] = \begin{bmatrix} S_{11}(0,0) & S_{11}(0,1) & S_{12}(0,0) & S_{12}(0,1) \\ S_{11}(1,0) & S_{11}(1,1) & S_{12}(1,0) & S_{12}(1,1) \\ S_{21}(0,0) & S_{21}(0,1) & S_{22}(0,0) & S_{22}(0,1) \\ S_{21}(1,0) & S_{21}(1,1) & S_{22}(1,0) & S_{22}(1,1) \end{bmatrix}. \tag{2.37}$$

If we consider a TE_{10} mode is the incident mode and that a TE_{20} mode propagates, then $S_{11}(0,0)$ is the reflection coefficient of the reflected TE_{10} mode at port 1 and $S_{11}(0,1)$ is

the reflection coefficient of the reflected TE_{20} mode at port 1 from the incident TE_{10} mode. Similarly, $S_{21}(1, 1)$ represents the transmission coefficient of the TE_{20} mode.

In many situations only the fundamental mode elements $(0, 0)$ are of interest. However, the contribution of the higher order modes to the fundamental mode is essential for accurate representation of the network.

2.4.2 Scattering Matrix Characteristics

For a reciprocal network the scattering matrix is symmetrical,

$$[S] = [S]^t. \tag{2.38}$$

The superscript "t" denotes the matrix transpose operation. When a two-port network is reciprocal, interchanging the ports does not alter its configuration or characteristics in any manner. A uniform transmission line is an example of a reciprocal network.

For a passive, reciprocal, lossless network,

$$[S]^t[S]^* = [U], \tag{2.39}$$

where $[U]$ is the identity matrix. The superscript "$*$" denotes the matrix conjugate operation. Equation (2.39) is known as the unitary condition and the proof is available in reference [3]. This relation is useful in verifying the correctness of scattering matrices.

2.4.3 Scattering Matrix of a Uniform Lossless Transmission Line

Consider a uniform lossless transmission line section of length L, propagation constant β and characteristic impedance Z_o, as seen in Figure 2.9. The transmission line is matched or terminated at both ends by characteristic impedances equal to Z_o.

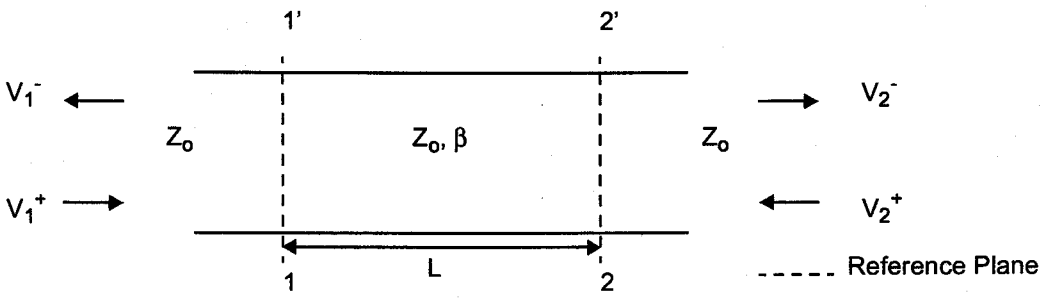

Figure 2.9. A Uniform Lossless Transmission Line

Consider the transmission line as a two-port network, with incident voltage waves V_1^+ and V_2^+, and reflected voltage waves V_1^- and V_2^- for ports 1 and 2, respectively. Since the

transmission line is uniform, lossless and there are no reflections at the two ends (it is matched), $S_{11} = S_{22} = 0$. By shifting the reference point from 1-1' to 2-2' there is a corresponding phase shift of βL and hence $S_{12} = S_{21} = e^{-j\beta L}$. Thus the scattering matrix for a transmission line is given by

$$[S] = \begin{bmatrix} 0 & e^{-j\beta L} \\ e^{-j\beta L} & 0 \end{bmatrix}. \tag{2.40}$$

When multiple electrical ports are considered the transmission line matrix defined equation (2.40) becomes a matrix of matrices with $[S_{11}] = [S_{22}] = [0]$ (a zero matrix) and $[S_{12}] = [S_{21}] = [TL]$. The transmission line matrix, $[TL]$, for the modes TE_{m0} that is used throughout this thesis is a diagonal matrix with elements

$$TL_{m0} = e^{-j\beta_{m0}L}. \tag{2.41}$$

2.4.3.1 Numerical Computations

The numerical computations required to calculate the diagonal transmission line matrix, $[TL]$, simply involves computing the exponential function. However, to improve spacial efficiency the sparse diagonal matrix may be stored as a column matrix.

2.4.4 Cascading Scattering Matrices

When two network elements with scattering matrices S_L and S_R are connected as shown in Figure 2.10, they can be represented by the overall resulting scattering matrix S_T. In this figure each of the scattering matrices represent one electrical port in a two-port network. However, there may be multiple electrical ports in which case the scattering matrices S_L, S_R and S_T represent matrices of matrices, which will be the case throughout this thesis.

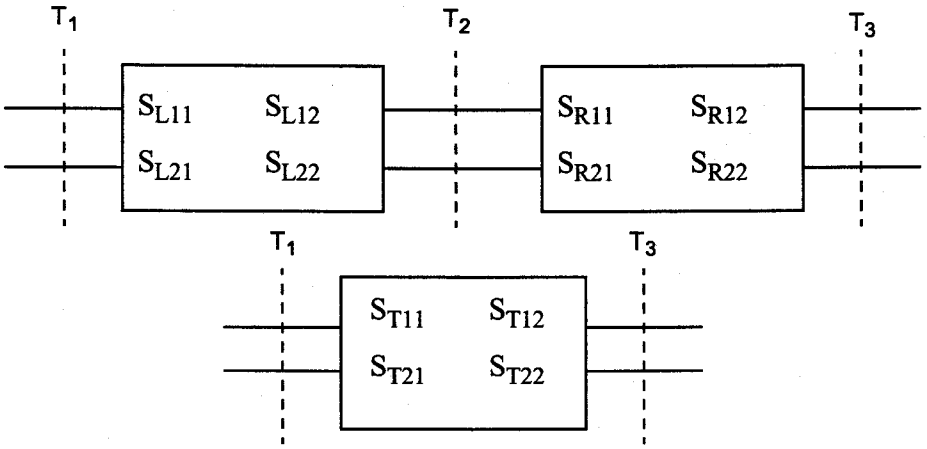

Figure 2.10. Cascading Scattering Matrices

The conventional equations used for cascading scattering matrices require two matrix inversions and can be found in reference [29]. The following set of equations for cascading scattering matrices from reference [31] are more efficient since they only require one matrix inversion:

$$S_{T11} = S_{L11} + S_{L12} S_{R11} W S_{L21}, \tag{2.42}$$

$$S_{T12} = S_{L12}(U + S_{R11} W S_{L22}) S_{R12}, \tag{2.43}$$

$$S_{T21} = S_{R21} W S_{L21}, \tag{2.44}$$

$$S_{T22} = S_{R22} + S_{R21} W S_{L22} S_{R12}, \tag{2.45}$$

where

$$W = \left[U - S_{L22} S_{R11}\right]^{-1}, \tag{2.46}$$

and U is the identity matrix.

When the scattering matrix S_R represents a transmission line, then $S_{R11} = S_{R22} = 0$ and $S_{R12} = S_{R21} = TL$ and these equations simplify to:

$$S_{T11} = S_{L11}, \tag{2.47}$$

$$S_{T12} = S_{L12} TL, \tag{2.48}$$

$$S_{T21} = TL S_{L21} \text{ and} \tag{2.49}$$

$$S_{T22} = TL S_{L22} TL. \tag{2.50}$$

Similar equations can be derived for when the scattering matrix S_L represents a transmission line.

Since scattering matrices are used throughout this thesis, it is simpler and more computationally efficient to cascade scattering matrices then to convert to ABCD or T parameters, which are simply cascaded by multiplication.

2.4.4.1 Numerical Computations

The number of numerical computations required to cascade two scattering matrices is:

- 11 matrix multiplications
- 4 matrix additions/subtractions
- 1 matrix inversion

The number of numerical computations required to cascade a scattering matrix with a transmission line matrix is:

- 4 diagonal matrix multiplications

Clearly the number of computations required to cascade two scattering matrices is more expensive than cascading a scattering matrix with a transmission line matrix, so to improve efficiency the type of matrix being cascaded should be considered before cascading.

2.5 Summary

In this chapter, information on the related research for bends, T-junctions and microwave CAD is presented. The three most common microwave transmission line discontinuities, steps, bends and T-junctions, are described. The general concept of scattering parameters and electrical and physical ports are also presented in this chapter.

Chapter 3. The Mode Matching Method

The mode matching method [22, 32, 33] is an efficient and accurate method for formulating boundary value problems, such as the analysis of electromagnetic fields at a waveguide discontinuity. This method is particularly useful for analyzing the junction of two or more regions that each have a set of well defined solutions of Maxwell's equations that satisfy all the boundary conditions except at the junction. The main advantage of this method is the inclusion of higher order modes and their interactions in the solution. The higher order modes are critical for the accurate characterization of a discontinuity as they account for the stored energy around the discontinuity. This method also has the advantage of being simpler than other numerical methods [22] such as the Finite Element Method (FEM), Finite Difference Time Domain (FDTD) method and the Transmission Line Modeling Method (TLM) [34] (also known as the Transmission Line Matrix Method).

The first step in the mode matching method is to expand the unknown electromagnetic fields in the regions in terms of their respective normal modes. With knowledge of the functional form of the normal modes, the problem is reduced to determining the modal coefficients to satisfy the boundary conditions at the discontinuity. Using the orthogonal property of normal modes eventually leads to an infinite set of linear simultaneous equations. Since it is impossible to obtain an exact solution to an infinite set of equations, an approximation is made by selecting a finite number of modes. By using a finite number of modes, the solution may not converge to the correct solution if the ratio of the number of modes is not selected properly, which is known as the relative convergence problem [35]. The solution of the equations leads directly to a multi-mode scattering matrix that characterizes the discontinuity.

In this chapter the mode matching method will be described by analyzing rectangular waveguide H-plane and microstrip step junctions.

3.1 Mode Matching Formulation

The mode matching method is best understood through an example, and in this section a rectangular waveguide with an arbitrary H-plane step is considered. The geometry of the step is shown in Figure 3.1. For the analysis, the dominant TE_{10} mode is assumed to be

propagating in region 1 (as long as the mode is TE_{n0} the analysis is independent of field excitation) and strikes the step junction. At the discontinuity there will be an infinite set of TE_{n0} modes reflected and transmitted in both regions, however, only N modes in region 1 and M modes in region 2 are considered. The electric and magnetic fields at the step junction are represented by the sum of the incident or forward fields, F_i, and the reflected or backward fields, B_i, as seen in Figure 3.1.

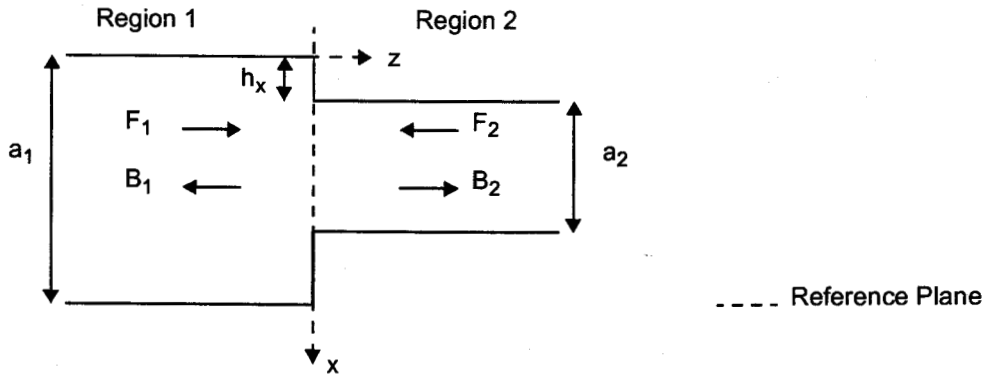

Figure 3.1. Arbitrary H-plane Step

The first step in the mode matching procedure is to expand the components of the electric and magnetic fields (E_y, H_x) in terms of the normal modes in the two regions:

$$E_{y1} = \sum_{i=1}^{N} (F^{i0}{}_1 + B^{i0}{}_1)\phi_{i1}(x), \tag{3.1}$$

$$H_{x1} = \sum_{i=1}^{N} \left(\frac{F^{i0}{}_1 - B^{i0}{}_1}{Z_{i1}}\right)\phi_{i1}(x), \tag{3.2}$$

$$E_{y2} = \sum_{i=1}^{M} (F^{i0}{}_2 + B^{i0}{}_2)\phi_{i2}(x), \tag{3.3}$$

$$H_{x2} = \sum_{i=1}^{M} \left(\frac{F^{i0}{}_2 - B^{i0}{}_2}{Z_{i2}}\right)\phi_{i2}(x), \tag{3.4}$$

where $\phi_{i1}(x)$ and $\phi_{i2}(x)$ are the normal modes or modal functions in regions 1 and 2, respectively, and for a H-plane step the normal modes are functions of x. The normal modes satisfy the orthogonality relation defined by

$$\int \phi_i(x)\phi_j(x)dx = \delta_{ij} = \begin{cases} 0 & i \neq j \\ 1 & i = j \end{cases}, \tag{3.5}$$

where δ_{ij} is the Kronecker delta function. The wave impedances, Z_{i1} and Z_{i2}, are given by equation (1.21).

Next we use the boundary conditions that the tangential component of the electric field and the normal component of the magnetic field must be continuous

$$E_{y1} = E_{y2} \text{ and} \tag{3.6}$$

$$H_{x1} = H_{x2}. \tag{3.7}$$

The electric field equation (3.6) is multiplied by $\phi_{m2}(x)$, where $m = 1 \ldots M$, and integrated with respect to x from 0 to a_2 to derive the following equation involving only the unknown coefficients:

$$\mathrm{F^{j0}}_2 + \mathrm{B^{j0}}_2 = \sum_{i=1}^{N} H_{ji}(\mathrm{F^{i0}}_1 + \mathrm{B^{i0}}_1) \qquad j = 1..\mathrm{M}, \tag{3.8}$$

$$\text{where } H_{ji} = \int_{h_x}^{(h_x + a_2)} \phi_{i1}(x)\phi_{j2}(x)dx. \tag{3.9}$$

The magnetic field equation (3.7) is multiplied by $\phi_{n1}(x)$, where $n = 1 \ldots N$, and integrated with respect to x from 0 to a_1 to derive the following equation involving only the unknown coefficients:

$$\frac{\mathrm{F^{j0}}_1 - \mathrm{B^{j0}}_1}{Z_{j1}} = \sum_{i=1}^{M} H_{ji} \frac{(\mathrm{F^{i0}}_2 - \mathrm{B^{i0}}_2)}{Z_{i2}} \qquad j = 1..\mathrm{N}. \tag{3.10}$$

It is easier to handle these simultaneous equations (3.8) and (3.10) in matrix form which are

$$F_2 + B_2 = H(F_1 + B_1) \text{ and} \tag{3.11}$$

$$Z_1^{-1}(F_1 - B_1) = H^t Z_2^{-1}(F_2 - B_2) \text{ or } Y_1(F_1 - B_1) = H^t Y_2(F_2 - B_2), \tag{3.12}$$

where H is the coupling matrix and is of the order (MxN), F_i is a column vector representing the incident field coefficients and is defined as

$$F_1 = \begin{bmatrix} \mathrm{F^{10}}_1 \\ \mathrm{F^{20}}_1 \\ . \\ \mathrm{F^{N0}}_1 \end{bmatrix} \qquad F_2 = \begin{bmatrix} \mathrm{F^{10}}_2 \\ \mathrm{F^{20}}_2 \\ . \\ \mathrm{F^{M0}}_2 \end{bmatrix}, \tag{3.13}$$

B_i is a column vector representing the reflected field coefficients and is defined as

$$B_1 = \begin{bmatrix} \mathrm{B^{10}}_1 \\ \mathrm{B^{20}}_1 \\ . \\ \mathrm{B^{N0}}_1 \end{bmatrix} \qquad B_2 = \begin{bmatrix} \mathrm{B^{10}}_2 \\ \mathrm{B^{20}}_2 \\ . \\ \mathrm{B^{M0}}_2 \end{bmatrix}, \tag{3.14}$$

Z_i is a diagonal matrix representing the wave impedance as defined in equation (1.23), and Y_i is a diagonal matrix representing the wave admittance as defined in equation (1.24).

Recalling the scattering matrix definition from Chapter 2:

$$B_1 = S_{11}F_1 + S_{12}F_2 \quad \text{and} \tag{3.15}$$

$$B_2 = S_{21}F_1 + S_{22}F_2. \tag{3.16}$$

By manipulating (3.11) and (3.12) into the above form the scattering matrices are determined

$$S_{11} = H^t S_{21} - U, \tag{3.17}$$

$$S_{12} = H^t(U + S_{22}), \tag{3.18}$$

$$S_{21} = 2(U + Z_2 H Y_1 H^t)^{-1} Z_2 H Y_1, \tag{3.19}$$

$$S_{22} = (U + Z_2 H Y_1 H^t)^{-1}(U - Z_2 H Y_1 H^t), \tag{3.20}$$

where U is the identity matrix, and S_{11}, S_{12}, S_{21} and S_{22} are matrices of order (NxN), (NxM), (MxN) and (MxM) respectively. H^t is the transpose of the coupling matrix H and when the number of modes approaches infinity $H^t = H^{-1}$ [36]. Another interesting property of the coupling matrix H for waveguides is that it is only a function of the geometry of the discontinuity and is independent of frequency. However for microstrip dispersion needs to be accounted for, so the effective width of the discontinuity is a function of frequency. These scattering matrix equations are not unique as there are eight ways to obtain the scattering matrices [22]. This formulation has been selected for numerical efficiency since only one matrix of order (MxM) needs to be inverted.

3.2 Rectangular Waveguide H-plane Step Junctions

As indicated in Section 2.3.1 there are three classifications of step junctions: symmetric, asymmetric and arbitrary. This section provides the coupling matrix for each of these three classifications.

3.2.1 Arbitrary Rectangular Waveguide H-plane Step

The modal functions for the arbitrary rectangular waveguide H-plane step shown in Figure 3.1, which satisfy the boundary condition that the tangential component of the electric field, E_y, is zero at the electric walls of the waveguide, are given by

$$\phi_{i1}(x) = \sqrt{\frac{2}{a_1}}\sin\left(\frac{i\pi x}{a_1}\right) \qquad i = 1..\mathrm{N} \quad \text{and} \tag{3.21}$$

$$\phi_{j2}(x) = \sqrt{\frac{2}{a_2}}\sin\left(\frac{j\pi(x-h_x)}{a_2}\right) \qquad j = 1..\mathrm{M}\ . \tag{3.22}$$

The resulting coupling matrix becomes [37]

$$H_{ji} = \begin{cases} \sqrt{\frac{a_2}{a_1}}\cos\left(\frac{i\pi h_x}{a_1}\right) & \text{when } \frac{i}{a_1} = \frac{j}{a_2} \\ \frac{2}{\sqrt{a_1 a_2}} \frac{\frac{j\pi}{a_2}}{\left(\frac{i\pi}{a_1}\right)^2 - \left(\frac{j\pi}{a_2}\right)^2} \left\{(-1)^j \sin\left(\frac{i\pi(h_x + a_2)}{a_1}\right) - \sin\left(\frac{i\pi h_x}{a_1}\right)\right\} & \text{otherwise} \end{cases} \tag{3.23}$$

where $j = 1 \ldots M$ and $i = 1 \ldots N$.

3.2.2 Asymmetric Rectangular Waveguide H-plane Step

The asymmetric rectangular waveguide H-plane step is a special case of the arbitrary rectangular waveguide H-plane step described in Section 3.2.1 with $h_x = 0$. The resulting coupling matrix becomes

$$H_{ji} = \begin{cases} \sqrt{\frac{a_2}{a_1}} & \text{when } \frac{i}{a_1} = \frac{j}{a_2} \\ \frac{2}{\sqrt{a_1 a_2}} \frac{\frac{j\pi}{a_2}}{\left(\frac{i\pi}{a_1}\right)^2 - \left(\frac{j\pi}{a_2}\right)^2} \left\{(-1)^j \sin\left(\frac{i\pi a_2}{a_1}\right)\right\} & \text{otherwise} \end{cases} \tag{3.24}$$

3.2.3 Symmetric Rectangular Waveguide H-plane Step

The symmetric rectangular waveguide H-plane step can be handled using equation (3.23) with $h_x = (a_1 - a_2)/2$ or a simpler more efficient derivation can be obtained by shifting the co-ordinate system as seen in Figure 3.2.

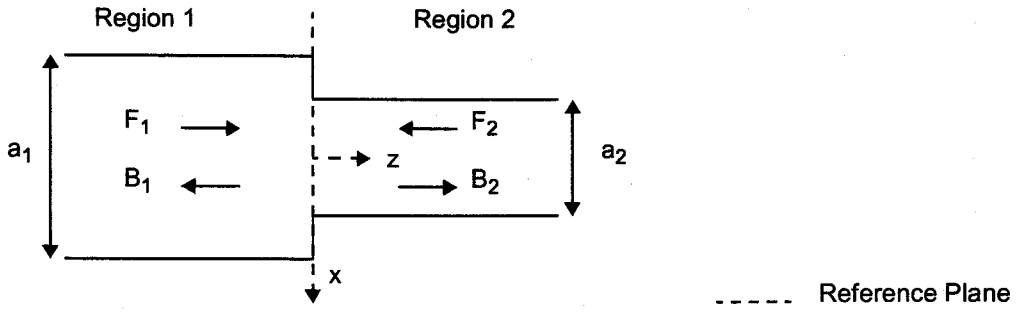

Figure 3.2. Symmetric H-plane Step

The modal functions, which satisfy the electric wall boundary condition, are given by

$$\phi_{i1}(x) = \sqrt{\frac{2}{a_1}}\cos\left(\frac{i\pi x}{a_1}\right) \qquad i = 1, 3, 5..\text{N and} \tag{3.25}$$

$$\phi_{j2}(x) = \sqrt{\frac{2}{a_2}}\cos\left(\frac{j\pi x}{a_2}\right) \qquad j = 1, 3, 5..\text{M}. \tag{3.26}$$

Only the odd modes need to be considered as the even modes are not excited by the incident TE_{10} wave due to the symmetric nature of the discontinuity. The region of integration becomes $x = -a_2/2$ to $a_2/2$. The resulting coupling matrix becomes

$$H_{ji} = \begin{cases} \sqrt{\dfrac{a_2}{a_1}} & \text{when } \dfrac{i}{a_1} = \dfrac{j}{a_2} \\ \dfrac{4}{\sqrt{a_1 a_2}} \dfrac{\frac{j\pi}{a_2}}{\left(\frac{i\pi}{a_1}\right)^2 - \left(\frac{j\pi}{a_2}\right)^2} \left\{(-1)^{\frac{(j-1)}{2}} \cos\left(\dfrac{i\pi a_2}{2a_1}\right)\right\} & \text{otherwise} \end{cases} \tag{3.27}$$

3.3 Microstrip Step

The mode matching method for microstrip follows the same formulation as described in Section 3.1, however there are two important differences between microstrip and a rectangular waveguide that need to be considered in the analysis:

- A rectangular waveguide has electric walls (the tangential components of the electric field are zero), while the microstrip planar waveguide model has magnetic walls (the tangential components of the magnetic field are zero or the normal component of the magnetic filed is a maximum).
- Modes for a rectangular waveguide begin with TE_{10}, while microstrip has a TE_{00} mode.

The first item affects the modal functions, and thus the formulation and derivation of the scattering matrices which become [22, 36]

$$S_{11} = U - Z_1 H^t Y_2 S_{21}, \tag{3.28}$$

$$S_{12} = Z_1 H^t Y_2 (U - S_{22}), \tag{3.29}$$

$$S_{21} = 2(HZ_1 H^t Y_2 + U)^{-1} H, \tag{3.30}$$

$$S_{22} = (HZ_1 H^t Y_2 + U)^{-1} (HZ_1 H^t Y_2 - U). \tag{3.31}$$

The second item affects the range of the modes, which need to begin at zero to account for the quasi-TEM mode, TE_{00}.

This section provides the coupling matrix for the three classifications of step junctions, as was done for in the previous section for rectangular waveguides.

3.3.1 Arbitrary Microstrip Step

The microstrip modal functions for the arbitrary microstrip step shown in Figure 3.1, which satisfy the boundary condition that the normal component of the magnetic field, H_x, is a maximum at the magnetic walls of the equivalent planar waveguide model, are given by

$$\phi_{i1}(x) = \sqrt{\frac{\varepsilon_{i0}}{a_1}}\cos\left(\frac{i\pi x}{a_1}\right) \qquad i = 0..N \text{ and} \tag{3.32}$$

$$\phi_{j2}(x) = \sqrt{\frac{\varepsilon_{j0}}{a_2}}\cos\left(\frac{j\pi(x-h_x)}{a_2}\right) \qquad j = 0..M, \tag{3.33}$$

where

$$\varepsilon_{n0} = \begin{cases} 1 & n = 0 \\ 2 & n \neq 0 \end{cases}. \tag{3.34}$$

The coupling matrix becomes

$$H_{ji} = \begin{cases} 0 & \text{when } i = 0 \;\&\; j \neq 0 \\ \sqrt{\frac{2a_1}{a_2}}\frac{1}{i\pi}\left\{\sin\left(\frac{i\pi(h_x+a_2)}{a_1}\right) - \sin\left(\frac{i\pi h_x}{a_1}\right)\right\} & \text{when } i \neq 0 \;\&\; j = 0 \\ \sqrt{\frac{a_2}{a_1}} & \text{when } i = 0 \;\&\; j = 0 \\ \sqrt{\frac{a_2}{a_1}}\cos\left(\frac{j\pi h_x}{a_2}\right) & \text{when } \frac{i}{a_1} = \frac{j}{a_2} \\ \frac{2}{\sqrt{a_1 a_2}}\frac{\frac{i\pi}{a_1}}{\left(\frac{i\pi}{a_1}\right)^2 - \left(\frac{j\pi}{a_2}\right)^2}\left\{(-1)^j\sin\left(\frac{i\pi(h_x+a_2)}{a_1}\right) - \sin\left(\frac{i\pi h_x}{a_1}\right)\right\} & \text{otherwise} \end{cases}. \tag{3.35}$$

As a reference, the derivation for this equation is shown in Appendix A, "Coupling Matrix Derivation" on page 116.

3.3.2 Asymmetric Microstrip Step

The asymmetric microstrip step is a special case of the arbitrary microstrip step described in Section 3.3 with $h_x = 0$. The resulting coupling matrix becomes

$$H_{ji} = \begin{cases} 0 & \text{when } i = 0 \;\&\; j \neq 0 \\ \sqrt{\dfrac{2a_1}{a_2}} \dfrac{1}{i\pi} \sin \dfrac{i\pi a_2}{a_1} & \text{when } i \neq 0 \;\&\; j = 0 \\ \sqrt{\dfrac{a_2}{a_1}} & \text{when } \dfrac{i}{a_1} = \dfrac{j}{a_2} \\ \dfrac{2}{\sqrt{a_1 a_2}} \dfrac{\dfrac{i\pi}{a_1}}{\left(\dfrac{i\pi}{a_1}\right)^2 - \left(\dfrac{j\pi}{a_2}\right)^2} \left\{ (-1)^j \sin\left(\dfrac{i\pi a_2}{a_1}\right) \right\} & \text{otherwise} \end{cases} \tag{3.36}$$

3.3.3 Symmetric Microstrip Step

The symmetric microstrip step can be handled using equation (3.35) with $h_x = (a_1 - a_2)/2$ or two simpler derivations can be obtained. One derivation is to use the same method that was applied to the symmetric rectangular waveguide H-plane step, which involves shifting the co-ordinate system as seen in Figure 3.2. However, for microstrip only the even modes need to be considered as the odd modes are not excited by the TE_{00} wave due to the symmetric nature of the discontinuity [38]. The other more popular derivation is to consider only one half of the original structure as seen in Figure 3.3 [22, 36].

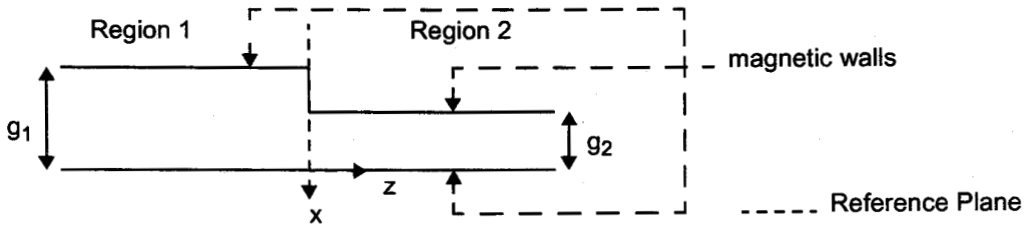

Figure 3.3. Auxiliary Geometry for a Symmetric Microstrip Step

With this approach the symmetric microstrip step can be analyzed as an asymmetric microstrip step. Thus equation (3.36) can be reused with widths $a_1 = g_1$ and $a_2 = g_2$.

3.4 Relative Convergence

As mentioned previously, the relative convergence problem occurs when a finite number of modes are used for the mode matching method and the solution does not converge to the correct solution. In order to avoid this problem, it is critical to choose the number of modes on both sides of the discontinuity such that the ratio of the number of modes equals the ratio of the widths of each side of the discontinuity [22, 36, 39]

$$\frac{M}{N} = \frac{a_2}{a_1}, \tag{3.37}$$

where M is the number of modes for the smaller dimension, a_2, and N is the number of modes for the larger dimension, a_1. This ratio is known as the relative convergence ratio.

3.5 Numerical Computations

The total number of numerical computations for finding the scattering matrices for the rectangular waveguide H-plane and microstrip step is:

- 1 matrix inversion, involving a matrix of order (MxM)
- 1 matrix transpose
- 4 matrix additions/subtractions
- 5 matrix multiplications
- 2 diagonal matrix multiplications, involving the impedance/admittance matrices

The coupling matrix H, a matrix of order (MxN), is computed using linear algebra.

The other factor that needs to be considered for the numerical computations of the step discontinuity is the number of modes required for the mode matching, which must be selected to satisfy the relative convergence ratio (equation (3.37)). This thesis uses at least 20 modes in the larger dimension for the analysis of step discontinuities. If the resulting number of modes becomes less than 5 for the smaller dimension, then 5 modes are used in the smaller dimension and the number of modes in the larger dimension are computed using the relative convergence ratio. The number of modes selected is a trade-off between accuracy and computational speed and storage requirements: a large number of modes may result in a more accurate solution but the computational speed is slow and the storage requirements for the matrices is large; a small number of modes may result in an inaccurate solution but the computational speed is fast and the storage requirements for the matrices is small. The use of 20 modes was chosen in attempt to balance accuracy with computational speed.

3.6 Summary

In this chapter the mode matching method and the application of the method to rectangular waveguide H-plane and microstrip step junctions are discussed in detail. The relative convergence problem that may be encountered when using the mode matching method is also discussed, along with a method for overcoming this problem. While this chapter focused on H-plane step discontinuities, the mode matching method can be applied to other types of discontinuity problems [40]. The mode matching method is an efficient and accurate method for formulating boundary value problems, such as the analysis of electromagnetic fields at a waveguide discontinuity.

Chapter 4. Discontinuity Analysis Method

The previous chapter explained the mode matching method and the characterization of rectangular waveguide H-plane and microstrip step junctions. In this chapter, a microwave CAD method for the analysis of transmission line right angle bend and T-junction discontinuities is presented and applied to rectangular waveguide H-plane and microstrip transmission lines. The implementation of the discontinuity analysis method in this thesis extensively uses mode matching to characterize the discontinuity. The method is also known as the port reduction method, which has been successfully used to analyze other structures [41, 42, 43, 44]. In this chapter the method is used to analysis a transmission line right angle bend, a T-junction, and finally compensated bends, T-junctions and steps. As a reference, the related elements provided by some commercial microwave CAD programs are listed in Appendix B. Finally, a description of the software routines developed to implement the discontinuity analysis method is presented.

When the port reduction method is applied to a n-port network, the resulting network is an $(n-x)$-port network, where $1 < x \leq n$, and by selecting various different locations of defined terminations the n-port scattering parameters are determined. In this chapter two-port networks (bends) and three-port networks (T-junctions) will be analyzed as one-port networks and two-port networks, respectively, using three different locations of defined terminations. While any defined termination could be used, for numerical efficiency a short circuit (an electric wall) is used for rectangular waveguides and an open circuit (a magnetic wall) is used for microstrip. The equivalent planar waveguide model is also used for microstrip because of its successful application in the analysis of dispersion.

4.1 Transmission Line Right Angle Bend

A transmission line bend is a two-port network that can be represented via the scattering parameters S_{11}, S_{12}, S_{21} and S_{22} as depicted in Figure 4.1. By placing a defined termination (an open circuit for microstrip, or a short circuit for a rectangular waveguide) at three different locations at port 2 the network can be analyzed as a one-port network which is composed of a step discontinuity and a transmission line. The scattering parameters of the two-port network are determined from the reflection coefficients of the three one-port networks, which are easily solved by the standard mode matching method for

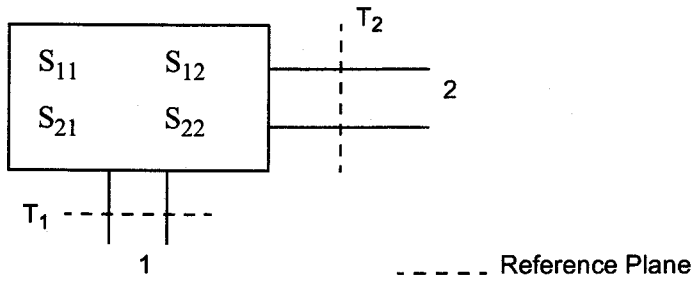

Figure 4.1. Two-port Network

step discontinuities. Let $[S]$ represent the scattering matrix of the two-port network, $\Gamma_{in}^{(i)}$ represent the reflection coefficient for the one-port network and $\Gamma_L^{(i)}$ represent the reflection coefficient for the terminated load. The scattering parameters are obtained by solving

$$\Gamma_{in}^{(i)} = S_{11} + \frac{S_{12}S_{21}\Gamma_L^{(i)}}{1 - S_{22}\Gamma_L^{(i)}}, \tag{4.1}$$

where

$$\Gamma_L^{(i)} = \pm e^{-j2\beta L_i}, \tag{4.2}$$

and β is the propagating constant of the principal mode for the transmission line connected between port 2 and the defined termination, and the value of $\Gamma_L^{(i)}$ is negative for a short circuit (waveguide) and positive for an open circuit (microstrip). By taking three different locations of L_i and equation (4.1) one can obtain:

$$\begin{bmatrix} 1 & \Gamma_{in}^{(1)}\Gamma_L^{(1)} & \Gamma_L^{(1)} \\ 1 & \Gamma_{in}^{(2)}\Gamma_L^{(2)} & \Gamma_L^{(2)} \\ 1 & \Gamma_{in}^{(3)}\Gamma_L^{(3)} & \Gamma_L^{(3)} \end{bmatrix} \begin{bmatrix} S_{11} \\ S_{22} \\ S_{12}S_{21} - S_{11}S_{22} \end{bmatrix} = \begin{bmatrix} \Gamma_{in}^{(1)} \\ \Gamma_{in}^{(2)} \\ \Gamma_{in}^{(3)} \end{bmatrix}. \tag{4.3}$$

Therefore the scattering parameters of the two-port network are obtained by accurately finding $\Gamma_{in}^{(i)}$ for three different terminations and solving this matrix equation (using the reciprocal nature of the two-port passive network, $S_{12} = S_{21}$). The $\Gamma_{in}^{(i)}$ parameters are found by analyzing the step discontinuity and transmission line using the mode matching method.

4.1.1 Microstrip Right Angle Bend

To demonstrate the method consider the case of a microstrip right angle bend, where the microstrip lines are analyzed using the planar waveguide model that can be viewed as a rectangular waveguide with magnetic side-walls with height h, effective dielectric constant ε_{eff} and effective width W_{eff}, as shown in Figure 4.2.

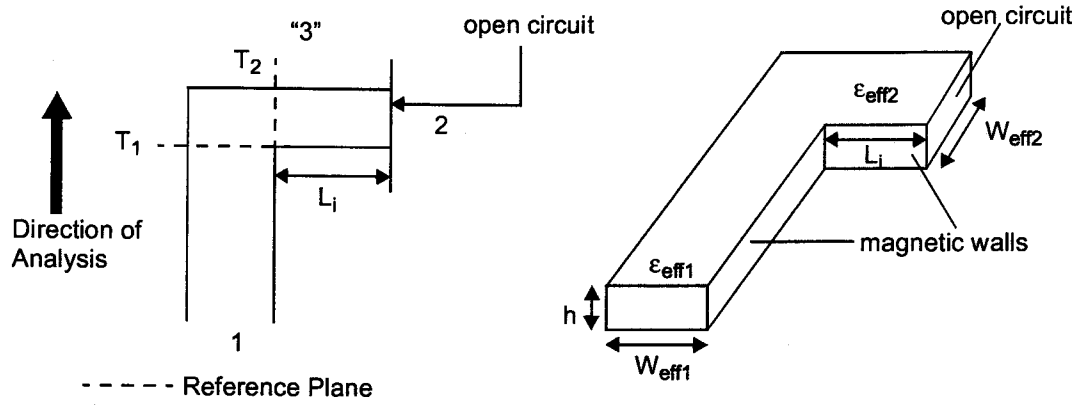

Figure 4.2. Microstrip Right Angle Bend

The two-port bend can be viewed from looking from port 1 as an asymmetric step discontinuity followed by a transmission line terminated by a magnetic wall (a perfect open circuit) at "port 3" that can be analyzed by using the standard mode matching method.

The first step in calculating $\Gamma_{in}^{(i)}$ is to perform mode matching for an asymmetric step discontinuity between a line of width W_{eff1} and a line of width $W_{eff1} + L_i$, as described in the previous chapter. The scattering matrices of the step discontinuity are then cascaded with the scattering matrix of a transmission line of length W_{eff2}, dielectric constant ε_{eff2} and propagation constant β_m, which can be represented by the transmission line matrix defined in equation (2.41). The resulting scattering matrices, S_{Lij}, are then cascaded with an open circuit, which can be represented by $[TERM_{11}] = [TERM_{22}] = [U]$ (an identity matrix) and $[TERM_{12}] = [TERM_{21}] = [0]$ (a zero matrix), by using a simplified equation (2.42):

$$S_{T11} = S_{L11} + S_{L12}(U - S_{L22})^{-1} S_{L21}. \tag{4.4}$$

The one-port reflection coefficient, $\Gamma_{in}^{(i)}$, is found by taking the principal mode from this resulting scattering matrix. Substituting this value, for the one-port reflection coefficient, and the reflection coefficient for the terminated load into equation (4.3) and solving the matrix equation results in the scattering parameters for the two-port right angle bend.

4.1.2 Rectangular Waveguide H-plane Right Angle Bend

The example described in the previous section can be applied to a rectangular waveguide H-plane bend with the following changes made:

- Port 2 is terminated with a short circuit instead of an open circuit so the reflection coefficient for the defined termination, $\Gamma_L^{(i)}$, is negative.

- The width of the transmission lines are a_1 and a_2 instead of W_{eff1} and W_{eff2}.
- The propagation constant is $\beta_{mn} = \sqrt{k_o^2 - k_{cmn}^2}$ instead of $\beta_m = \sqrt{k_o^2 \varepsilon_{eff} - \left(\frac{m\pi}{W_{eff}}\right)^2}$.
- The walls of the rectangular waveguide are electric walls, which are perfect short circuits, instead of magnetic walls so the termination matrix becomes $[TERM_{11}] = [TERM_{22}] = -[U]$.
- The modes begin at 1 instead of 0.
- The dielectric constant is $\varepsilon_r = 1$, for an air-filled waveguide, instead of ε_{eff}.

4.1.3 Numerical Computations

The total number of numerical computations for finding the reflection coefficient $\Gamma_{in}^{(i)}$ is:

- 1 asymmetric step discontinuity (as described in Section 3.5)
- 1 transmission line (as described in Section 2.4.3.1)
- 1 cascade of a scattering matrix with a transmission line matrix (as described in Section 2.4.4.1)
- 1 cascade of a scattering matrix with an open circuit or short circuit termination, which could be handled by cascading two scattering matrices as described in Section 2.4.4.1, but should be handled as a special case for efficiency:
  - 1 matrix inversion
  - 2 matrix additions/subtractions
  - 2 matrix multiplications

The other factor that needs to be considered for the numerical computations of the bend is the number of modes required for the mode matching in order to satisfy the relative convergence ratio (equation (3.37)). If the value of L_i is large relative to W_{eff1} then a large number of modes may be required.

Thus, the overall numerical computations for finding the scattering parameters for the two-port transmission line right angle bend is:

- 3 reflection coefficients, $\Gamma_{in}^{(i)}$, as described above
- 1 matrix inversion of order (3x3)
- 1 matrix multiplication of order (3x3)

4.2 Transmission Line T-junction

The analysis of the T-junction is very similar to the above analysis for the bend, except there are three ports to consider instead of two. A transmission line T-junction is a three-port network that is represented via the scattering parameters S_{11}, S_{12}, S_{13}, S_{21}, S_{22}, S_{23}, S_{31}, S_{32} and S_{33} as depicted in Figure 4.3.

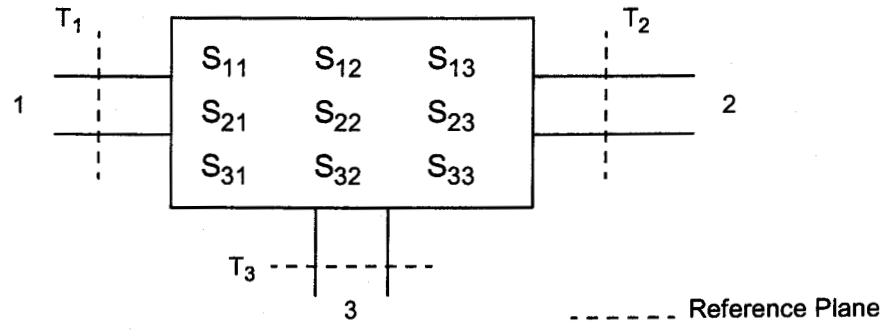

Figure 4.3. Three-port Network

By placing a defined termination (an open circuit for microstrip, or a short circuit for a rectangular waveguide) at three different locations at port 3 the network can be analyzed as a two-port network, which is composed of two step discontinuities connected by a finite length of transmission line. The scattering parameters of the three-port network are determined from the scattering parameters of the three two-port networks, which are easily solved by the standard mode matching method for step discontinuities. Let $[S]$ represent the scattering matrix of the three-port network, $[R^{(i)}]$ represent the scattering matrix of the two-port network and $\Gamma_L^{(i)}$ represent the reflection coefficient for the terminated load. The scattering parameters of the two-port network after terminating port 3 can be written as

$$R_{11}^{(i)} = S_{11} + \frac{S_{13}S_{31}\Gamma_L^{(i)}}{1 - S_{33}\Gamma_L^{(i)}}, \tag{4.5}$$

$$R_{12}^{(i)} = S_{12} + \frac{S_{13}S_{32}\Gamma_L^{(i)}}{1 - S_{33}\Gamma_L^{(i)}}, \tag{4.6}$$

$$R_{21}^{(i)} = S_{21} + \frac{S_{23}S_{31}\Gamma_L^{(i)}}{1 - S_{33}\Gamma_L^{(i)}} \text{ and} \tag{4.7}$$

$$R_{22}^{(i)} = S_{22} + \frac{S_{23}S_{32}\Gamma_L^{(i)}}{1 - S_{33}\Gamma_L^{(i)}}. \tag{4.8}$$

Where, as before,

$$\Gamma_L^{(i)} = \pm e^{-j2\beta L_i}, \tag{4.9}$$

and β is the propagating constant of the principal mode for the transmission line connected between port 3 and the defined termination, and the value of $\Gamma_L^{(i)}$ is negative for a short circuit (waveguide) and positive for an open circuit (microstrip). By taking three different locations of L_i and equation (4.5) one can obtain:

$$\begin{bmatrix} 1 & R_{11}^{(1)}\Gamma_L^{(1)} & \Gamma_L^{(1)} \\ 1 & R_{11}^{(2)}\Gamma_L^{(2)} & \Gamma_L^{(2)} \\ 1 & R_{11}^{(3)}\Gamma_L^{(3)} & \Gamma_L^{(3)} \end{bmatrix} \begin{bmatrix} S_{11} \\ S_{33} \\ S_{13}S_{31} - S_{11}S_{33} \end{bmatrix} = \begin{bmatrix} R_{11}^{(1)} \\ R_{11}^{(2)} \\ R_{11}^{(3)} \end{bmatrix}. \tag{4.10}$$

Hence, three of the scattering parameters (S_{11}, S_{13} and S_{33}) for the T-junction are found by accurately obtaining the parameter $R_{11}^{(i)}$ for three different locations of a terminated load. Similarly another matrix equation can be easily found from equation (4.8) involving $R_{22}^{(i)}$ and from this S_{22} and S_{23} can be obtained

$$\begin{bmatrix} 1 & R_{22}^{(1)}\Gamma_L^{(1)} & \Gamma_L^{(1)} \\ 1 & R_{22}^{(2)}\Gamma_L^{(2)} & \Gamma_L^{(2)} \\ 1 & R_{22}^{(3)}\Gamma_L^{(3)} & \Gamma_L^{(3)} \end{bmatrix} \begin{bmatrix} S_{22} \\ S_{33} \\ S_{23}S_{32} - S_{22}S_{33} \end{bmatrix} = \begin{bmatrix} R_{22}^{(1)} \\ R_{22}^{(2)} \\ R_{22}^{(3)} \end{bmatrix}. \tag{4.11}$$

So far, five of the six independent variables have been solved for. The remaining parameter S_{12} can be determined by either equation (4.6), involving $R_{12}^{(i)}$, or equation (4.7), involving $R_{21}^{(i)}$, i.e.

$$S_{12} = R_{12}^{(i)} - \frac{S_{13}S_{32}\Gamma_L^{(i)}}{1 - S_{33}\Gamma_L^{(i)}}. \tag{4.12}$$

Thus, all the scattering parameters of the T-junction have been obtained from the scattering parameters of the two-port networks. The $[R^{(i)}]$ parameters of the two-port networks are found by analyzing the two step discontinuities and transmission line using the mode matching method.

4.2.1 Alternative Port Reduction Analysis of a T-junction

In the previous section, a three-port T-junction was analyzed by terminating one port with a defined termination at three locations and examining the resulting three two-port networks. The circuit could also be analyzed by terminating two ports at seven different locations and examining the resulting seven one-port networks. Taken to the extreme, the circuit could be analyzed by terminating all three ports at seven locations and examining the resulting seven resonators. However, terminating additional ports can actually increase the number of numerical computations [44].

In general, a multi-port network can be analyzed by selectively choosing some ports of the network to be terminated by a defined termination so that the reflection coefficients can be found at the remaining ports. The scattering parameters of the multi-port network can then be found using a formulation involving the reflection coefficients, similar to the one used in the previous section. For more information refer to reference [44], which analyzes a five-port network by terminating three ports and calculating the reflection coefficients for the remaining two ports fifteen times.

Also note, that while the mode matching method is used to analyze the various structures in this chapter, the port reduction method can be used with any suitable numerical method. Thus, more rigorous full-wave numerical methods can be combined with the port reduction method.

4.2.2 Microstrip T-junction

As an example of how the $[R^{(i)}]$ parameters are computed consider a microstrip T-junction as shown in Figure 4.4, where the microstrip lines are equivalent to rectangular waveguides with magnetic side-walls that have height h, effective dielectric constant ε_{eff} and effective width W_{eff}.

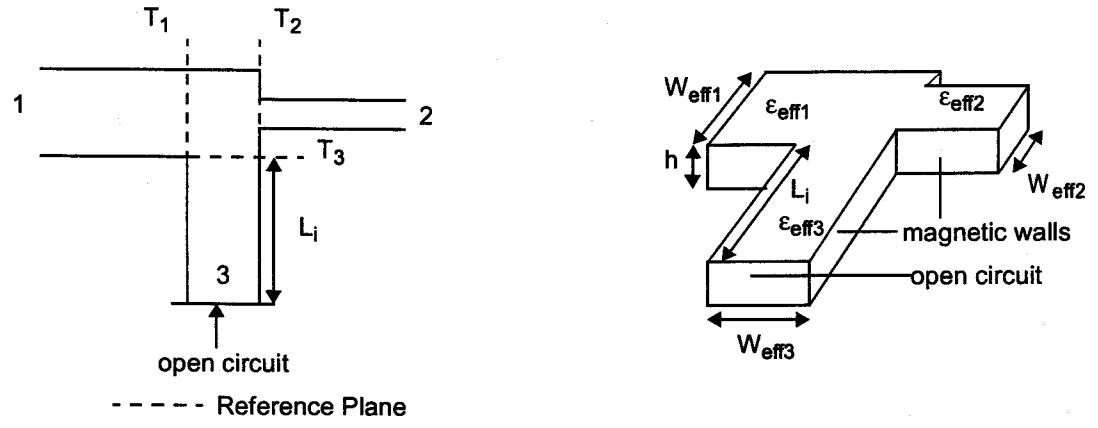

Figure 4.4. Microstrip T-junction

With an open circuit at port 3 the network consists of three sections of rectangular waveguides with magnetic walls involving two step discontinuities, which can be analyzed using the standard mode matching method using the same approach that was used for the bend in the previous section.

The first step in calculating $[R^{(i)}]$ is to perform mode matching for an asymmetric step discontinuity between a line of width W_{eff1} and a line of width $W_{eff1} + L_i$, as described in

the previous chapter. The scattering matrices of the step discontinuity are then cascaded with the scattering matrix of a transmission line of length W_{eff3}, dielectric constant ε_{eff3} and propagation constant β_m, which can be represented by the transmission line matrix defined in equation (2.41). The resulting scattering matrices are then cascaded with the scattering matrices for an arbitrary step discontinuity of width $W_{eff1} + L_i$ to W_{eff2}.

The two-port scattering parameters $[R^{(i)}]$ are found by taking the principal mode from the resulting scattering matrices. Substituting these values and the reflection coefficient for the terminated load into equations (4.10), (4.11) and (4.12) and solving the matrix equations results in the scattering parameters for the three-port T-junction.

4.2.3 Rectangular Waveguide H-plane T-junction

The example described in the previous section can be applied to a rectangular waveguide H-plane T-junction by making the changes described in Section 4.1.2 and accounting for the additional transmission line in a T-junction.

4.2.4 Numerical Computations

The total number of numerical computations for finding the two-port scattering parameters $[R^{(i)}]$ is:

- 2 step discontinuities (as described in Section 3.5)
- 1 transmission line (as described in Section 2.4.3.1)
- 1 cascade of a scattering matrix with a transmission line matrix (as described in Section 2.4.4.1)
- 1 cascade of scattering matrices (as described in Section 2.4.4.1)

The other factor that needs to be considered for the numerical computations of the bend is the number of modes required for the mode matching in order to satisfy the relative convergence ratio (equation (3.37)). If the value of L_i is large relative to W_{eff1} and W_{eff2} then a large number of modes may be required.

Thus, the overall numerical computations for finding the scattering parameters for the three-port transmission line T-junction is:

- 3 scattering parameters, $[R^{(i)}]$, as described above
- 2 matrix inversions of order (3x3)
- 2 matrix multiplications of order (3x3)

4.3 Compensated Transmission Line Right Angle Bends

In Section 4.1 the analysis of a transmission line uncompensated right angle bend discontinuity was presented. The right angle bend was not compensated in an attempt to reduce the effects of the reactances arising from the sharp discontinuity. This section describes some of the compensation methods for right angle bend discontinuities, how they can be analyzed and their numerical computations. While these compensated bends can be used for both microstrip and rectangular waveguides, the diagrams in this section show microstrip transmission lines.

For simplicity the widths of the transmission lines shown in this section are the same, however they do not need to be (ie. W_{eff1} does not have to equal W_{eff2}).

4.3.1 Outside Cut Right Angle Bend

An outside cut right angle bend has a rectangular portion of the bend removed in an attempt to reduce the effects of discontinuity reactances as shown in Figure 4.5. The rectangular portion removed has dimensions $d1$ by $d2$, and in this figure $d1 < W_{eff1}$ and $d2 < W_{eff2}$, as is the typical case. The only constraint on the values of $d1$ and $d2$ is that they cannot both be larger the transmission lines (ie. $d1 > W_{eff1}$ and $d2 > W_{eff2}$) at the same time since that would result in two lines that do not touch.

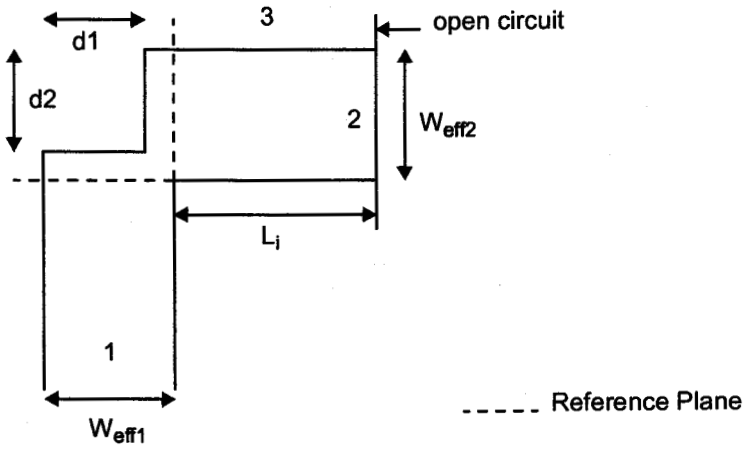

Figure 4.5. Outside Cut Right Angle Bend

The reflection coefficient $\Gamma_{in}^{(i)}$ is found by:

1. Computing the scattering matrices for an asymmetric step discontinuity from a transmission line of width W_{eff1} to $W_{eff1} + L_i$.
2. The scattering matrix for a transmission line of length $W_{eff2} - d2$ and width $W_{eff1} + L_i$ is computed and cascaded with the scattering matrices from the previous step.

3. Computing the scattering matrices for an asymmetric step discontinuity from a transmission line of width $W_{eff1} + L_i$ to $W_{eff1} + L_i - d1$.
4. The scattering matrix for a transmission line of length $d2$ and width $W_{eff1} + L_i - d1$ is computed and cascaded with the scattering matrices from the previous step.
5. The scattering matrices computed in step 2 are cascaded with the scattering matrices computed in the previous step and then with the scattering matrices for an open circuit. The reflection coefficient $\Gamma_{in}^{(i)}$ is found by taking the principal mode from the resulting reflection coefficient scattering matrix.

Note that if $d2 > W_{eff2}$ the first asymmetric step discontinuity would be from W_{eff1} to $W_{eff1} - d1$ and the second asymmetric step discontinuity would be from $W_{eff1} - d1$ to $W_{eff1} - d1 + L_i$.

4.3.1.1 Numerical Computations

As described in the previous section, the total number of numerical computations for finding the reflection coefficient $\Gamma_{in}^{(i)}$ for the outside cut right angle bend is:

- 2 step discontinuities (as described in Section 3.5)
- 2 transmission lines (as described in Section 2.4.3.1)
- 2 cascades of a scattering matrix with a transmission line matrix (as described in Section 2.4.4.1)
- 1 cascade of scattering matrices (as described in Section 2.4.4.1)
- 1 cascade of a scattering matrix with an open circuit matrix (as described in Section 4.1.3)

The other factor that needs to be considered for the numerical computations of the outside cut right angle bend is the number of modes required for the mode matching. Depending on the values of W_{eff1}, $d1$ and L_i a large number of modes may be required for each step discontinuity to satisfy the relative convergence ratio (equation (3.37)).

The overall numerical computations required for computing the scattering parameters of an outside cut right angle bend is as described in Section 4.1.3 with the cost of $\Gamma_{in}^{(i)}$ adjusted as described above.

4.3.2 Double Outside Cut Right Angle Bend

A double outside cut right angle bend is very similar to the outside cut right angle bend described in the previous section, except that it has two rectangular portions of the bend removed in an attempt to reduce the effects of discontinuity reactances as shown in Figure

4.6. The rectangular portions removed can be described as having dimensions $d1a + d1b$ by $d2b$ and $d1a$ by $d2a$.

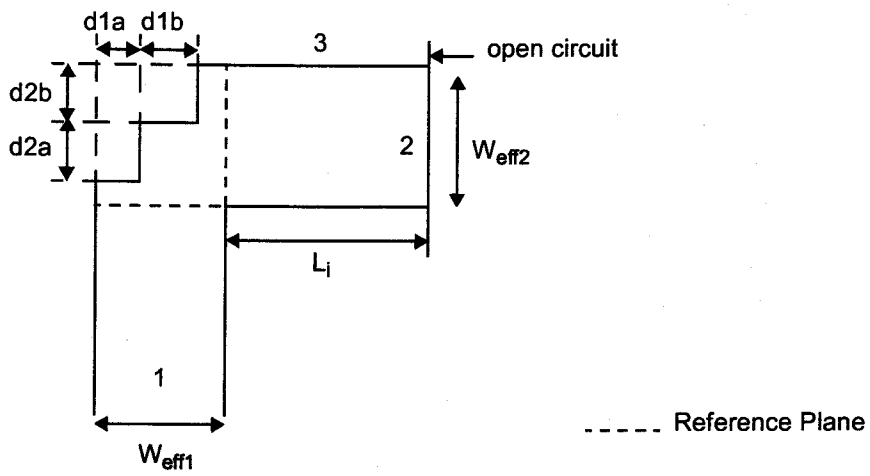

Figure 4.6. Double Outside Cut Right Angle Bend

The reflection coefficient $\Gamma_{in}^{(i)}$ is found by:

1. Computing the scattering matrices for an asymmetric step discontinuity from a transmission line of width W_{eff1} to $W_{eff1} + L_i$.
2. The scattering matrix for a transmission line of length $W_{eff2} - d2a - d2b$ and width $W_{eff1} + L_i$ is computed and cascaded with the scattering matrices from the previous step.
3. Computing the scattering matrices for an asymmetric step discontinuity from a transmission line of width $W_{eff1} + L_i$ to $W_{eff1} + L_i - d1a$.
4. The scattering matrix for a transmission line of length $d2a$ and width $W_{eff1} + L_i - d1a$ is computed and cascaded with the scattering matrices from the previous step.
5. Computing the scattering matrices for an asymmetric step discontinuity from a transmission line of width $W_{eff1} + L_i - d1a$ to $W_{eff1} + L_i - d1a - d1b$.
6. The scattering matrix for a transmission line of length $d2b$ and width $W_{eff1} + L_i - d1a - d1b$ is computed and cascaded with the scattering matrices from the previous step.
7. The scattering matrices computed in steps 2, 4 and 6 are cascaded together and then with the scattering matrices for an open circuit. The reflection coefficient $\Gamma_{in}^{(i)}$ is found by taking the principal mode from the resulting reflection coefficient scattering matrix.

Note that for the uncommon cases of $(d2a + d2b) > W_{eff2}$, $d2a > W_{eff2}$ or $d2b > W_{eff2}$ the asymmetric step discontinuities would be different.

4.3.2.1 Numerical Computations

As described in the previous section, the total number of numerical computations for finding the reflection coefficient $\Gamma_{in}^{(i)}$ for the double outside cut right angle bend is:

- 3 step discontinuities (as described in Section 3.5)
- 3 transmission lines (as described in Section 2.4.3.1)
- 3 cascades of a scattering matrix with a transmission line matrix (as described in Section 2.4.4.1)
- 2 cascades of scattering matrices (as described in Section 2.4.4.1)
- 1 cascade of a scattering matrix with an open circuit matrix (as described in Section 4.1.3)

The other factor that needs to be considered for the numerical computations of the double outside cut right angle bend is the number of modes required for the mode matching. Depending on the values of W_{eff1}, $d1a$, $d1b$ and L_i a large number of modes may be required for each step discontinuity to satisfy the relative convergence ratio (equation (3.37)).

The overall numerical computations required for computing the scattering parameters of a double outside cut right angle bend is as described in Section 4.1.3 with the cost of $\Gamma_{in}^{(i)}$ adjusted as described above.

4.3.3 Mitered Right Angle Bend

A mitered right angle bend has a triangular portion of the bend removed in an attempt to reduce the effects of discontinuity reactances as shown in Figure 4.7.

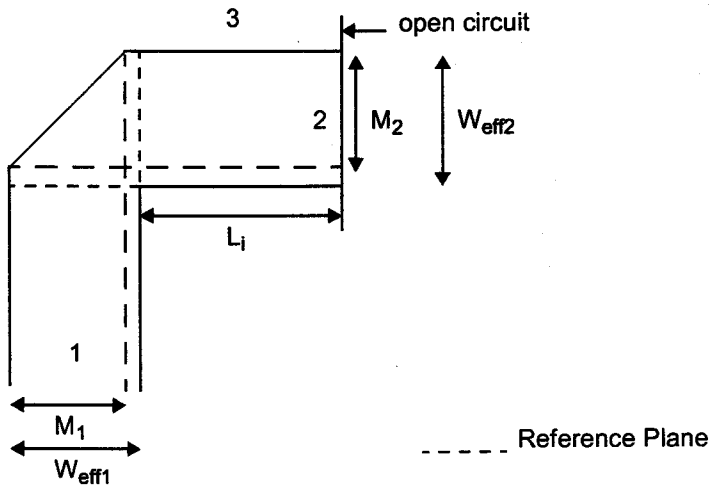

Figure 4.7. Mitered Right Angle Bend

To analyze the mitered right angle bend, the miter is approximated by a stair-case approximation as shown in Figure 4.8, that can be viewed as a number of step discontinuities and transmission lines. Another way to view the stair-case approximation of the miter is to consider it as an "n" outside cut right angle bend, where n represents the number of steps in the stair-case approximation of the miter.

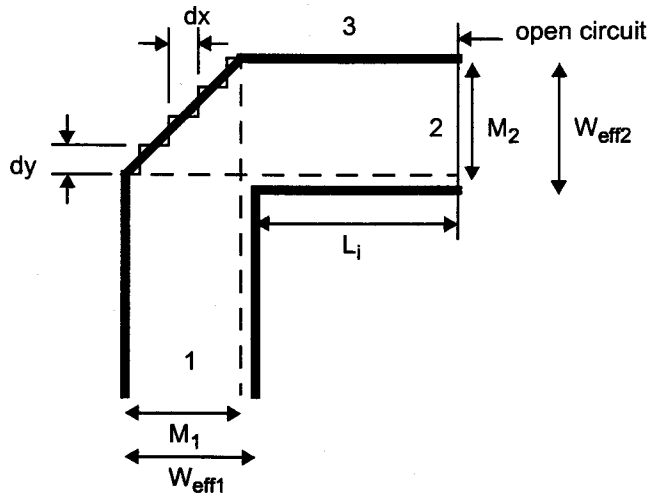

Figure 4.8. Mitered Right Angle Bend Analysis

The reflection coefficient $\Gamma_{in}^{(i)}$ is found by cascading the scattering matrices for the various step discontinuities and transmission lines with an open circuit at port 3 (a perfect magnetic wall), using ε_{eff2} as the effective dielectric constant for the transmission lines, in a similar fashion to the analysis of the double outside cut right bend. The difference in the height and width of the steps, dy and dx, respectively are

$$dy = \frac{M_2}{n} \quad \text{and} \quad dx = \frac{M_1}{n}. \tag{4.13}$$

The analysis of the mitered bend shown in Figure 4.8, which has $n = 4$, can be summarized by asymmetric step discontinuities followed by transmission lines as outlined in Table 4.1.

Table 4.1. Mitered Right Angle Bend Analysis

Step Discontinuity	Transmission Line Length
$W_{eff1} \rightarrow W_{eff1} + L_i$	$W_{eff2} - 4dy$
$W_{eff1} + L_i \rightarrow W_{eff1} + L_i - dx/2$	dy
$W_{eff1} + L_i - dx/2 \rightarrow W_{eff1} + L_i - 3dx/2$	dy
$W_{eff1} + L_i - 3dx/2 \rightarrow W_{eff1} + L_i - 5dx/2$	dy
$W_{eff1} + L_i - 5dx/2 \rightarrow W_{eff1} + L_i - 7dx/2$	dy

There are two other types of mitering compensation that can be applied to a right angle bend as shown in Figure 4.9. The mitering of a right angle bend can be classified by the value of M_1 and M_2, as Figure 4.7 shows $M_i < W_{effi}$, Figure 4.9 (a) shows $M_i = W_{effi}$, and Figure 4.9 (b) shows $M_i > W_{effi}$. Note the shift in reference planes for the mitered bend in Figure 4.9 (b).

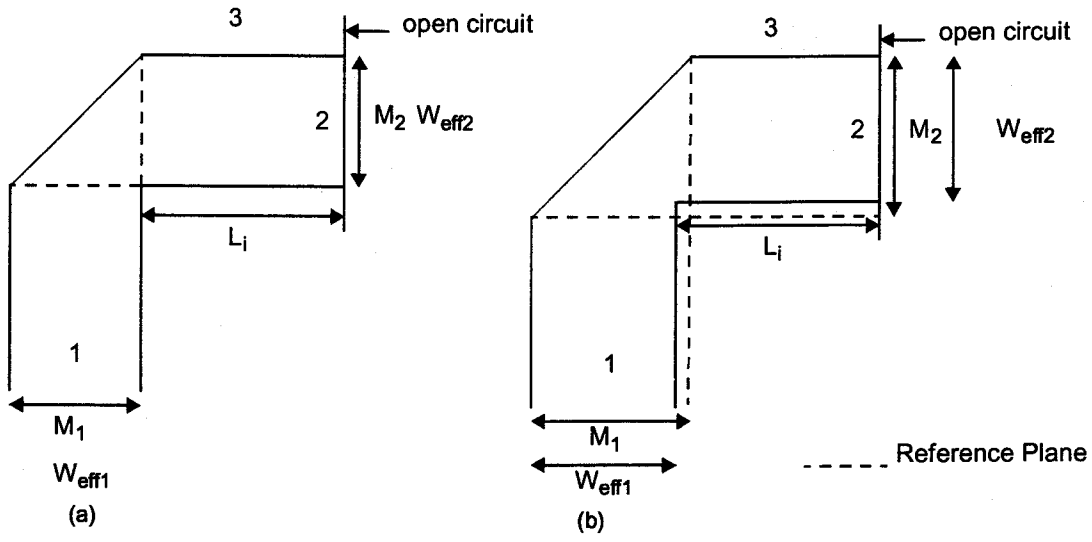

Figure 4.9. Alternative Mitered Right Angle Bends

These alternative mitered right angle bends are analyzed using the same approach as described above, using a stair-case approximation of step discontinuities and transmission lines.

4.3.3.1 Numerical Computations

The total number of numerical computations for finding the reflection coefficient $\Gamma_{in}^{(i)}$ for the mitered right angle bend shown in Figure 4.7 using the analysis method described above is:

- $n+1$ step discontinuities (as described in Section 3.5)
- $n+1$ transmission lines (as described in Section 2.4.3.1)
- $n+1$ cascades of a scattering matrix with a transmission line matrix (as described in Section 2.4.4.1)
- n cascades of scattering matrices (as described in Section 2.4.4.1)
- 1 cascade of a scattering matrix with an open circuit matrix (as described in Section 4.1.3)

A similar number of numerical computations is required for the alternative mitered right angle bends shown in Figure 4.9.

The other factor that needs to be considered for the numerical computations of the mitered right angle bend is the number of modes required for the mode matching. For the first step, W_{eff1} to $W_{eff1} + L_i$ a large number of modes may be needed to satisfy the relative convergence ratio (equation (3.37)). Since the remaining step discontinuities only differ in width by dx, the number of modes required for the mode matching will be relatively constant for all steps to satisfy the relative convergence ratio.

The overall numerical computations required for computing the scattering parameters of a mitered right angle bend is as described in Section 4.1.3 with the cost of $\Gamma_{in}^{(i)}$ adjusted as described above.

4.3.4 Curved Right Angle Bend

A curved right angle bend has a rounded contour in an attempt to reduce the effects of discontinuity reactances as shown in Figure 4.10. While the curved taper in Figure 4.10 is a quarter circle, the contour could be an arbitrarily curved shape. The analysis method for the curved right angle bend also uses a stair-case approximation, as the curved bend is segmented into a number of smaller steps using a constant value of dx and a variable value for dy.

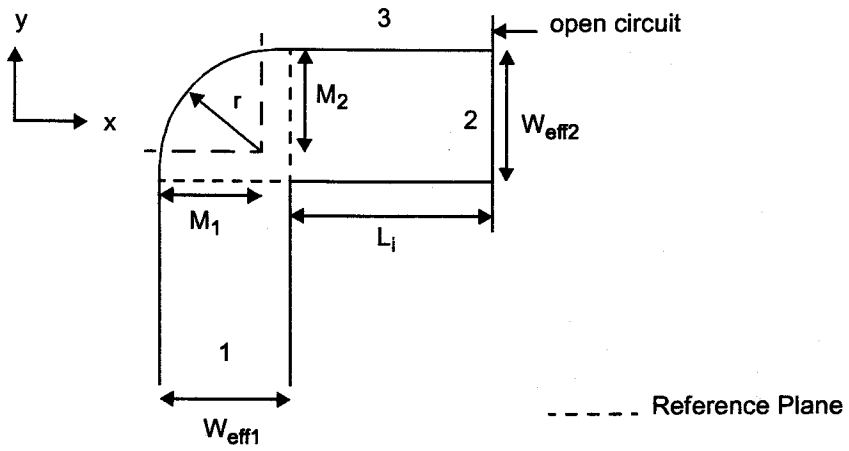

Figure 4.10. Curved Right Angle Bend

By representing the curvature as a function, such as $y = f(x)$ and using n steps of

$$dx = \frac{M_1}{n} \tag{4.14}$$

the curve can be approximated by n step discontinuities and $n-1$ transmission lines. Other than the first step, W_{eff1} to $W_{eff1} + L_i$, all of the step discontinuities vary by dx,

such as the step: $W_{eff1} + L_i$ to $W_{eff1} + L_i - dx$. The lengths of the transmission lines in the y direction are dependent on both dx and which step $i = 1 \ldots n$ where

$$dy_i = f(i \times dx) - f((i-1)dx). \tag{4.15}$$

As was the case for the mitered right angle bend, the value of M_1 and M_2 may be selected to be larger, equal or smaller than the width of the two microstrip lines.

4.3.4.1 Numerical Computations

By choosing to use step discontinuities that only vary by dx, the numerical computations for the curved right angle bend are the same as for the mitered right angle bend. The varying length of the transmission lines, dy_i, does not change the number of numerical computations.

4.4 Compensated Transmission Line T-junctions

In Section 4.2 the analysis of a transmission line T-junction that was not compensated in an attempt to reduce the effects of the reactances arising from the discontinuity was presented. This section describes some of the alternative structures and compensation methods for T-junctions, how they can be analyzed and their numerical computations. While these T-junctions can be used for both microstrip and rectangular waveguides, the diagrams in this section show rectangular waveguides.

For simplicity the widths for most of the transmission lines shown in this section are the same, however they do not need to be (ie. a_1 does not have to equal a_2 and a_3).

4.4.1 Alternative T-junction Structures

In Section 4.2.2 the T-junction that was presented had an asymmetric and an arbitrary step junction. Minor changes in the configuration of the placement of the three transmission lines forming the T-junction will require different analysis using the method described in this chapter. To characterize the geometry of the T-junction the additional parameters *top-edge* and *side-edge* are introduced as seen in Figure 4.11.

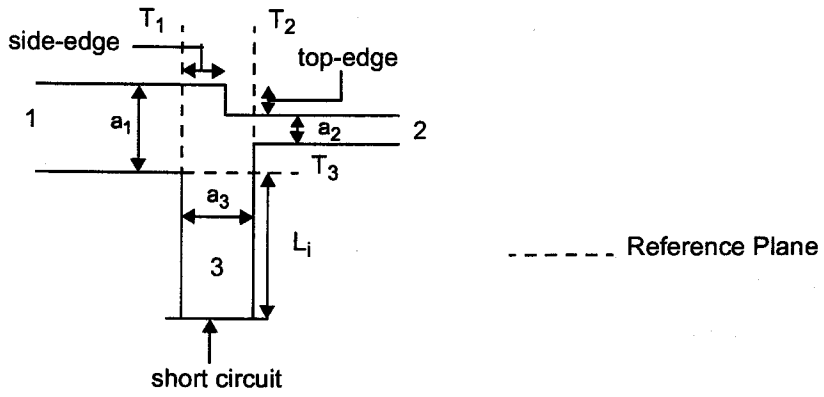

Figure 4.11. Alternative T-junction Structure

The analysis methods for a T-junction with line widths $a_1 > a_2$ as shown in Figure 4.11 depend on the value of the *side-edge* and *top-edge* parameters as follows:

- *top-edge* = 0:
  - analysis involves two asymmetric steps (a_1 to $a_1 + L_i$ and a_2 to $a_1 + L_i$) and a transmission line of length a_3
- *side-edge* = 0:
  - analysis involves an offset step that is described in Section 4.5.4 (a_1 to $a_1 + L_i$ with $e = (a_2 + L_i + \textit{top-edge} - a_1)/2$), an asymmetric step ($a_2$ to $a_1 + L_i$) and a transmission line of length a_3
- *side-edge* = a_3:
  - as described in Section 4.2.2, analysis involves an asymmetric step, an arbitrary step and a transmission line of length a_3
- $0 <$ *side-edge* $< a_3$:
  - analysis involves three asymmetric steps (a_1 to $a_1 + L_i$, a_2 to $a_1 + L_i - \textit{top-edge}$, and $a_1 + L_i - \textit{top-edge}$ to $a_1 + L_i$), and two transmission lines of length $a_3 - \textit{side-edge}$ and *side-edge*

Thus, minor changes in the positioning of the transmission lines forming the T-junction requires modifications to the discontinuity analysis method for the T-junction.

4.4.1.1 Numerical Computations

The numerical computations for the alternative T-junctions are basically the same as described in Section 4.2.4 with the following exceptions:

- the second case, *side-edge* = 0, uses an offset step whose computational requirements are described in Section 4.5.4.1

- the last case, $0 < side\text{-}edge < a_3$, requires an additional step and transmission line.

4.4.2 Shaped T-junction

A shaped T-junction has rectangular portions removed from lines 1 and 2, and rectangular portions added to line 3 in an attempt to reduce the effects of discontinuity reactances as shown in Figure 4.12. The rectangular portions removed from both lines 1 and 2 in this figure have dimensions nd by nw. However, the values removed from each of the two lines does not need to be the same which would likely be the case when the values of a_1 and a_2 are different. The rectangular portions added to line 3 have dimensions $(sw - a_3)/2$ by $sd - a_2 - nd$.

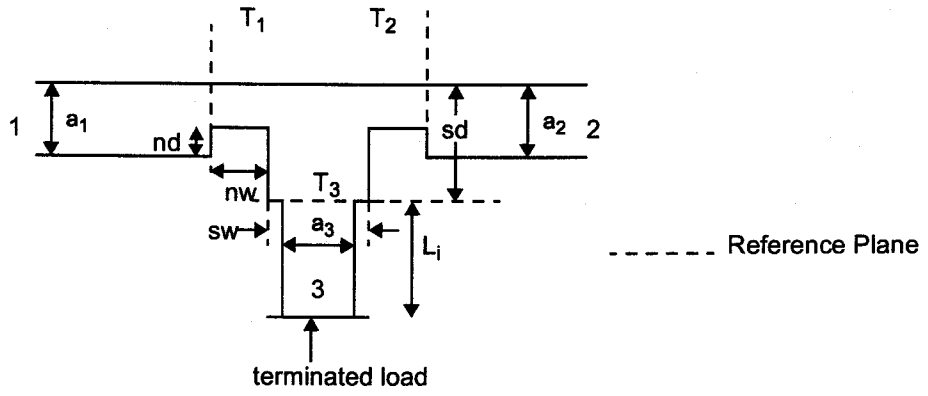

Figure 4.12. Shaped T-junction

The $[R^{(i)}]$ parameters are found by analyzing the structure from left to right as follows:

1. Computing the scattering matrices for an asymmetric step discontinuity from a transmission line of width a_1 to $a_1 - nd$.
2. The scattering matrix for a transmission line of length nw and width $a_1 - nd$ is computed and cascaded with the scattering matrices from the previous step.
3. Computing the scattering matrices for an asymmetric step discontinuity from a transmission line of width $a_1 - nd$ to sd.
4. The scattering matrix for a transmission line of length $(sw - a_3)/2$ and width sd is computed and cascaded with the scattering matrices from the previous step.
5. Computing the scattering matrices for an asymmetric step discontinuity from a transmission line of width sd to $sd + L_i$.
6. The scattering matrix for a transmission line of length a_3 and width $sd + L_i$ is computed and cascaded with the scattering matrices from the previous step.

7. The scattering matrices for the asymmetric step discontinuities on the right side of the structure are computed and cascaded with the transmission line matrices using the same approach described in the previous steps to analyze the left side of the structure. If the structure is symmetric the results from the first five steps can be reused. The resulting scattering matrices from the cascaded step discontinuities and transmission lines are than all cascaded together. The two-port scattering parameters $[R^{(i)}]$ are found by taking the principal mode from the resulting scattering matrices.

4.4.2.1 Numerical Computations

As described in the previous section, the total number of numerical computations for finding the $[R^{(i)}]$ parameters for the shaped T-junction is, in the worst case where the left and right sides of the structure are not symmetrical:

- 6 step discontinuities (as described in Section 3.5)
- 5 transmission lines (as described in Section 2.4.3.1)
- 5 cascades of a scattering matrix with a transmission line matrix (as described in Section 2.4.4.1)
- 5 cascades of scattering matrices (as described in Section 2.4.4.1)

The other factor that needs to be considered for the numerical computations of the shaped T-junction is the number of modes required for the mode matching. Depending on the values of a_1, a_2, nd, sd and L_i a large number of modes may be required for the step discontinuities to satisfy the relative convergence ratio (equation (3.37)).

The overall numerical computations required for computing the scattering parameters of a shaped T-junction is as described in Section 4.2.4 with the cost of $[R^{(i)}]$ adjusted as described above.

4.4.3 Square Notched T-junction

A square notched T-junction has a rectangular portion of transmission line removed in an attempt to reduce the effects of discontinuity reactances as shown in Figure 4.13. The rectangular portion removed has dimensions nd by nw. Usually $nw < a_3$ as is the case in this figure. When $nw > a_3$ then there are additional step discontinuities that need to be accounted for in the analysis.

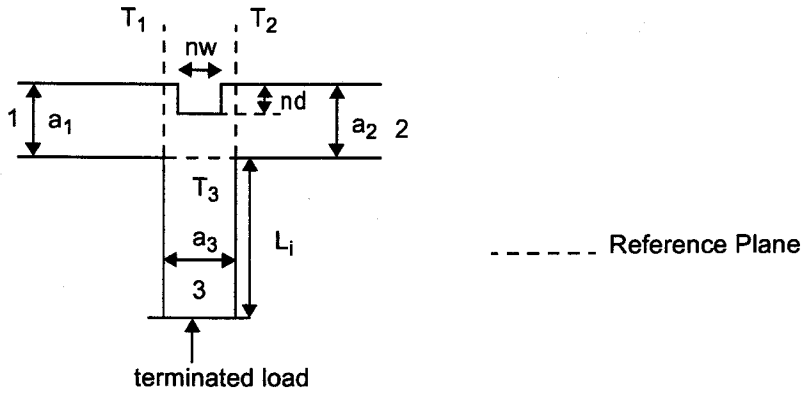

Figure 4.13. Square Notched T-junction

The $[R^{(i)}]$ parameters are found by analyzing the structure from left to right as follows:

1. Computing the scattering matrices for an asymmetric step discontinuity from a transmission line of width a_1 to $a_1 + L_i$.
2. The scattering matrix for a transmission line of length $(a_3 - nw)/2$ and width $a_1 + L_i$ is computed and cascaded with the scattering matrices from the previous step.
3. Computing the scattering matrices for an asymmetric step discontinuity from a transmission line of width $a_1 + L_i$ to $a_1 + L_i - nd$.
4. The scattering matrix for a transmission line of length nw and width $a_1 + L_i - nd$ is computed and cascaded with the scattering matrices from the previous step.
5. The scattering matrices for the asymmetric step discontinuities on the right side of the structure are computed and cascaded with transmission line matrices using the same approach described in the previous steps to analyze the left side of the structure. If the structure is symmetric the results from the first three steps can be reused. The resulting scattering matrices from the cascaded step discontinuities and transmission lines are than all cascaded together. The two-port scattering parameters $[R^{(i)}]$ are found by taking the principal mode from the resulting scattering matrices.

4.4.3.1 Numerical Computations

As described in the previous section, the total number of numerical computations for finding the $[R^{(i)}]$ parameters for the square notched T-junction is, in the worst case where the left and right sides of the structure are not symmetrical:

- 4 step discontinuities (as described in Section 3.5)
- 3 transmission lines (as described in Section 2.4.3.1)
- 3 cascades of a scattering matrix with a transmission line matrix (as described in Section 2.4.4.1)
- 3 cascades of scattering matrices (as described in Section 2.4.4.1)

The other factor that needs to be considered for the numerical computations of the square notched T-junction is the number of modes required for the mode matching. Depending on the values of a_1, a_2, nd and L_i a large number of modes may be required for the step discontinuities to satisfy the relative convergence ratio (equation (3.37)).

The overall numerical computations required for computing the scattering parameters of a square notched T-junction is as described in Section 4.2.4 with the cost of $[R^{(i)}]$ adjusted as described above.

4.4.4 Tapered Notch T-junction

A tapered notch T-junction has a triangular portion of transmission line removed in an attempt to reduce the effects of discontinuity reactances as shown in Figure 4.14. The triangular portion removed has height nd and width nw and the tip of the triangle is aligned with the center line of transmission line 3. However, the values removed from each of the two lines does not need to be the same which would likely be the case when the values of a_1 and a_2 are different.

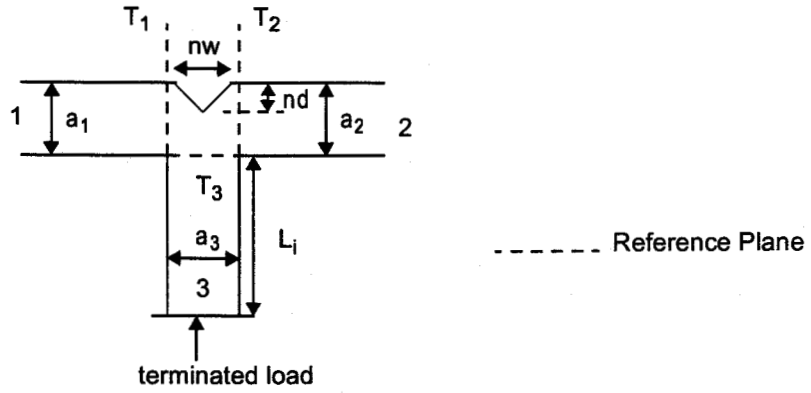

Figure 4.14. Tapered Notch T-junction

The triangular portion is analyzed using a stair-case approximation of n steps as shown in Figure 4.15, where the difference in the height and width of the steps, dy and dx, respectively are

$$dy = \frac{nw}{n} \quad \text{and} \quad dx = \frac{nd}{n}. \tag{4.16}$$

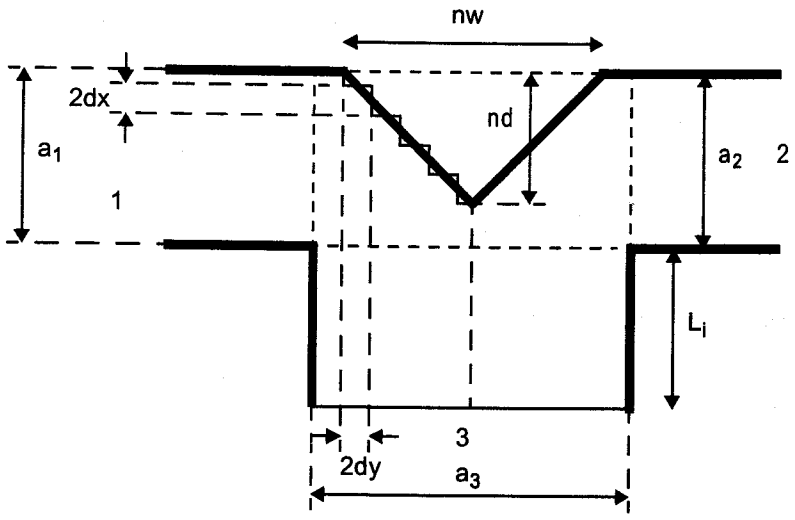

Figure 4.15. Tapered Notch T-junction Analysis

The analysis of the tapered notch T-junction shown in Figure 4.15, which has $n = 9$, can be summarized by step discontinuities followed by transmission lines as outlined in Table 4.2.

Table 4.2. Tapered Notch T-junction Analysis

Step Discontinuity	Transmission Line Length
$a_1 \rightarrow a_1 + L_i$	$(a_3 - nw)/2$
$a_1 + L_i \rightarrow a_1 + L_i - dx$	2dy
$a_1 + L_i - dx \rightarrow a_1 + L_i - 3dx$	2dy
$a_1 + L_i - 3dx \rightarrow a_1 + L_i - 5dx$	2dy
$a_1 + L_i - 5dx \rightarrow a_1 + L_i - 7dx$	2dy
$a_1 + L_i - 7dx \rightarrow a_1 + L_i - 9dx$	dy

This analysis is used to find the $[R^{(i)}]$ parameters for the left half of the T-junction, which is obtained by cascading each of the scattering matrices for the asymmetric step discontinuities with the scattering matrix of each of the transmission lines, and cascading all these resulting scattering matrices together. The same approach will be used to analysis the right half of the T-junction, unless the structures is symmetric in which case the results from the left side can be reused. The two-port scattering parameters $[R^{(i)}]$ are found by taking the principal mode from the resulting scattering matrices.

If the size of the removed triangular portion exceeds the dimensions a_3 by a_1 or a_2 then the reference planes will move and additional step discontinuities may be required to analysis the T-junction.

4.4.4.1 Numerical Computations

As described in the previous section, the total number of numerical computations for finding the $[R^{(i)}]$ parameters for the tapered notch T-junction is, in the worst case where the left and right sides of the structure are not symmetrical:

- $2((n+1)/2+1)$ step discontinuities (as described in Section 3.5)
- $2((n+1)/2+1)$ transmission lines (as described in Section 2.4.3.1)
- $2((n+1)/2+1)$ cascades of a scattering matrix with a transmission line matrix (as described in Section 2.4.4.1)
- $2(n+1)/2+1$ cascades of scattering matrices (as described in Section 2.4.4.1)

The other factor that needs to be considered for the numerical computations of the tapered notch T-junction is the number of modes required for the mode matching. Depending on the values of a_1, a_2, nd and L_i a large number of modes may be required for the step discontinuities to satisfy the relative convergence ratio (equation (3.37)).

The overall numerical computations required for computing the scattering parameters of a tapered notch T-junction is as described in Section 4.2.4 with the cost of $[R^{(i)}]$ adjusted as described above.

4.5 Compensated Transmission Line Step Junctions

In the previous chapter the mode matching analysis of three types of step junctions were presented: arbitrary, asymmetric and symmetric. None of these steps were compensated in an attempt to reduce the effects of the reactances arising from the discontinuity. This section describes some of the compensation methods for step junctions and the offset step, how they can be analyzed and their numerical computations. While these compensated steps can be used for both microstrip and rectangular waveguides, the diagrams in this section show rectangular waveguides.

4.5.1 Linear Taper Step

A linear taper symmetrical step has triangular portions of the step removed in an attempt to reduce the effects of discontinuity reactances as shown in Figure 4.16.

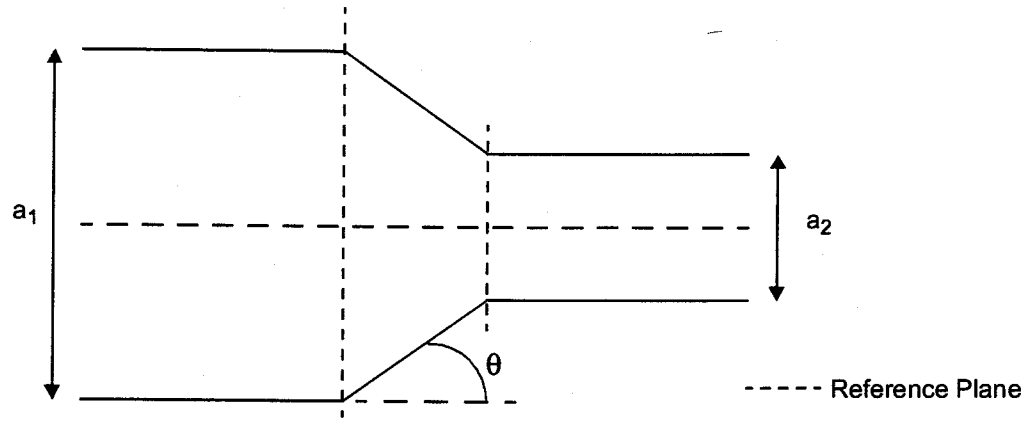

Figure 4.16. Linear Taper Step

If $\theta = 90°$ the uncompensated symmetric step is recovered. To analyze the linear taper step the triangular portion is approximated by a stair-case of step discontinuities with transmission lines as shown in Figure 4.17.

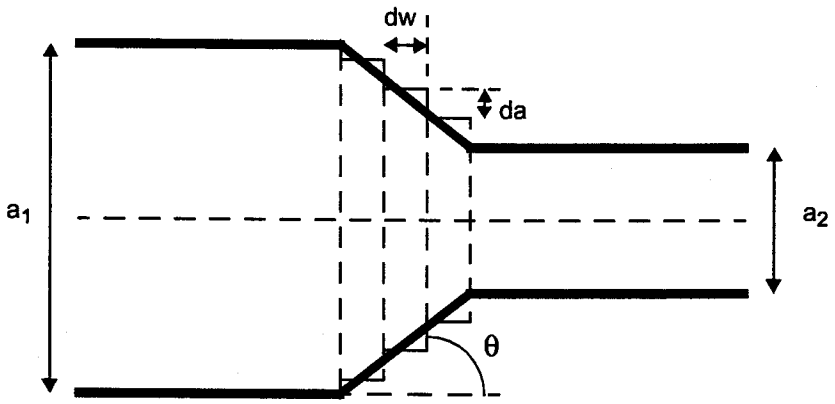

Figure 4.17. Linear Taper Step Analysis

The difference in the height and width of the steps, da and dw, respectively are

$$da = \frac{(a_1 - a_2)}{2n} \quad \text{and} \quad dw = \frac{nda}{(n-1)\tan\theta} \tag{4.17}$$

where n represents the number of steps in the stair-case approximation of the taper and for the step in Figure 4.17, $n = 4$. The scattering matrices for the linear taper step are found by cascading the scattering matrices for the various step discontinuities and transmission lines, moving from right to left, as outlined in Table 4.3.

Table 4.3. Linear Taper Step Analysis

Step Discontinuity	Transmission Line Length
$a_2 \rightarrow a_2 + 2da$	dw
$a_2 + 2da \rightarrow a_2 + 4da$	dw
$a_2 + 4da \rightarrow a_2 + 6da$	dw
$a_2 + 6da \rightarrow a_2 + 8da = a_1$	

4.5.1.1 Numerical Computations

In order to compute the overall scattering matrices for the linear taper step the total number of numerical computations required is:

- n step discontinuities (as described in Section 3.5)
- $n-1$ transmission line (as described in Section 2.4.3.1)
- $n-1$ cascades of a scattering matrix with a transmission line matrix (as described in Section 2.4.4.1)
- $n-1$ cascades of scattering matrices (as described in Section 2.4.4.1)

Since the step discontinuities only have a difference in the width of the transmission line of $2da$, the number of modes required for the mode matching will be relatively constant for all steps to satisfy the relative convergence ratio (equation (3.37)).

4.5.2 Partial Linear Taper Step

A partial linear taper symmetrical step is similar to the linear taper step with smaller triangular portions of the step removed as shown in Figure 4.18.

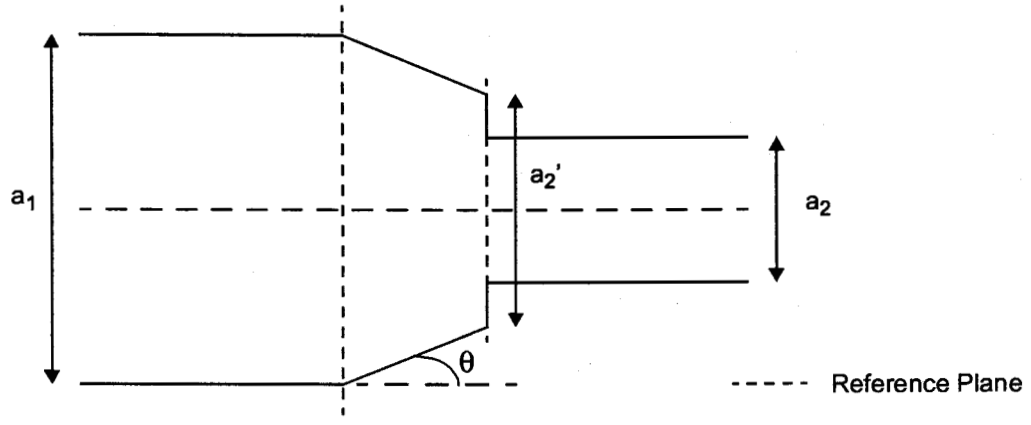

Figure 4.18. Partial Linear Taper Step

The analysis method for the partial linear taper step is the same as for the linear taper step in that it uses a stair-case approximation, with the first step discontinuity being a_2 to a_2'.

4.5.2.1 Numerical Computations

The numerical computations for the partial linear taper step are essentially the same as for the linear taper step. The only difference is that for the first step discontinuity additional modes may need to be used to satisfy the relative convergence ratio (equation (3.37)).

4.5.3 Curved Taper

A curved taper symmetrical step has a rounded contour to join the lines of width a_1 and a_2 in an attempt to reduce the effects of discontinuity reactances as shown in Figure 4.19. While the curved taper in Figure 4.19 is a quarter circle, the contour could be an arbitrarily curved shape.

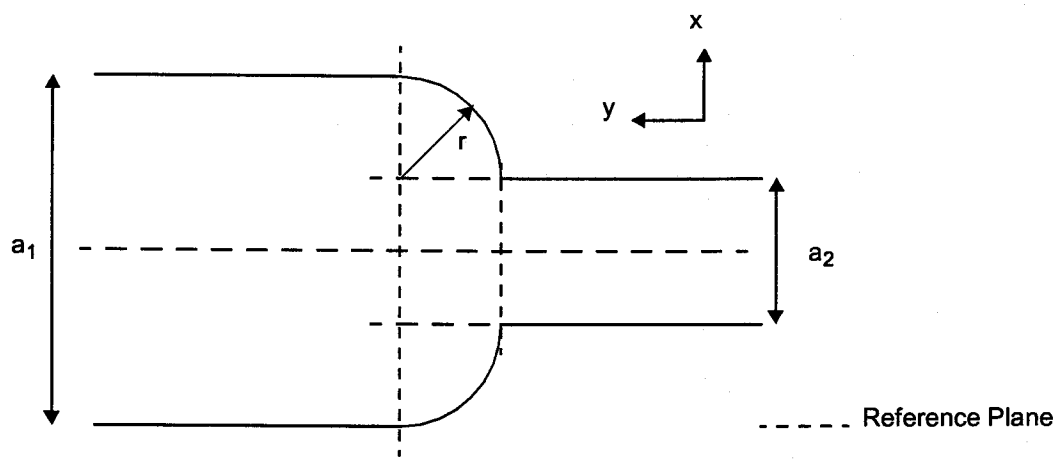

Figure 4.19. Curved Taper Step

The analysis method for the curved taper step also uses a stair-case approximation. By representing the curvature as a function, such as $y = f(x)$ and using n steps of

$$dx = \frac{a_1 - a_2}{2n} \tag{4.18}$$

the curve can be approximated by n step discontinuities and $n-1$ transmission lines. All of the step discontinuities vary by $2dx$, such as the first step from a_2 to $a_2 + 2dx$. The lengths of the transmission lines in the y direction are dependent on both dx and which step $i = 1 \ldots n$ where

$$dy_i = f(i \times dx) - f((i-1)dx). \tag{4.19}$$

4.5.3.1 Numerical Computations

By choosing to use step discontinuities that only vary in width by $2dx$ the numerical computations for the curved taper are the same as for the linear taper step. The varying length of the transmission lines, dy_i, does not change the numerical computations.

4.5.4 Offset Step

An offset step does not have one line completely overlapped by the other, and is characterized by the eccentricity (difference in the center of the lines), e, as shown in Figure 4.20. While it is not a compensated step, it has been included here to complete the characterization of step discontinuities and since it is required for one of the alternative T-junction structures described in Section 4.4.1.

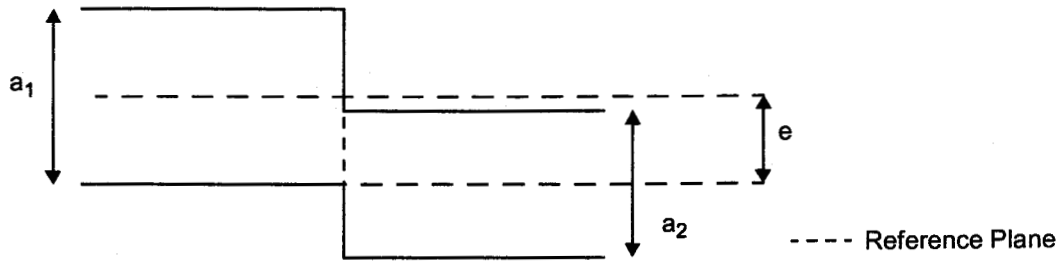

Figure 4.20. Offset Step

The offset step is analyzed by introducing an auxiliary structure of length dl and width

$$W = \frac{a_1}{2} + \frac{a_2}{2} + e \tag{4.20}$$

as shown in Figure 4.21.

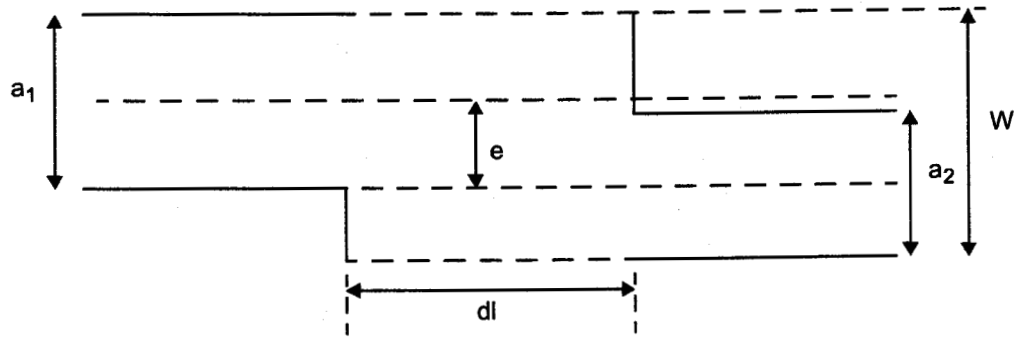

Figure 4.21. Offset Step Auxiliary Structure

The structure is analyzed from left to right as follows:

1. The scattering matrices for an asymmetric step discontinuity from a transmission line of width a_1 to W are computed.
2. The scattering matrix for a transmission line of length dl and width W is computed and cascaded with the scattering matrices from step 1. To recover the original structure dl approaches zero ($dl \rightarrow 0$) so the value of dl that is used is one hundredth of the guided wavelength for a transmission line of width W.
3. The scattering matrices for an asymmetric step discontinuity from a transmission line of width W to a_2 are computed and cascaded with the scattering matrices from step 2.

4.5.4.1 Numerical Computations

As described in the previous section, the total number of numerical computations for the offset step is:

- 2 step discontinuities (as described in Section 3.5)
- 1 transmission line (as described in Section 2.4.3.1)
- 1 cascade of a scattering matrix with a transmission line matrix (as described in Section 2.4.4.1)
- 1 cascade of scattering matrices (as described in Section 2.4.4.1)

The other factor that needs to be considered for the numerical computations of the offset step is the number of modes required for the mode matching. Depending on the transmission line widths and the eccentricity value, e, a large number of modes may be required for each step discontinuity to satisfy the relative convergence ratio (equation (3.37)).

4.6 Software Implementation

The objective of this thesis was to develop a set of routines that can be used as a foundation for a microwave CAD program that can provide an accurate solution, quickly and efficiently. The software was implemented in a manner to specifically meet this goal by using a modular approach with the programming language that has the best performance for scientific computing.

4.6.1 Modular Approach

In order to provide a versatile solution that would allow for code reuse, the program was written as a collection of routines. Even the core of the program was written as a subroutine so that it could be incorporated into a library such as SPICE [17, 45] or Dobrowolski's Jadmic2 microwave CAD program [20] which provides a graphical interface. By developing the program in a modular fashion a set of routines become available for future

microwave CAD programs. A modular approach was used instead of an object oriented approach for performance reasons described in the next section.

The specific routines developed for this thesis are:

- Bend: a set of routines to analyze right angle bends
- Constant: define constants used in the routines
- Coupling: a set of routines to compute the coupling matrix of a step discontinuity
- Main: a driver routine
- Math: a collection of mathematical array routines
- Planar: a set of routines for calculating properties of planar transmission lines
- Scas: a set of routines to cascade scattering matrices
- Step: a set of routines to analyze step junctions
- Tjunc: a set of routines to analyze T-junctions

Appendix C, "Sample Source Code" on page 122 contains some of the source code for some of these routines.

4.6.2 Programming Language

The programming language that was selected to implement these routines was Fortran because of its superior performance in scientific computing, particularly the handling of complex numbers and arrays. While Java, C++ and C are more popular, especially with the shift to an object oriented programming paradigm, they do not provide the performance for numerical processing [46, 47, 48, 49]. Advances in Java, C++ and C to improve performance are underway but they have not reached the speed of Fortran, which is the major reason why Fortran continues to be popular for scientific computing. There are also advances in Fortran as FORTRAN 77[1] has been replaced with Fortran 90 and now there is work underway for object oriented Fortran and High Performance Fortran (HPF) to further improve the performance and usability of Fortran 90 for computationally intensive applications [50].

Initially, the routines developed for this thesis were done using FORTRAN 77 but some of the features of Fortran 90 provided improved usability without sacrificing performance (for more information see Appendix D, "FORTRAN 77 versus Fortran 90 Performance Comparison" on page 129). Some of these new features are:

- The MODULE and USES constructs allows constants to be defined in one location and used throughout the program.
- The CASE construct allows for improved readability over IF-ELSE IF constructs that are based on the same expression.

1 Note that the correct spellings are "FORTRAN 77" and "Fortran 90."

- Dynamic memory allocation including allocatable arrays, which use the ALLOCATE and DEALLOCATE statements. Without allocatable arrays standard arrays have to be declared with bounds that are large enough to accommodate any situation, which usually results in declaring an array that is too large and wastes memory. This is an inefficient, error-prone way of using arrays [51].
- New predefined functions for processing matrices, including MATMUL (matrix multiplication) and TRANSPOSE.
- The source for Fortran 90 programs can be in a free-form style instead of the fixed-form layout required by FORTAN 77.

The specific compiler used to develop the program was the Microsoft Fortran PowerStation compiler (now the Digital Visual Fortran compiler), which runs on Windows 95 and supports the Fortran 90 standard. In order to further improve the performance of the program, the routines were compiled using compiler options to perform: full optimization, automatic inlining and code generation optimized for an Intel Pentium processor. The routines were written to adhere to the Fortran 90 standard so that they may be easily ported to other platforms.

4.7 Summary

In this chapter the discontinuity analysis method for right angle bends and T-junctions and the application of the method to rectangular waveguide H-plane and microstrip planar transmission lines are discussed in detail. The method is initially presented to describe the analysis of uncompensated right angle bends and T-junctions, and is extended to analyze compensated right angle bends, T-junctions and step junctions. Information about the numerical computations required to analyze each of the discontinuities is also provided. Finally, details about the software implementation of the discontinuity analysis method are presented.

Chapter 5. Results and Discussion

The previous chapters presented the mode matching method and the discontinuity analysis method, implemented as a set of software routines written in Fortran 90, to analyze rectangular waveguide H-plane and microstrip transmission line step junctions, right angle bends and T-junctions. In this chapter results from these methods are compared to published results. Comments on the numerical efficiency of the discontinuity analysis method are also presented.

5.1 Transmission Line Step Junctions

Since the mode matching method described in Chapter 3 is used extensively with the discontinuity analysis method described in Chapter 4, this section validates the mode matching method by comparing results for microstrip transmission line and rectangular waveguide H-plane uncompensated step junctions to published results. The behaviour of the relative convergence ratio is also presented.

5.1.1 Microstrip Step Junctions

The results obtained for an uncompensated symmetric step junction by using the mode matching method described in Section 3.3 are compared to the results presented in reference [12], which uses Green's Function and the segmentation and desegmentation methods. Figures 5.1 and 5.2 show the reflection coefficients (magnitude of S_{11}) for impedance ratios of $1:2$ and $1:\sqrt{2}$, respectively.

These figures show good agreement for the mode matching method. While it may appear that there is a large discrepancy for the reflection coefficient between the methods shown in Figure 5.1, the vertical scale on the graph has a range of only 0.06 and the largest difference between the results from reference [12] and the calculated results is only 0.008 or 2.33%. Since there is excellent agreement at low frequencies, one possible explanation for the difference between the results at higher frequencies is that dispersion may be handled differently in reference [12]. This would result in different effective dielectric constants and widths for the two methods, which are the parameters that define the step junction.

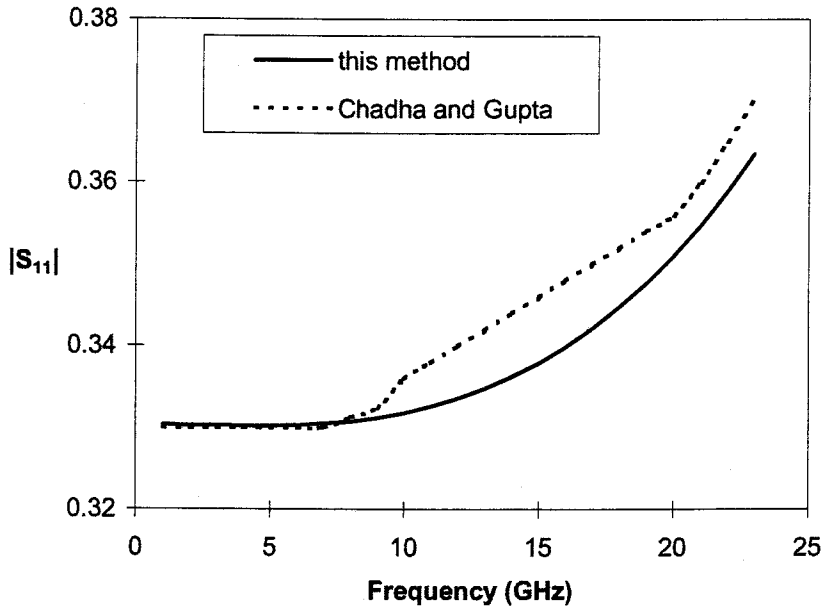

Figure 5.1. Green's Function (Chadha and Gupta [12]) and calculated S_{11} magnitude of a microstrip uncompensated symmetric step with ε_r=2.53, h=0.79mm, Z_1=35.35Ω and Z_2=70.71Ω

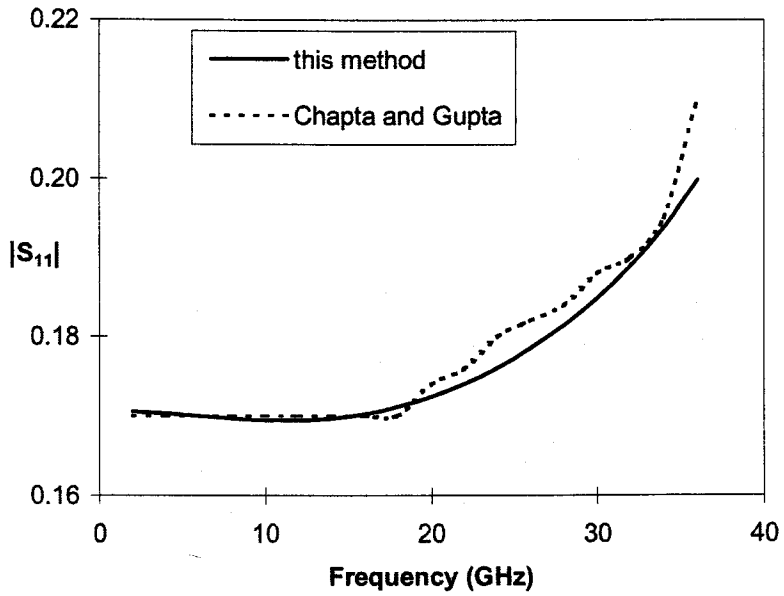

Figure 5.2. Green's Function (Chadha and Gupta [12]) and calculated S_{11} magnitude of a microstrip uncompensated symmetric step with ε_r=2.53, h=0.79mm, Z_1=42.09Ω and Z_2=59.46Ω

To further validate the mode matching method, results for another uncompensated symmetric step junction are compared to Kompa [52], as shown in Figure 5.3. Kompa uses the planar waveguide model with a method similar to the mode matching method which has been validated with the modified residue calculus technique in reference [36].

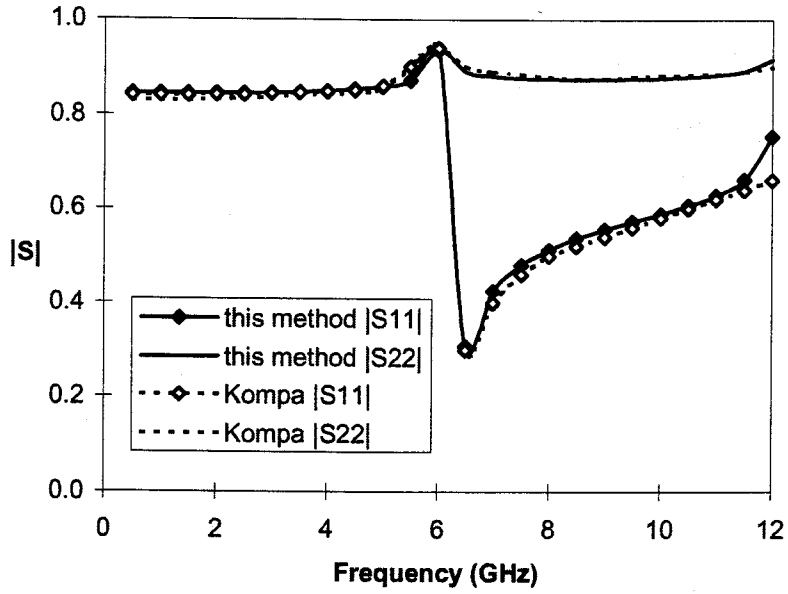

Figure 5.3. Kompa [52] and calculated S_{11} and S_{22} magnitude of a microstrip uncompensated symmetric step with ε_r=9.7, h=0.635mm, W_1=0.05cm and W_2=1.5cm

This figure shows excellent agreement for the mode matching method.

Additional comparisons for a microstrip uncompensated symmetric step were also done with the following references:

- [53], which uses the source method, which models the discontinuity using an equivalent circuit with current sources
- [54, 55 and 56], which all analyzed the same step geometry by using full-wave approaches: spectral domain, time-domain method of lines and time-domain finite difference, respectively
- [57], which uses a full-wave approach incorporating the method of lines with the source method

All comparisons were also found to be in good agreement and thus validates the accuracy of the mode matching method for microstrip step junctions.

5.1.2 Rectangular Waveguide H-plane Step Junctions

To validate the mode matching method for the rectangular waveguide H-plane step junctions described in Chapter 3, the susceptance of the dominant mode normalized with respect to the admittance of the larger guide (Y_1) of an uncompensated symmetric step junction is computed from

$$\frac{Y}{Y_1} = \frac{G+jB}{Y_1} = g+jb = \frac{1-S_{11}(1,1)}{1+S_{11}(1,1)}, \tag{5.1}$$

and compared to the asymptotic value of 7.7 from [35, 58, 59] for the equivalent circuit shown in Figure 5.4. Normalized susceptance is used to represent the step junction in the equivalent circuit since the narrow guide is below cutoff at the chosen frequency so the normalized input admittance from the larger guide is purely susceptance.

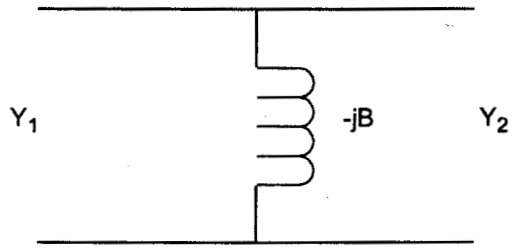

Figure 5.4. Equivalent circuit of a rectangular waveguide H-plane Step Junction

The calculated normalized susceptance for different number of modes on the two sides of the step junction are shown in Table 5.1 with $a_1/\lambda_g = 0.71$ and $a_2/a_1 = 1/3$.

Table 5.1. Normalized Susceptance of a Rectangular Waveguide H-plane Symmetric Step

N	M	b
10	4	7.678
20	7	7.731
30	10	7.746
40	14	7.738
50	17	7.741
60	20	7.743
10	10	7.599
20	20	7.687
30	30	7.711
40	40	7.720

These results compare within the specified 1% accuracy of the result determined in [58].

To further validate the mode matching method, results are compared in Figures 5.5 and 5.6 to reference [60], which uses an equivalent circuit to represent an uncompensated asymmetric step junction.

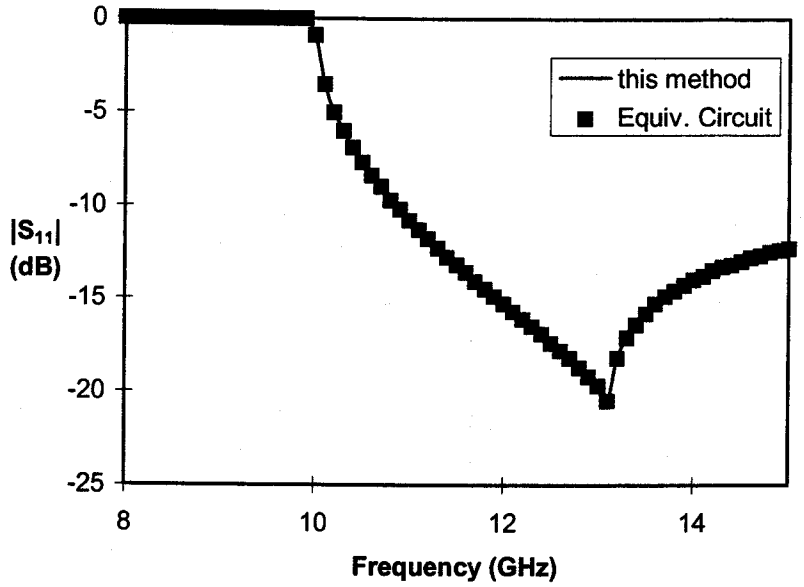

Figure 5.5. Equivalent Circuit [60] and calculated S_{11} magnitude of a rectangular waveguide uncompensated asymmetric step with a_1=22.86mm and a_2=15mm

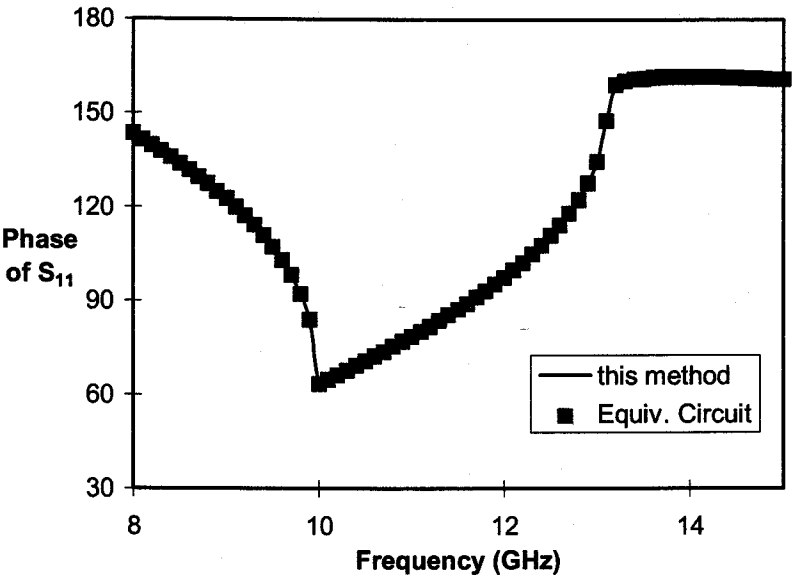

Figure 5.6. Equivalent Circuit [60] and calculated S_{11} phase in degrees of a rectangular waveguide uncompensated asymmetric step with a_1=22.86mm and a_2=15mm

It should be noted that the smaller waveguide (waveguide 2) is cutoff below 10 GHz, whereas above 13.1 GHz two modes can propagate in the larger waveguide (waveguide 1). Both the phase and magnitude are in excellent agreement with the referenced results. Thus validating the accuracy of the mode matching method for rectangular waveguide H-plane step junctions.

5.1.3 Relative Convergence

To validate the relative convergence ratio defined in equation (3.37), the normalized susceptance for the rectangular waveguide H-plane uncompensated symmetric step junction described in the previous section was computed for various values of M and N [35]. In Figure 5.7 the susceptance normalized with respect to the admittance of the larger guide is plotted versus N for the fixed ratios $M/N = 1/3, 1/2, 3/3$.

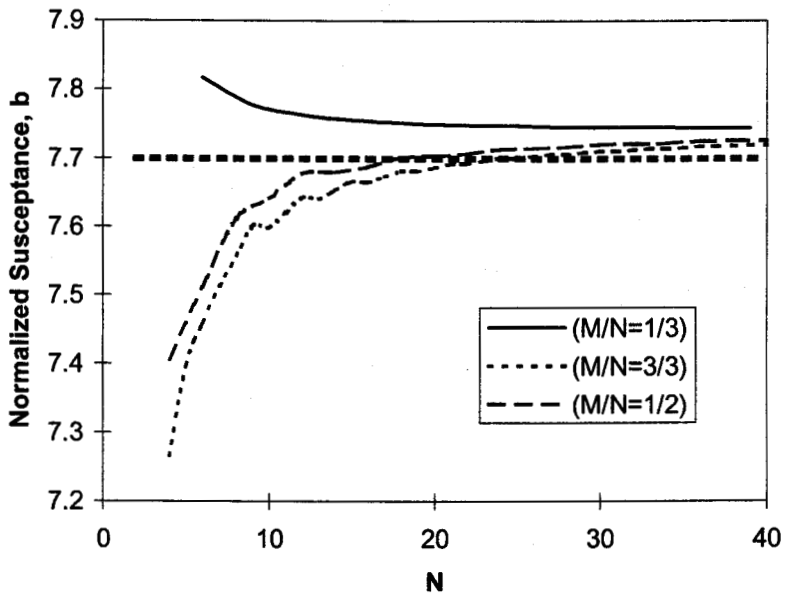

Figure 5.7. Convergence study of TE_{10} mode normalized susceptance of a rectangular waveguide H-plane uncompensated symmetric step discontinuity with fixed M/N

While all three curves converge within 1% of the asymptotic 7.7 value, the curve $M/N = a_2/a_1 = 1/3$ reaches the asymptotic value most rapidly.

In Figure 5.8 the normalized susceptance, b, is calculated with a fixed N and varying M.

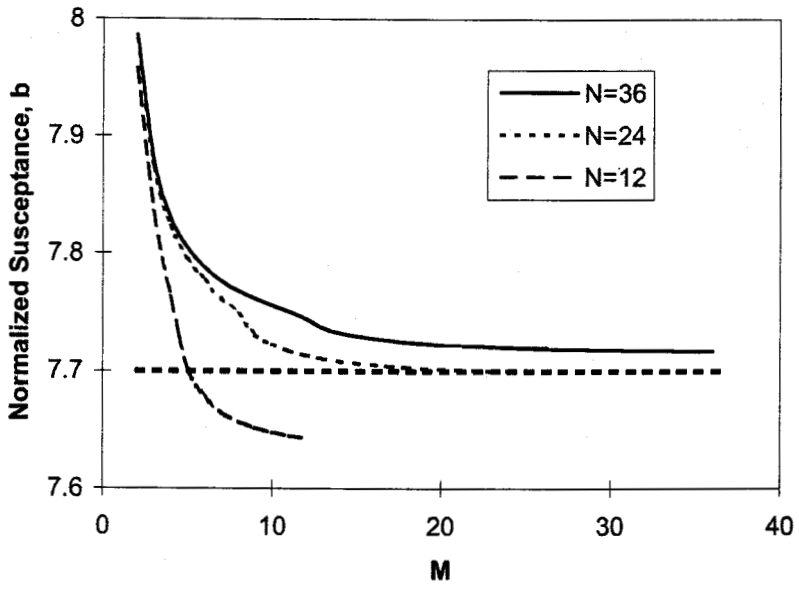

Figure 5.8. Convergence study of TE_{10} mode normalized susceptance of a rectangular waveguide H-plane uncompensated symmetric step discontinuity with fixed N

It is noticed that the normalized susceptance converges to a value other than the asymptotic value, however the error is not large and is within the 1% accuracy. This indicates that as long as M and N are large, the M/N ratio does not significantly affect the solution accuracy. However, for efficient numerical computations one should keep the relative convergence ratio, $M/N = a_2/a_1$.

5.1.4 Summary

The preceding sections validate the accuracy of the mode matching method for rectangular waveguide H-plane and microstrip step junctions and validate the relative convergence ratio. The remaining sections of the chapter compare the discontinuity analysis method described in the previous chapter, which extensively uses the mode matching method, to published results for right angle bends and T-junctions.

5.2 Transmission Line Right Angle Bends

The discontinuity analysis method described in Section 4.1 details how a two-port transmission line uncompensated right angle bend can be analyzed with three one-port networks. This section validates the method by comparing results for microstrip and rectangular waveguide H-plane uncompensated right angle bends to published results.

5.2.1 Microstrip Right Angle Bends

The results obtained by using the method described in Section 4.1.1 were compared to the results presented in reference [12], which uses Green's Function and the segmentation and desegmentation methods. The length of the transmission line connected between port 2 and the open circuit, L_i is

$$L_i = i\lambda_g \qquad i = 1, 2, 3 \tag{5.2}$$

where λ_g is the guided wavelength of the principal mode. Figure 5.9 shows the results for a microstrip uncompensated right angle bend.

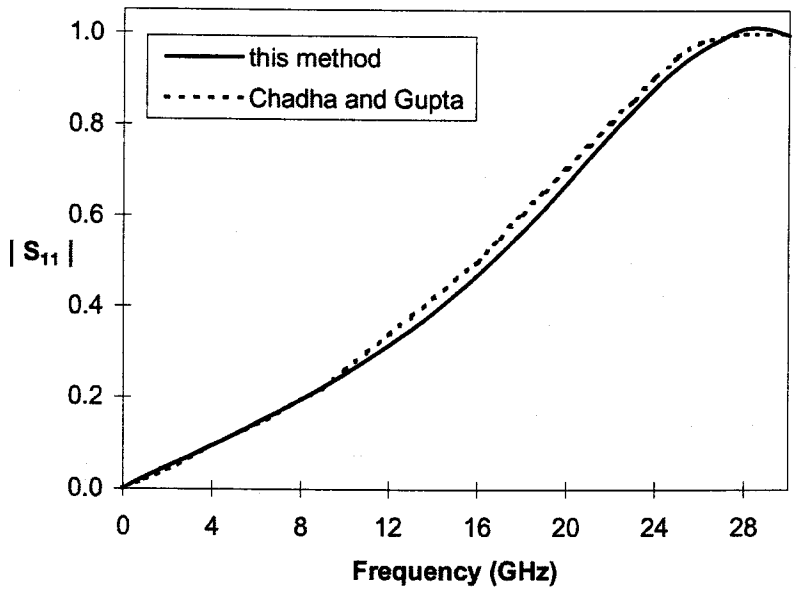

Figure 5.9. Green's Function (Chadha and Gupta [12]) and calculated S_{11} magnitude of a microstrip uncompensated right angle bend with ε_r=2.53, h=0.65mm and Z_1=Z_2=50Ω

The results for the microstrip uncompensated right angle bend show excellent agreement with reference [12] over the frequency range 0-30 GHz. The results are also in agreement with reference [11], which uses the boundary integral method to analyze the same bend.

To further validate the discontinuity analysis method, results for another uncompensated right angle bend are compared to reference [61], which uses the full-wave FDTD method, as shown in Figure 5.10.

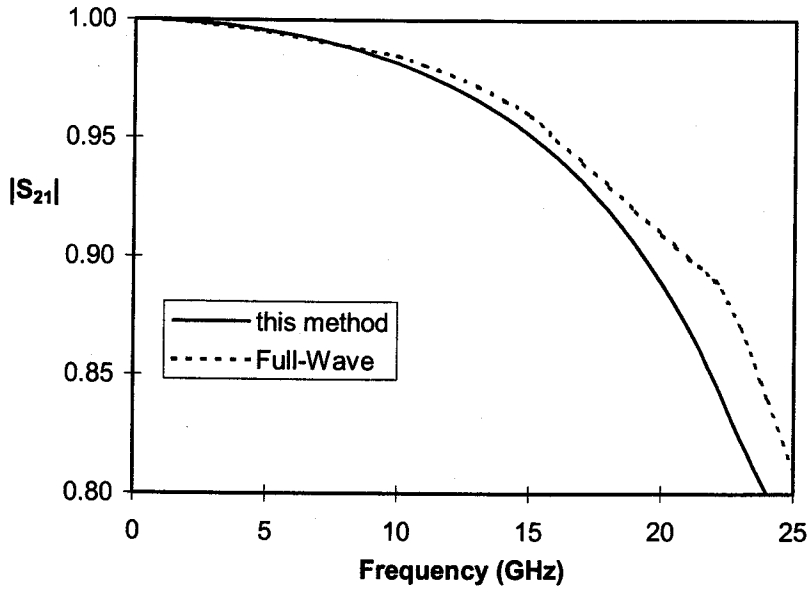

Figure 5.10. Full-wave FDTD [61] and calculated S_{21} magnitude of a microstrip uncompensated right angle bend with ε_r=2.33, h=0.51mm and W_1=W_2=1.53mm

The results for the microstrip uncompensated right angle bend show good agreement. Again, the discrepancy at higher frequencies could be due to different dispersion models for the two methods, as explained in Section 5.1.1. Reference [61] also reports that it takes 235 CPU seconds to compute the transmission coefficient on a Cray YMP supercomputer, which is capable of sustaining 1 billion float point operations per second (1 giga-flops). For the discontinuity analysis routines developed in this thesis it took approximately 8 seconds to calculate on a Pentium 166 MHz. This shows a very significant savings in computation time using the discontinuity analysis method over the full-wave FDTD approach since the Cray computer is at least six times faster than the Pentium and it took 39 times longer to compute the results (for more details see Appendix E).

Additional comparisons were also done with the following references:

- [62], which uses the full-wave method of moments
- [63], which uses the full-wave spatial domain moment method
- [64], which uses a full-wave involving the mixed potential integral equation

All comparisons were also found to be in relatively good agreement and thus validates the accuracy of the mode matching method for microstrip uncompensated right angle bends. Some other published results were examined but since the accuracy of the results was not established (they were not compared to other methods or experimental measurements), they have not been referenced.

5.2.2 Rectangular Waveguide H-plane Right Angle Bends

The results obtained by using the method described in Section 4.1.2 were compared to the results presented in reference [65], which uses the boundary element method (BEM) for an uncompensated rectangular waveguide H-plane right angle bend, as seen in Figure 5.11. The length of the transmission line connected between port 2 and the short circuit, L_i is

$$L_i = \frac{i\lambda_g}{3} \qquad i = 1, 2, 3 \tag{5.3}$$

where λ_g is the guided wavelength of the principal mode.

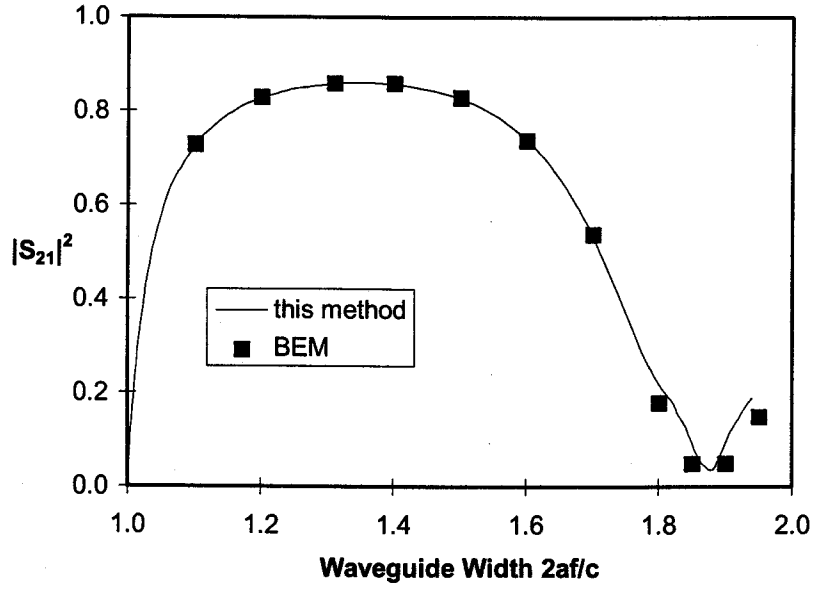

Figure 5.11. BEM [65] and calculated S_{21} parameter of a rectangular waveguide H-plane uncompensated right angle bend

Note that the waveguide width, $2af/c$, is used for the dependent axis of the graph since it is more general to plot the graph using this than a specific frequency and waveguide width. The results for the rectangular waveguide H-plane uncompensated right angle bend show excellent agreement with reference [65].

The results obtained by using the discontinuity analysis method were also compared to the results presented in reference [66], which uses Green's Theorem and presents data from Marcuvitz [58], which uses empirical equations, for an uncompensated rectangular waveguide H-plane right angle bend, as seen in Figures 5.12 and 5.13.

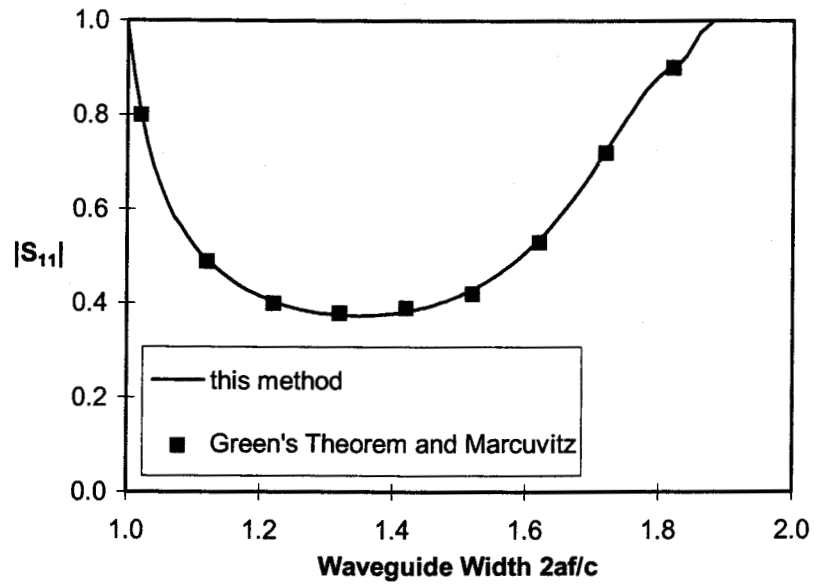

Figure 5.12. Green's Theorem [66] and Marcuvitz [58] (black squares) and calculated S_{11} magnitude of a rectangular waveguide H-plane uncompensated right angle bend

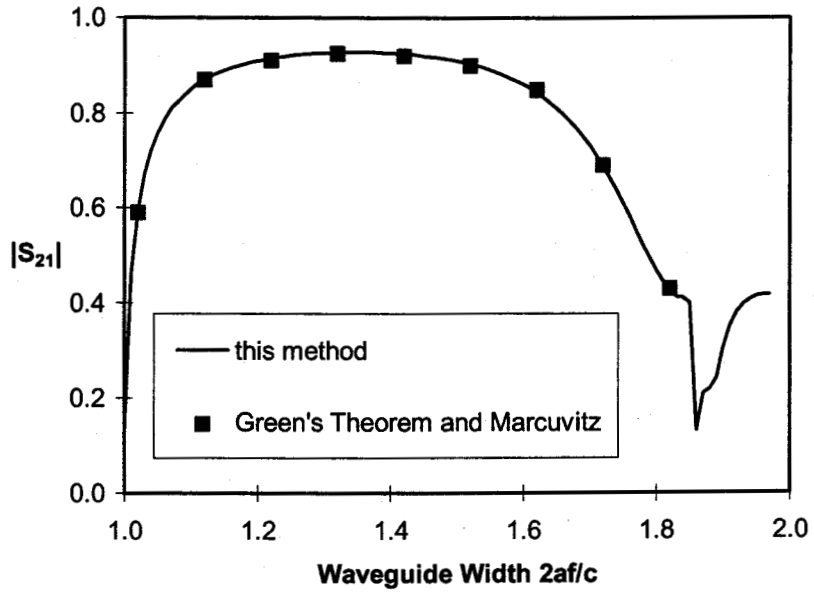

Figure 5.13. Green's Theorem [66] and Marcuvitz [58] (black squares) and calculated S_{21} magnitude of a rectangular waveguide H-plane uncompensated right angle bend

The results for the rectangular waveguide H-plane uncompensated right angle bend show excellent agreement with both references [58 and 66].

5.2.3 Summary

The analysis of microstrip and rectangular waveguide H-plane uncompensated right angle bends using the discontinuity analysis method described in this thesis has been presented. The results show good agreement with previously published results. The discrepancy between the results for microstrip at higher frequencies is likely due to dispersion since the rectangular waveguide results did not exhibit the discrepancy at higher frequencies. The CPU savings for the discontinuity analysis are very significant in comparison with the full-wave FDTD approach.

5.3 Transmission Line T-junctions

The discontinuity analysis method described in Section 4.2 details how a three-port transmission line uncompensated T-junction can be analyzed with three two-port networks. This section validates the method by comparing results for rectangular waveguide H-plane and microstrip uncompensated T-junctions to published results.

5.3.1 Microstrip T-junctions

Results from discontinuity analysis method described in Section 4.2.2 are compared with previously published results to validate the accuracy of the method. The length of the transmission line connected between port 3 and the open circuit, L_i is

$$L_i = \frac{i\lambda_g}{3} \qquad i = 1, 2, 3. \tag{5.4}$$

The reference plane is chosen to be the wider lines of transmission lines 1 and 2 (see Figure 2.7 on page 19).

Figure 5.14 to Figure 5.17 show the comparison of some of the scattering parameters calculated by this method and the results of measurement taken from reference [67]. All the results are given in the form of absolute values and phases, for a T-junction with $top\text{-}edge = 0$, as defined in Figure 4.11 on page 52.

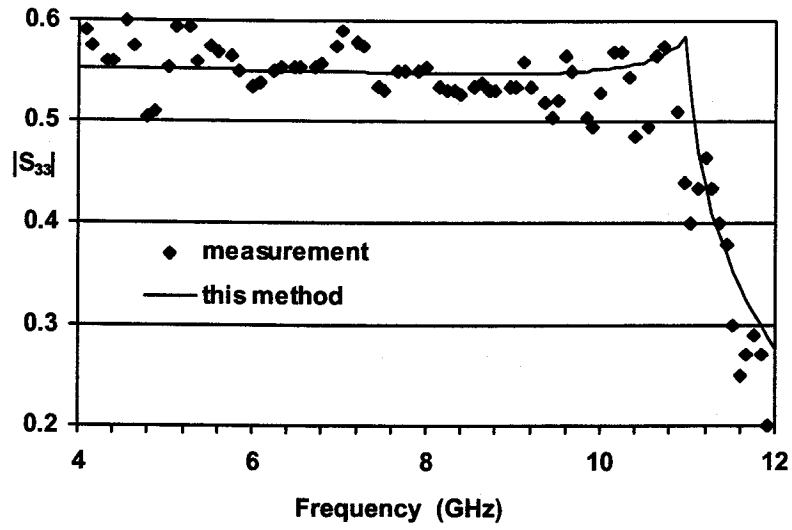

Figure 5.14. Measured [67] and calculated S_{33} magnitude of a microstrip T-junction with Z_1=20Ω, Z_2=Z_3=50Ω, h=0.8mm and ε_r=2.32

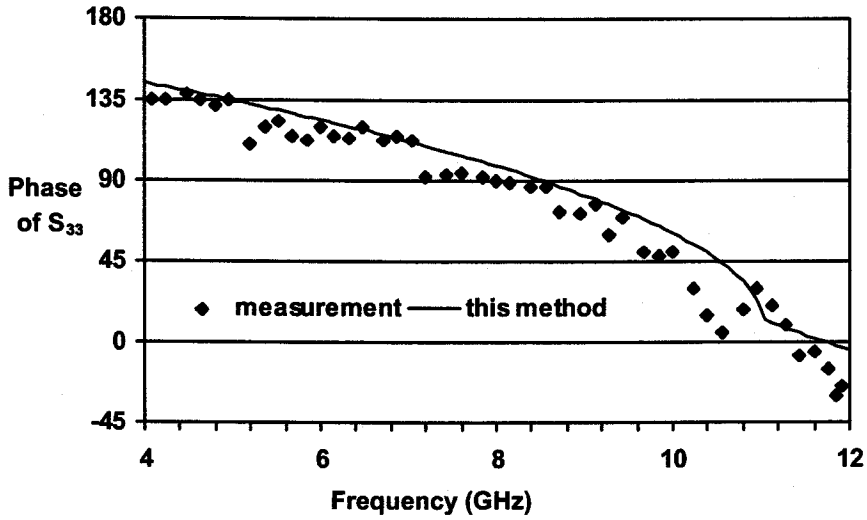

Figure 5.15. Measured [67] and calculated S_{33} phase in degrees of a microstrip T-junction with Z_1=20Ω, Z_2=Z_3=50Ω, h=0.8mm and ε_r=2.32

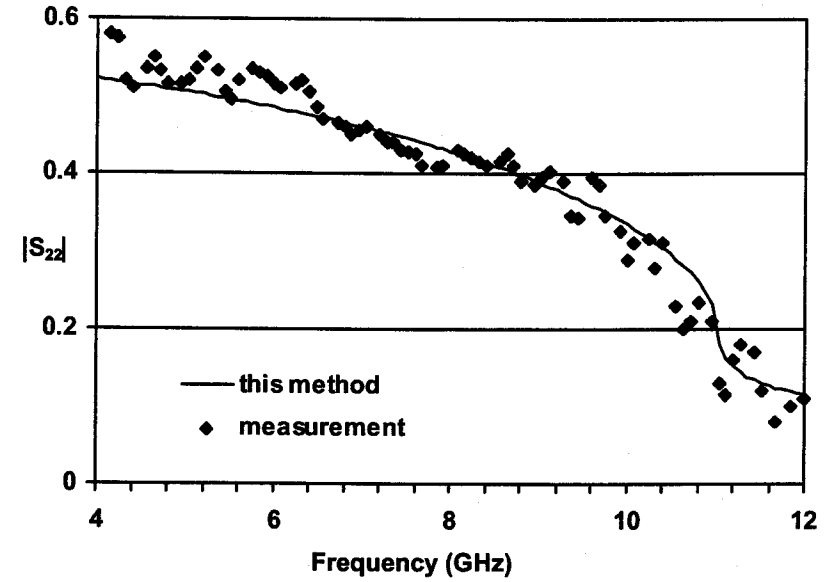

Figure 5.16. Measured [67] and calculated S_{22} magnitude of a microstrip T-junction with Z_1=20Ω, Z_2=Z_3=50Ω, h=0.8mm and ε_r=2.32

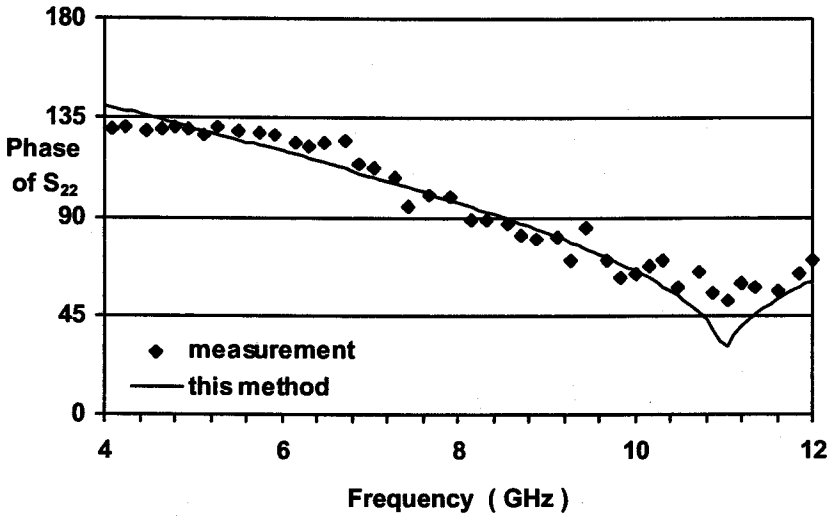

Figure 5.17. Measured [67] and calculated S_{22} phase in degrees of a microstrip T-junction with Z_1=20Ω, Z_2=Z_3=50Ω, h=0.8mm and ε_r=2.32

It can be seen that the agreement is excellent except when the frequency is near the cutoff frequencies, where the radiated power becomes large. Usually, in this frequency range, the first higher order mode will emerge and so this frequency region is not of great interest for practical applications.

Figure 5.18 shows the comparison of some of the scattering parameters calculated by this method and the calculated full-wave results taken from reference [68].

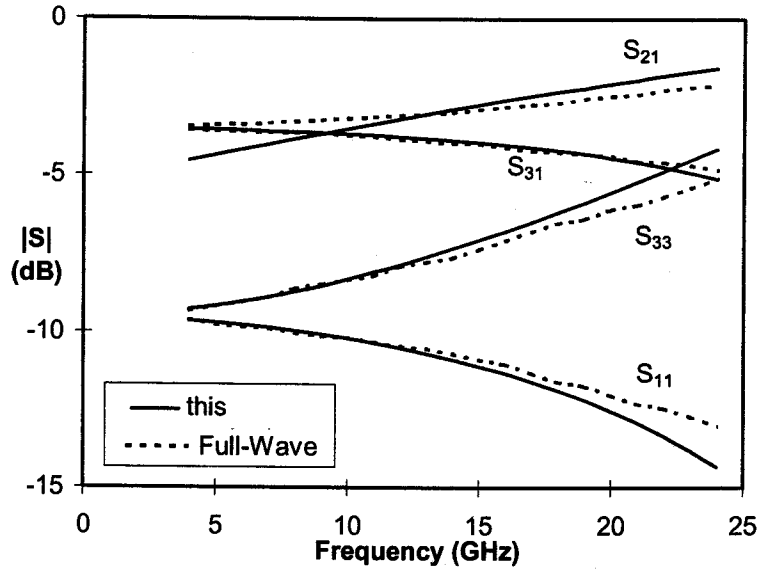

Figure 5.18. Full-wave [68] and calculated S-parameters of a microstrip T-junction with $Z_1=Z_2=Z_3=20\Omega$, h=0.635mm and $\varepsilon_r=9.9$

It can be seen that the results are in excellent agreement.

Figure 5.19 to Figure 5.21 show some of the scattering parameters for symmetrical and asymmetrical microstrip T-junctions calculated by this method. These figures show the affect of varying the impedance of transmission line 1 (Z_1) from 50Ω to 40Ω to 30Ω with $top\text{-}edge = 0$, as defined in Figure 4.11 on page 52.

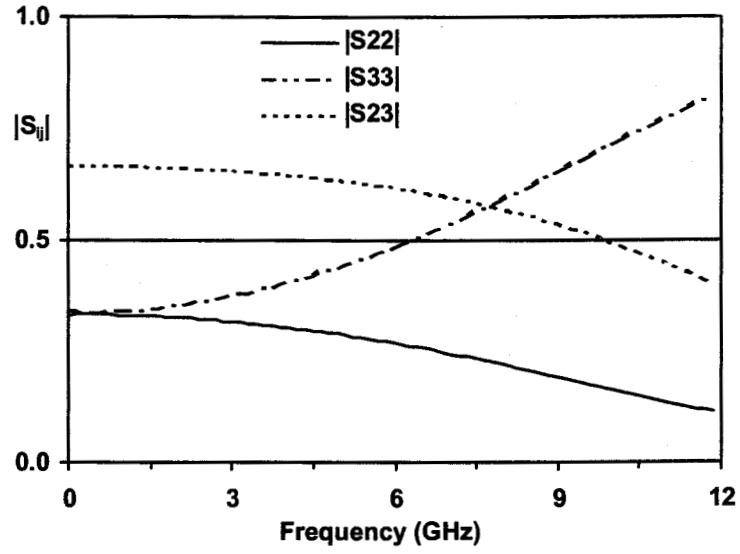

Figure 5.19. Calculated S-parameters of a microstrip T-junction with $Z_1=Z_2=Z_3=50\Omega$, h=1.58mm and $\varepsilon_r=2.32$

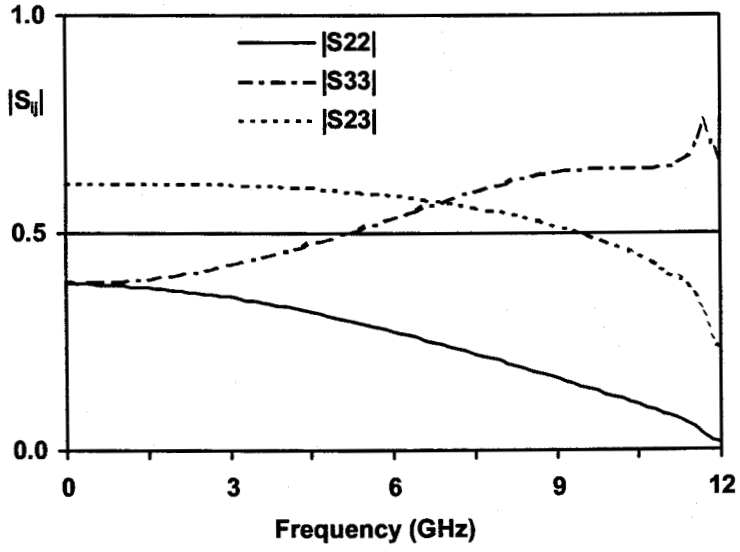

Figure 5.20. Calculated S-parameters of a microstrip T-junction with $Z_1=40\Omega$, $Z_2=Z_3=50\Omega$, h=1.58mm and $\varepsilon_r=2.32$

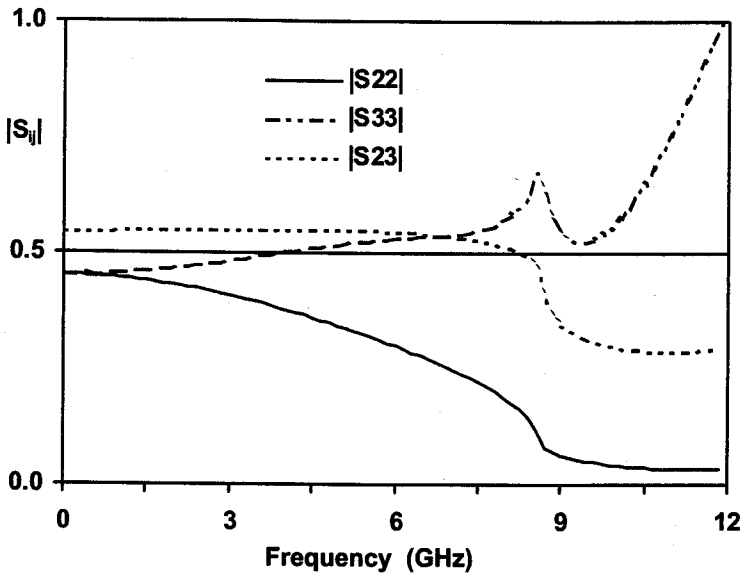

Figure 5.21. Calculated S-parameters of a microstrip T-junction with Z_1=30Ω, Z_2=Z_3=50Ω, h=1.58mm and ε_r=2.32

It is interesting to note that as the impedance of transmission line 1 decreases the magnitude of S_{22} and S_{23} decrease and local maximums are observed with S_{33}.

5.3.2 Rectangular Waveguide H-plane T-junctions

Results from discontinuity analysis method described in Section 4.2.3 are compared with previous published results to validate the accuracy of the method. The length of the transmission line connected between port 3 and the short circuit, L_i is

$$L_i = \frac{i\lambda_g}{3} \qquad i = 1, 2, 3. \tag{5.5}$$

The reference plane is chosen to be the wider lines of transmission lines 1 and 2 (see Figure 2.7 on page 19).

Figure 5.22 shows the comparison of some of the scattering parameters calculated by this method and the results of measurement taken from reference [69], which uses a variation of the mode matching method. A symmetric rectangular waveguide T-junction has the same dimensions for all three waveguides.

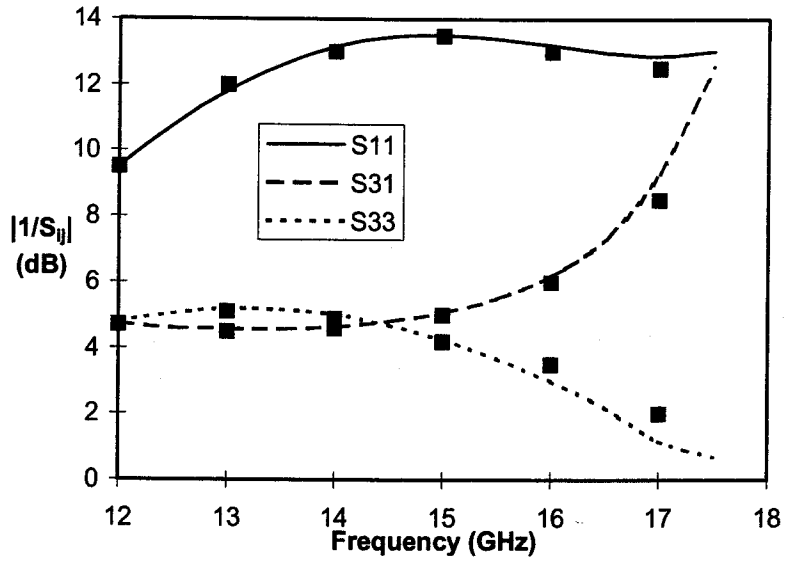

Figure 5.22. Measured (black squares) [69] and calculated S_{11}, S_{31} and S_{33} magnitude of a symmetric rectangular waveguide H-plane T-junction with a=15.799mm and b=7.889mm

The results for the rectangular waveguide H-plane symmetric T-junction show good agreement.

Figure 5.23 shows the comparison of the scattering parameters S_{11} and S_{23} calculated by this method and the results of measurement and analysis taken from reference [70], which in addition to having measured results has results for FDTD and FEM approaches. Results for the same discontinuity analyzed using BEM were published in reference [65].

The results for the rectangular waveguide H-plane symmetric T-junction show good agreement with both sets of published results [65 and 70]. Reference [70] also reports that it takes 120 CPU seconds to compute the scattering parameters for a single frequency on a IBM 6000/520. For the discontinuity analysis routines it took approximately 3 seconds to calculate the scattering parameters for the 20 frequencies shown in Figure 5.23 on a Pentium 166 MHz. Using a normalization factor of 18, as described in Appendix E, to account for the difference in the computers the discontinuity analysis method is still faster than the full-wave FDTD approach ($3/20 = 0.15$ seconds versus $120/18 \approx 6.5$ seconds). Further information on the numerical efficiency of the discontinuity analysis method is presented in Section 5.5.

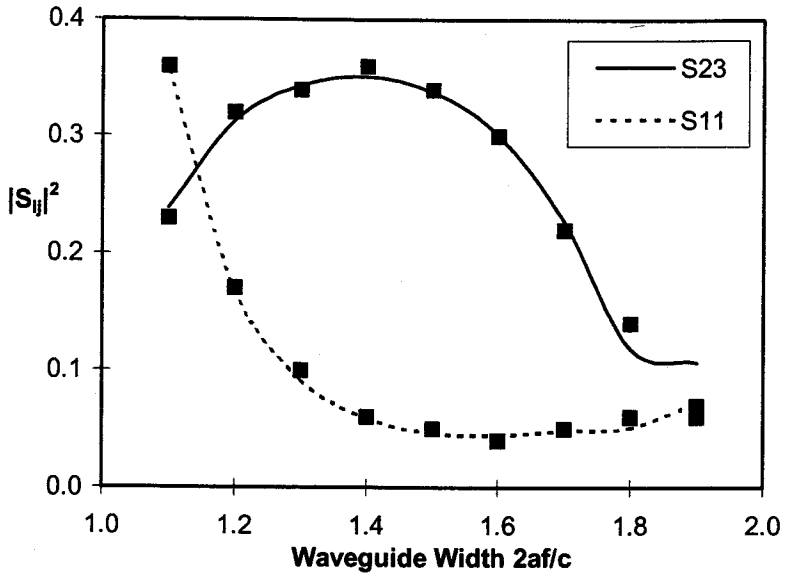

Figure 5.23. Measured (black squares) [70] and calculated S_{11} and S_{23} magnitude of a symmetric rectangular waveguide H-plane T-junction with a=22.86mm and b=10.16mm

During the literature search for published results it was discovered that the discontinuity analysis method described in this thesis has also been successfully used by Liang and Zaki [41] to analyze rectangular waveguide E-plane and H-plane uncompensated T-junctions.

5.3.3 Summary

The analysis of microstrip and rectangular waveguide H-plane uncompensated T-junctions using the discontinuity analysis method described in this thesis has been presented. The results show good agreement with previously published results. The discontinuity analysis method is also quicker to compute the scattering parameters than the full-wave FDTD approach.

5.4 Compensated Transmission Line Discontinuities

While the compensated bends, T-junctions and steps shown in Chapter 4 are referenced in literature, published results are not available for many of these compensated discontinuities, particularly for waveguide discontinuities. This section will compare results from the discontinuity analysis method described in this thesis to some of the available published results for compensated discontinuities.

5.4.1 Microstrip Offset Step

The results computed by the proposed method described in Section 4.5.4 are compared with published results to check the accuracy of the method. Figure 5.24 shows the comparison of the transmission coefficient calculated by this method and the results of measurement taken from reference [71].

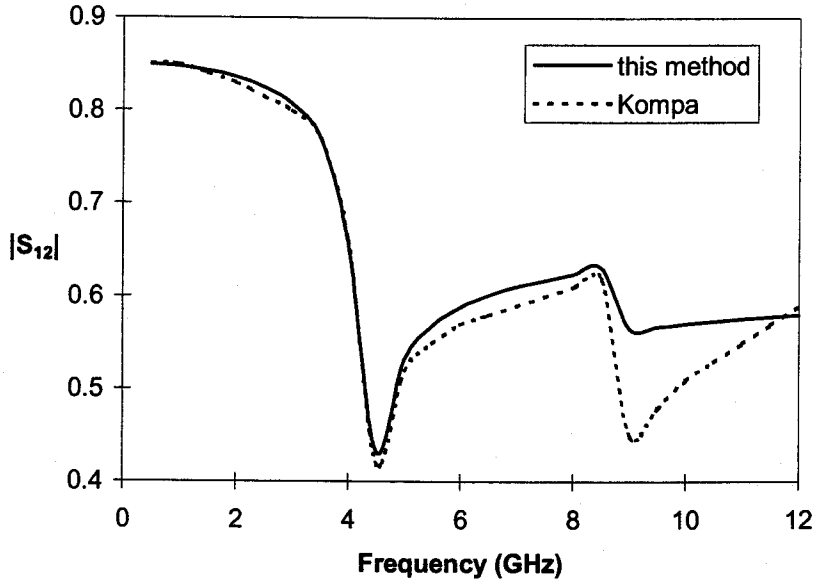

Figure 5.24. Kompa [71] and calculated S_{12} magnitude of a microstrip offset step with ε_r=2.32, h=1.5mm, W_1=0.5cm, W_2=2.0cm and e=0.75cm

The results show good agreement up to approximately 9 GHz. The same structure was also analyzed in reference [72], which uses a similar approach to the one used in this thesis, and has similar results. Once possible explanation for the loss of accuracy at higher frequencies could be the loss of accuracy in the dispersion equations which are essential for computing both the effective dielectric constant and width for which the discontinuity analysis is based upon.

5.4.2 Microstrip Linear Taper Step

The results obtained for a linear taper step by using the method described in Section 4.5.1 are compared to the results presented in reference [12], which uses Green's Function and the segmentation and desegmentation methods. Figures 5.25 and 5.26 show the reflection coefficients (magnitude of S_{11}) for impedance ratios of $1:2$ and $1:\sqrt{2}$.

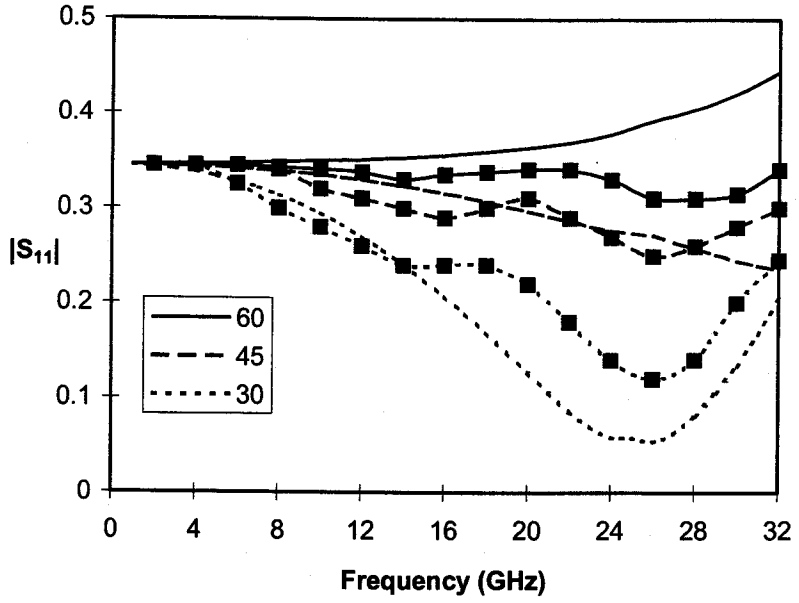

Figure 5.25. Green's Function [12] (black squares) and calculated S_{11} magnitude of a microstrip linear taper step with ε_r=2.53, h=0.79mm, Z_1=35.35Ω and Z_2=70.71Ω for angles of 60, 45 and 30 degrees

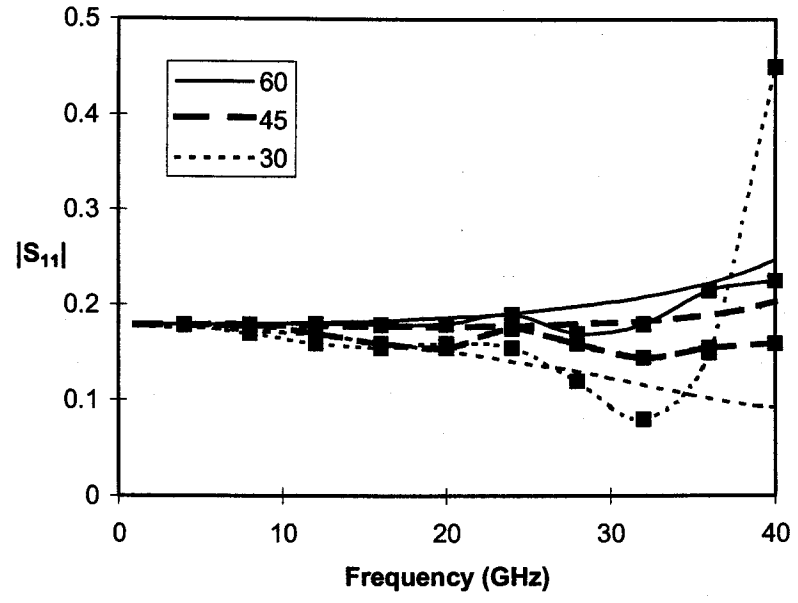

Figure 5.26. Green's Function [12] (black squares) and calculated S_{11} magnitude of a microstrip linear taper step with ε_r=2.53, h=0.79mm, Z_1=42.09Ω and Z_2=59.46Ω for angles of 60, 45 and 30 degrees

The results show relatively good accuracy at low frequencies but at higher frequencies the results become less accurate. Surprisingly the number of steps used to approximate the taper was only 2, as when more steps were used the results became even less accurate (this behaviour is explained on the following page).

To further analyze the accuracy of the discontinuity analysis method for a linear taper step, results were compared with the full-wave approach used in reference [73], as seen in Figure 5.27.

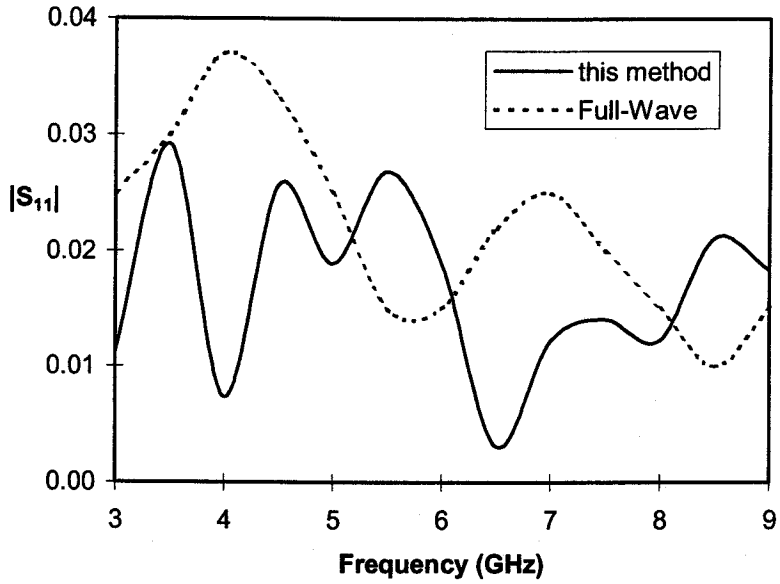

Figure 5.27. Full-wave [73] and calculated S_{11} magnitude of a microstrip linear taper step with ε_r=10, h=1.27mm, W_1=0.25mm, W_2=0.635mm and the length of the taper is 20mm

While the results are in the correct range, they are obviously not in very good agreement and investigation in to the discrepancy has resulted in the following observations:

- The number of steps used to approximate the linear taper with a stair-case was 32. It was observed that the results are highly influenced by the number of steps taken and that the results may not converge when more steps are used. Consider the geometries shown in Figure 5.28.

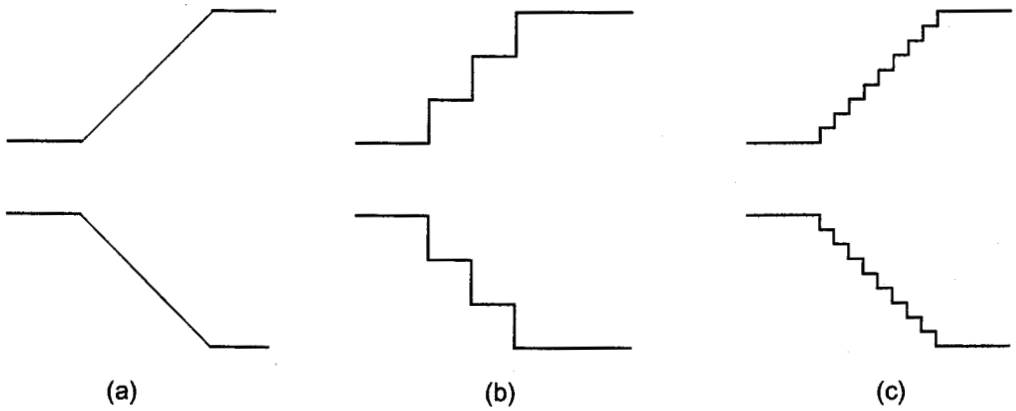

Figure 5.28. Stair-case Geometries Affect on the Number of Steps:
(a) Original; (b) Small Number of Steps; (c) Large Number of Steps

As the number of steps are increased the difference in the widths of adjacent steps become smaller and eventually each step will start to act as a transmission line as the step junction has practically been removed. Thus, increasing the number of steps can actually result in decreased accuracy. However, for this particular taper, using a smaller number of steps did not seem to improve the accuracy.

- Surprisingly the number of modes used for the mode matching did not seem to make a difference. Results were very similar with 1 mode, 5 modes and using the number modes to satisfy the relative converge ratio (equation (3.37)). This indicates that the mode matching is not the limiting factor on the overall accuracy.
- Analysis of the linear taper introduces the difficultly in determining how to account for the dispersion characteristics for the stair-case approximation, which affects both the effective dielectric constant and the effective width of each step. Consider the geometries shown in Figure 5.29.

  The dispersion for the stair-case is normally accounted for by splitting the taper into n steps of equal width based on the physical dimensions of the original taper and then accounting for dispersion [74]. This results in effective dielectric constants and effective widths for each step; and the steps are no longer equal (as seen in Figure 5.29 (c)). An alternative approach would be to apply dispersion to the two transmission lines and then split the taper into n steps of equal width based on the effective widths. However, in either approach, it is critical that both the effective dielectric constant and width are very accurate as all the

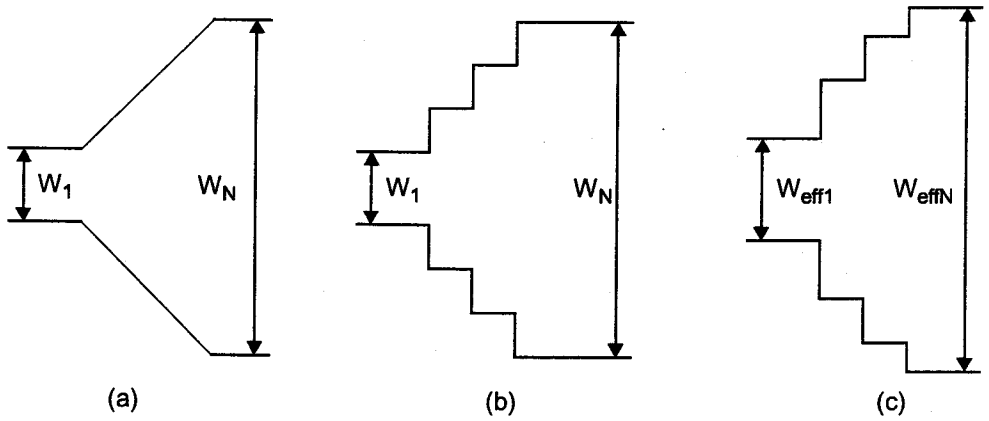

Figure 5.29. Stair-case Geometries Affect on Dispersion: (a) Original; (b) Step-segmented; (c) Effective Step-segmented

computations for each of the steps rely on them. In this case neither approach seemed to have a significant impact on the results. Reference [73] indicates that approximating the taper as a stair-case approximation can be successful but in order to account for the fields and dispersion for each of the step discontinuities, the spectral domain method is used to account for both the longitudinal and transverse current density distributions.

While the results for the linear taper step were not very accurate, it should be noted that for reference [73] it took 25 minutes and required approximately 5.3 MB of storage on a SUN SPARC Model 10 workstation to compute S_{11} at a single frequency point. Using the discontinuity analysis method, it took 4 seconds and 1.1 MB of storage to generate data for 15 frequencies. Using a normalization factor of 8, as described in Appendix E, to account for the difference in the computers the discontinuity analysis method is still significantly faster than the full-wave FDTD approach ($4/15 = 0.27$ seconds versus $25 \times 60/8 \approx 187$ seconds). The discontinuity analysis program also uses significantly less storage (almost 80% less). Further information on the numerical efficiency of the discontinuity analysis method is presented in Section 5.5. This vast difference in computational speed highlights the need for quick and accurate programs for analysis. While reference [73] may provide extremely accurate results, one can not afford to spend several minutes analyzing a single frequency point for a linear taper step, which is likely only one element of the circuit.

5.4.3 Microstrip Outside Cut Right Angle Bend

The results computed by the proposed method described in Section 4.3.1 are compared with published results to check the accuracy of the method. Figure 5.30 shows the comparison of the transmission coefficient calculated by this method and the full-wave FDTD method taken from reference [61].

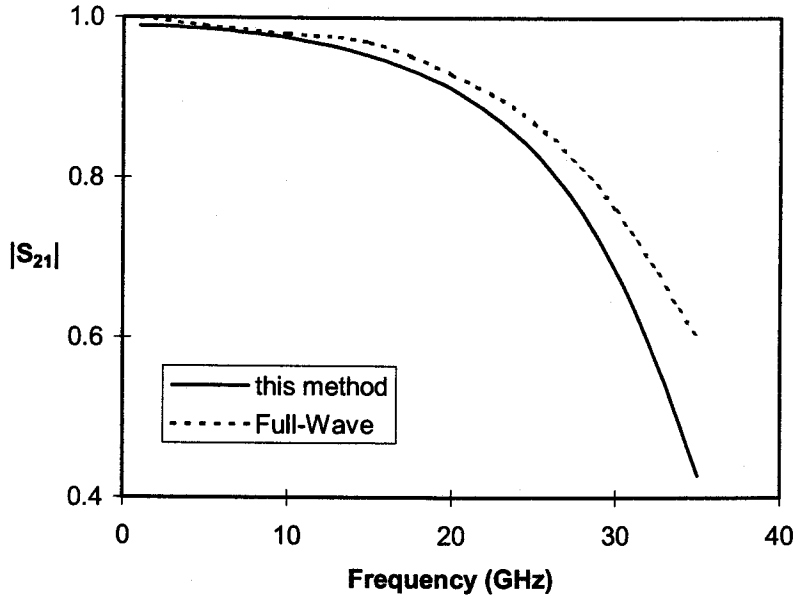

Figure 5.30. Full-wave FDTD [61] and calculated S_{21} magnitude of a microstrip outside cut right angle bend with ε_r=2.33, h=0.51mm, W_1=W_2=1.53mm and d_1=d_2=0.25W_1

Once again the results show relatively good accuracy at low frequencies but at higher frequencies the results become less accurate. In addition to the explanations for the discrepancy given in the previous sections there is another factor for the discrepancy when using the discontinuity analysis method for a right angle bend, the choice of the location of the termination, L_i. The selection of L_i is critical in trying to obtain valid results as it is defining the size of the step junctions as seen in Figure 5.31.

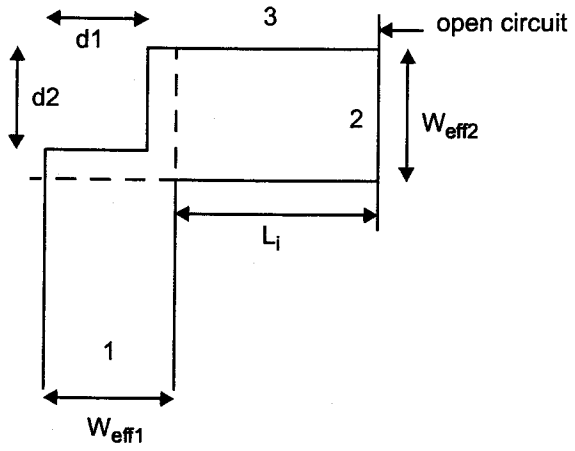

Figure 5.31. Outside Cut Right Angle Bend

As mentioned in the previous section about the number of steps to use for a linear taper, the selection of L_i is important so that the two step junctions do not behave as transmission lines. For an outside cut right angle bend, the two steps are: W_{eff1} to $W_{eff1} + L_i$ and $W_{eff1} + L_i$ to $W_{eff1} + L_i - d1$. If L_i is quite small then the first discontinuity may behave as a transmission line. Similarly, if L_i is quite large then the second discontinuity may behave as a transmission line.

For the outside cut, various attempts were made at trying to find the best value of L_i, including selecting L_i to be a function of W_{eff1} or a function of wavelength. The best results obtained were when L_i was a function of wavelength, using equation (5.4).

5.4.4 Mitered and Curved Right Angle Bends and Tapered T-junctions

Attempts to use the discontinuity analysis method for microstrip and rectangular waveguide H-plane mitered and curved right angle bends described in Sections 4.3.3 and 4.3.4 and tapered notch T-junctions described in Section 4.4.4 were unsuccessful. Explanations for the behaviour are attributed to the reasons given for the problems with the microstrip linear taper step, as described in Section 5.4.2, and the selection of L_i, as described in the previous section. For the selection of L_i, the use of a stair-case approximation causes additional problems, as when a number of steps are used to approximate the miter or curve they behave as transmission lines since the difference in transmission line widths are small.

Another possible explanation for the poor results was found in reference [75], where they use triangular approximations for mitered and curved boundaries since the structures cannot always be accurately modelled with a rectangular grid. Even with triangular

approximations they found that results were extremely sensitive to the position of the boundary, and that accuracy can only be expected when the boundary is adequately approximated. They found that using a stair-case approximation of mitered and curved boundaries in the FDTD method may yield converged but unreliable results. A slight displacement of two or four elements to approximate the contour, whether they be triangular or rectangular, can cause quite a large variation in results.

5.4.5 Summary

The analysis of microstrip and rectangular waveguide H-plane compensated discontinuities using the discontinuity analysis method described in this thesis has been presented. While the results are obtained quickly they unfortunately do not show good agreement with previously published results, particularly at higher frequencies, for the various reasons described in the previous sections. The use of the mode matching method to analyze these compensated structures should be avoided in situations where there are step junctions with minimal difference in line widths. Another numerical method could be used in conjunction with the port reduction method to analyze these compensated structures.

5.5 Numerical Computations

In this chapter the time to compute the scattering parameters for a discontinuity was presented for three cases:

- In Section 5.2.1, "Microstrip Right Angle Bends" a Cray YMP supercomputer took 235 CPU seconds to compute the transmission line coefficient, while it took the discontinuity analysis method 8 seconds on a Pentium 166 MHz, a slower computer.
- In Section 5.3.2, "Rectangular Waveguide H-plane T-junctions" an IBM 6000/520 took 120 CPU seconds to compute the scattering parameters, while it took the discontinuity analysis method 0.15 seconds on a Pentium 166 MHz, a faster computer. Using a normalization factor of 18, as described in Appendix E, to account for the difference in the computers the discontinuity analysis method is still faster than the full-wave FDTD approach (0.15 seconds versus 6.5 seconds).
- In Section 5.4.2, "Microstrip Linear Taper Step" a SUN SPARC Model 10 took 25 minutes to compute the reflection coefficient, while it took 0.27 seconds on a Pentium 166 MHz, a faster machine. Using a normalization factor of 8, as described in Appendix E, to account for the difference in the computers the discontinuity analysis method is still faster than the full-wave FDTD approach (0.27 seconds versus 187 seconds).

Even after normalizing the computer speeds, as described in Appendix E, these examples show that the discontinuity analysis method has an advantage over the FDTD method in computing the scattering parameters. This is not surprising if you consider the following:

- The FDTD method uses discretization to analyze the circuit so for an acceptable accuracy a large number of discretizations is required. The number of discretizations determines the matrix size in the numerical computation, which in turn determines the required memory and speed of the circuit analysis.
- With the discontinuity analysis method described in this thesis an n-port network is analyzed as three $(n-1)$-port networks. Specifically, T-junctions are analyzed as three two-port networks and right angle bends are analyzed as three one-port networks. Reducing the size of the network to analyze is a significant factor in improving the numerical efficiency (both in terms of CPU time and memory). Also, the number of modes used in the mode matching determines the matrix size in the numerical computation and by choosing the number of modes to satisfy the relative convergence ratio (3.37) further improves the storage efficiency of the discontinuity analysis method.

5.6 Summary

Results from the discontinuity analysis method described in the previous chapter were compared to published results for rectangular waveguide H-plane and microstrip transmission line step junctions, right angle bends and T-junctions. The results for uncompensated steps, bends and T-junctions agreed quite well with the published results and had the advantage of obtaining the results in significantly less time. The method could be implemented in a microwave CAD program for use in an iterative design process since it has good accuracy and significantly reduced computer time over the full-wave FDTD method.

With the excellent agreement with the uncompensated bends and T-junctions the method was expanded to the analysis of compensated discontinuities, and unfortunately the results were not as accurate at higher frequencies. However, the lack of accuracy only means that a more rigorous numerical method is required for the analysis of the compensated discontinuities at higher frequencies. The port reduction method is still a valid approach for these structures but the simple approach using the mode matching method is limited to more regular geometries, and specifically should be avoided when using stair-case approximations.

Chapter 6. Application of Discontinuity Analysis Method

The previous chapters show a discontinuity analysis method that can be used to analyze rectangular waveguide H-plane T-junctions. This chapter deals with an application of the method in the design and analysis of an entire rectangular waveguide H-plane diplexer. A diplexer is a three-port network that is used to separate an input signal into two output signals. The diplexer analyzed in this chapter consists of three units: two septum-coupled bandpass filters as the channel filters and a T-junction. A schematic diagram of the diplexer is shown in Figure 6.1.

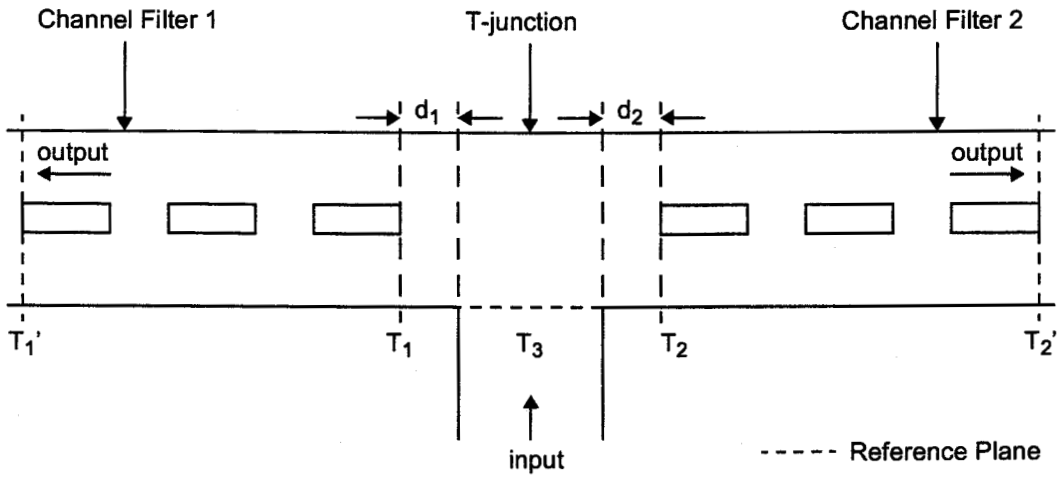

Figure 6.1. Diplexer Schematic Diagram

Rectangular waveguide H-plane T-junction diplexers are indispensable in many microwave and millimeter wave systems and subsystems used in radar and communication. With the explosive growth in millimeter wave communication systems there has been a strong need for low cost rectangular waveguide H-plane T-junction diplexers. A good overview of the subject is available in reference [31].

6.1 Background

The diplexer shown in this chapter is an example of how the discontinuity analysis method described in Chapter 4 can be applied to other structures. Additional terms and concepts necessary to describe the diplexer will be briefly covered in this section.

6.1.1 Bandpass Filter

Filters are two-port networks used to control the frequency response in a circuit by selectively attenuating those components of the input signal which are undesired, relative to those which it is desired to enhance (providing transmission at frequencies within the passband of the filter, and attenuation in the stopband of the filter). Figure 6.2 shows the general representation of a filter network.

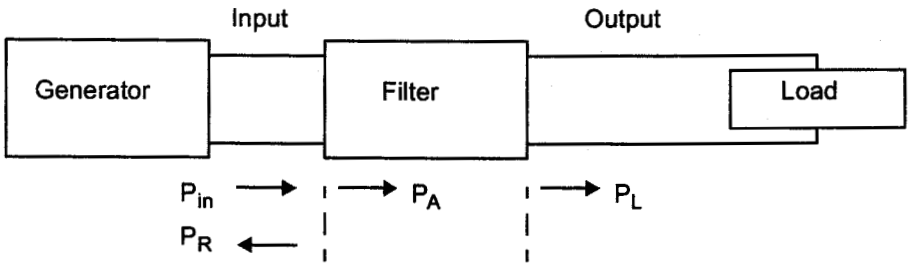

Figure 6.2. General Representation of a Filter Network

In the diagram the power is represented by:

- P_{in}: the incident power from the generator
- P_R: the power reflected from the generator
- P_A: the power absorbed by the filter
- P_L: the power transmitted to the load

From the conservation of energy,

$$P_{in} = P_R + P_A, \qquad P_L \leq P_A \tag{6.1}$$

The insertion loss (IL) and return loss (RL) at a particular frequency is defined as,

$$IL = -10\log\frac{P_L}{P_{in}}, \qquad RL = -10\log\frac{P_R}{P_{in}} \tag{6.2}$$

The units for both IL and RL are decibels (dB). Ideally, the baseband IL should be 0 dB and the stopband RL should be infinity.

A bandpass filter is characterized by its frequency response as shown in Figure 6.3, which shows that a band of frequencies are passed with minimum attenuation and the frequencies outside the band are attenuated. Some of the common terms used to describe the frequency response are:

- Lower cutoff frequency, f_{LC}
- Upper cutoff frequency, f_{UC}
- Lower isolation frequency, f_{LI}
- Upper isolation frequency, f_{UI}
- Center frequency, f_o

- Passband return loss, RL
- Isolation, L_A

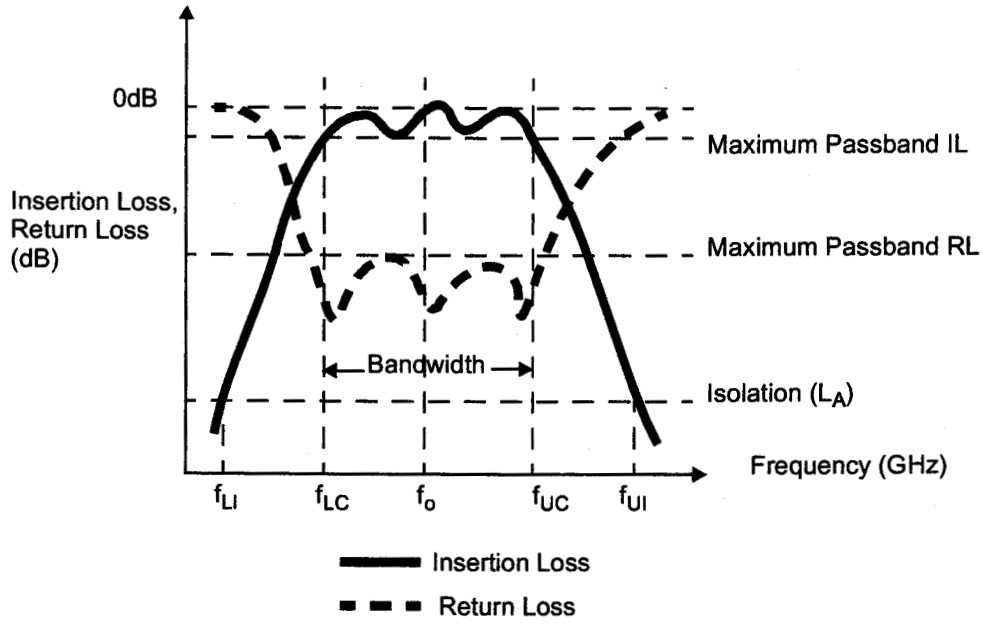

Figure 6.3. Bandpass Filter Frequency Characteristics

Another parameter used to characterize a filter is the order of the filter, which is the number of resonators or elements required to implement the filter. At lower frequencies, filters are realized by lumped elements (capacitors and inductors). At microwave frequencies, filters are realized by distributed elements (transmission lines and waveguides). Rectangular waveguide bandpass filters are realized using coupled resonators and the coupling is achieved using either irises or septums. In the diplexer example shown in this chapter, the filters are realized using septum-coupling.

For more information on microwave filters refer to references [76, 77, 78].

6.1.2 Septum-coupled Bandpass Waveguide Filter

A septum-coupled bandpass waveguide filter is a section of rectangular waveguide that has a dividing partition, usually made up of metal rectangular inserts, along the axis of the waveguide as shown in Figure 6.4, which shows a seventh order filter.

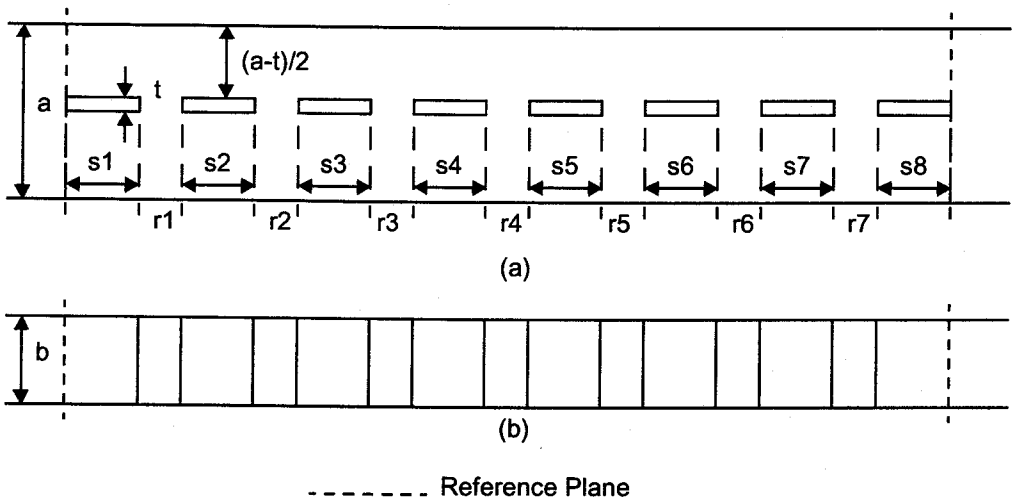

Figure 6.4. Septum-coupled Bandpass Filter Geometry: (a) top view; (b) front view

The septum-coupled bandpass filter consists of 8 septum-couplers, which act as parallel resonators, connected by 7 transmission lines, which act as series resonators since their length is approximately one-half of the guide wavelength of the line at the center frequency of the filter. A low frequency equivalent circuit of the septum-coupled bandpass filter is shown in Figure 6.5 and can be viewed as 7 series resonators connecting 8 parallel resonators.

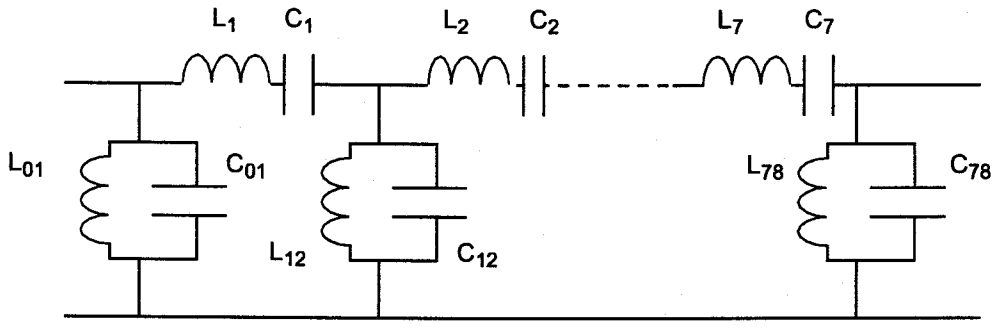

Figure 6.5. Equivalent Model of a Low Frequency Bandpass Filter

For more information on septum-coupled rectangular waveguide filters refer to reference [79].

6.2 Conventional Diplexer Design

The following steps are performed in a conventional diplexer design:

1. Each channel filter is designed individually using a method from reference [76, 80 or 81] and the multi-mode scattering matrices of each filter are obtained.
2. The multi-mode scattering matrices of the T-junction are calculated. This can be accomplished by using the resonator method described in reference [31], since the T-junction is uncompensated. With the resonator method, the order of the matrices is equal to approximately three times the number of modes in each waveguide.
3. The multi-mode scattering matrices of the two channel filters are cascaded with those from the T-junction in order to obtain the overall three-port scattering matrices of the diplexer, as shown in Figure 6.6.

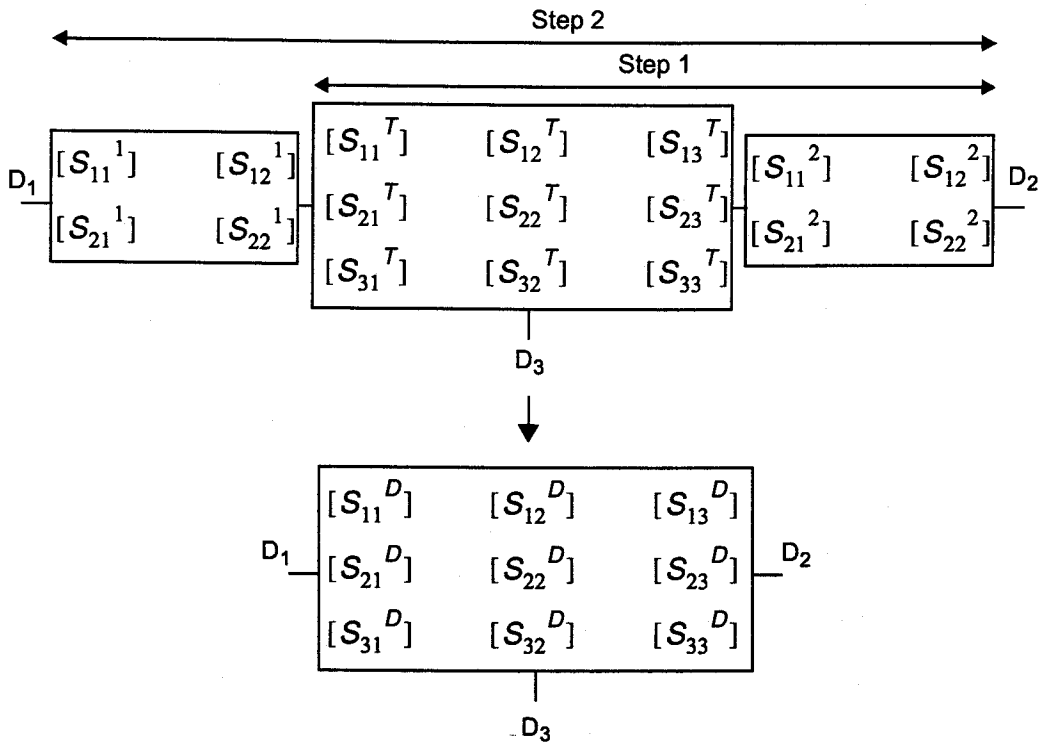

Figure 6.6. Combination of Three Scattering Matrices

The overall procedure of combining the three scattering matrices, as shown in Figure 6.6, involves two steps. At first, the scattering matrices of one of the two channel filters are combined with that of the T-junction. Subsequently the resulting three-port scattering matrices are combined with the two-port scattering matrices of the remaining filter. In each of the two step procedure a two-port network is combined with a three-port network. The scattering matrices computed in each step is calculated as follows [31]:

$$[S_{11}{}^{R}] = [S_{11}{}^{2}] + [S_{12}{}^{2}]([U] - [S_{11}{}^{T}][S_{22}{}^{2}])^{-1}[S_{11}{}^{T}][S_{21}{}^{2}], \quad (6.1)$$

$$[S_{12}{}^{R}] = [S_{12}{}^{2}]([U] - [S_{11}{}^{T}][S_{22}{}^{2}])^{-1}[S_{12}{}^{T}], \quad (6.2)$$

$$[S_{13}{}^{R}] = [S_{12}{}^{2}]([U] - [S_{11}{}^{T}][S_{22}{}^{2}])^{-1}[S_{13}{}^{T}], \quad (6.3)$$

$$[S_{21}{}^{R}] = [S_{21}{}^{T}]([S_{21}{}^{2}] + ([U] - [S_{11}{}^{T}][S_{22}{}^{2}])^{-1}[S_{11}{}^{T}][S_{21}{}^{2}]), \quad (6.4)$$

$$[S_{22}{}^{R}] = [S_{22}{}^{T}] + [S_{21}{}^{T}][S_{22}{}^{2}]([U] - [S_{11}{}^{T}][S_{22}{}^{2}])^{-1}[S_{12}{}^{T}], \quad (6.5)$$

$$[S_{23}{}^{R}] = [S_{23}{}^{T}] + [S_{21}{}^{T}][S_{22}{}^{2}]([U] - [S_{11}{}^{T}][S_{22}{}^{2}])^{-1}[S_{13}{}^{T}], \quad (6.6)$$

$$[S_{31}{}^{R}] = [S_{31}{}^{T}]([S_{21}{}^{2}] + [S_{22}{}^{2}]([U] - [S_{11}{}^{T}][S_{22}{}^{2}])^{-1}[S_{11}{}^{T}][S_{21}{}^{2}]), \quad (6.7)$$

$$[S_{32}{}^{R}] = [S_{32}{}^{T}] + [S_{31}{}^{T}][S_{22}{}^{2}]([U] - [S_{11}{}^{T}][S_{22}{}^{2}])^{-1}[S_{12}{}^{T}] \text{ and} \quad (6.8)$$

$$[S_{33}{}^{R}] = [S_{33}{}^{T}] + [S_{31}{}^{T}][S_{22}{}^{2}]([U] - [S_{11}{}^{T}][S_{22}{}^{2}])^{-1}[S_{13}{}^{T}]. \quad (6.9)$$

4. Optimization of the fundamental mode frequency response as desired.

The conventional diplexer design has two major drawbacks. First of all, the diplexer configuration shown in Figure 6.1 does not offer good passband return loss [31]. Also, the designer has to completely rely on brute force optimization routine for the common junction input matching. Therefore, two things are necessary:

1. The rectangular waveguide H-plane T-junction should be modified in order to incorporate some tuning mechanism.
2. Reduction of optimization time by using a more accurate initial design.

6.3 Modified Diplexer Design

In an approach suggested by Morini and Rozzi [82] it was shown that the fundamental mode scattering matrix of the T-junction should satisfy the following condition for good matching

$$|S_{11}| \approx |S_{22}| \approx |S_{33}| \geq 1/3 \quad (6.10)$$

at the center frequencies of the two channel filters. In addition, the two filters should be located at distances l_1 and l_2 for a perfect match, which are given by

$$l_1 = -\frac{1}{2j\beta}\ln\left(\frac{S_{22}}{\Delta S(S_{33}{}^{*})P_{L1}}\right) \text{ at } f = f_2 \text{ and} \quad (6.11)$$

$$l_2 = -\frac{1}{2j\beta}\ln\left(\frac{S_{11}}{\Delta S(S_{33}^{*})P_{L2}}\right) \text{ at } f = f_1 . \qquad (6.12)$$

Where f_1 and f_2 are the center frequencies of the two channel filters, respectively, P_{L1} and P_{L2} are the reflection coefficients of the filters under matched condition at their center frequencies, β is the propagation constant, and ΔS is the determinant of the T-junction scattering matrix.

Equation (6.10) cannot be satisfied by the rectangular waveguide H-plane T-junction used in the diplexer in Figure 6.1 [31]. Therefore, a compensated square notched T-junction is proposed as shown in Figure 6.7.

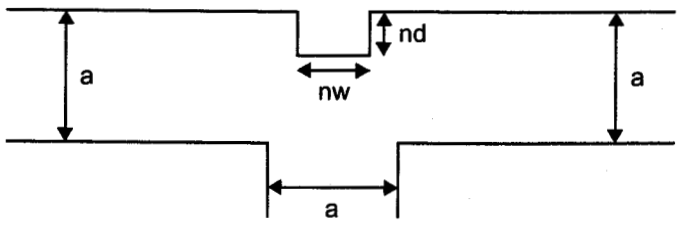

Figure 6.7. Square Notched T-junction

Dimensions nw and nd are adjusted so that equation (6.10) is satisfied as closely as possible. Such a T-junction can be analyzed using the method described in Section 4.4.3. Keeping the above facts in mind we can now summarize the design steps for the modified approach as follows:

1. Each channel filter is designed individually using a method from reference [76, 80 or 81] and the multi-mode scattering matrices of each filter are obtained, as was done in the conventional diplexer design.
2. Design the square notched rectangular waveguide H-plane T-junction as shown in Figure 6.7. Adjust the parameters nw and nd and use the discontinuity analysis method described in Section 4.4.3 so that equation (6.10) is satisfied. Only the fundamental mode needs to be used in this analysis.
3. The rectangular waveguide H-plane diplexer shown in Figure 6.8 is analyzed using the discontinuity analysis method described in Chapter 4 as follows:

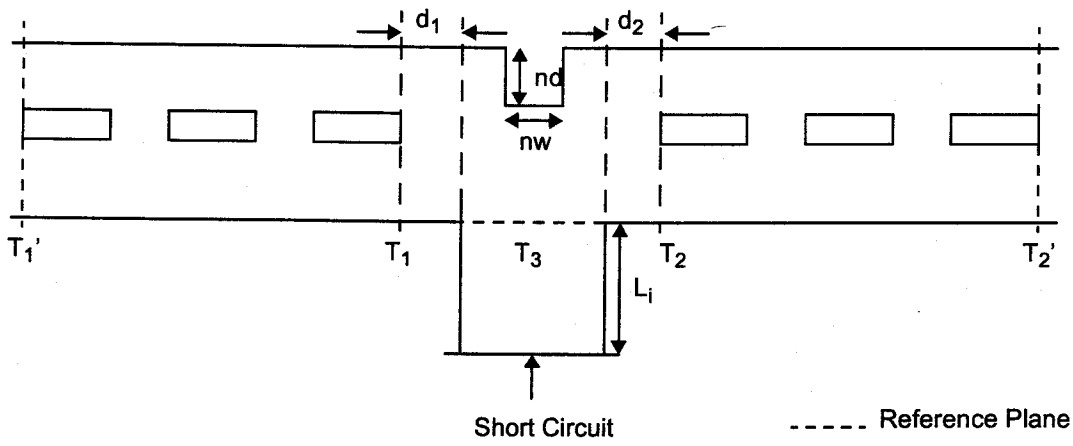

Figure 6.8. Modified Diplexer Schematic Diagram

a. The multi-mode scattering matrices of each channel filter are calculated and stored.
b. Calculate the two-port multi-mode scattering matrices for the two-port networks between the reference planes T_1 and T_2, which are created by placing a short circuit termination at three different locations at port 3.
c. Cascading the multi-mode scattering matrices of the two channel filters at T_1 and T_2 and obtain three new sets of two-port multi-mode scattering matrices between T_1' and T_2'.
d. Extracting the fundamental mode three-port scattering parameters of the diplexer for the reference planes at T_1', T_2' and T_3.

It is interesting to note that one only needs the scattering matrix of the compensated square notched T-junction in the initial design stage (step 2), and not during the analysis. Also, in the above analysis the cascading of multi-mode scattering matrices only involves two-port networks. Also, with the discontinuity analysis method, the order of the matrices involved is equal to the number of modes in each waveguide. This saves a great deal of memory and time when compared with conventional method described in Section 6.2.

4. Optimization of the design is achieved by using a method proposed by references [81, 83]. Figure 6.9 shows the optimization procedure.

Note that the compensated T-junction shown in Figure 6.8 cannot be analyzed by the conventional resonator method [31], as was the case for the conventional diplexer design, because it can only be used to analyze uncompensated discontinuities.

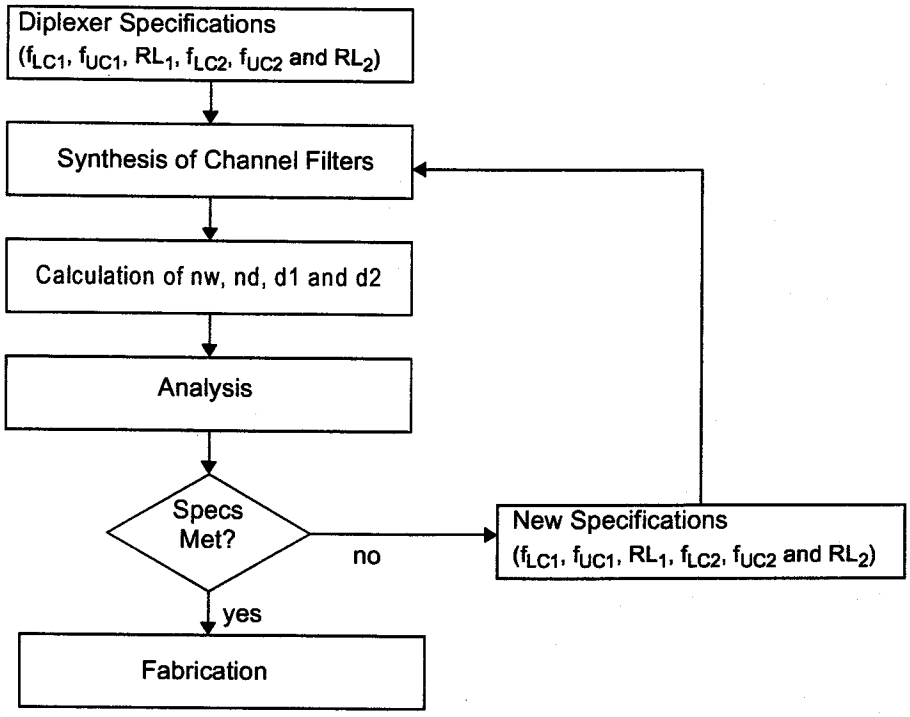

Figure 6.9. Optimization Procedure

6.4 Design and Analysis of a Ka-band Diplexer

Using the modified diplexer design described in the previous section a Ka-band diplexer was designed and analyzed. Ka-band is an industry standard designation for a rectangular waveguide that operates in the frequency range 26.5 to 40 GHz and has dimensions a=0.28" and b=0.14" (rectangular waveguide dimensions are often specified in inches). The design specifications for the diplexer are as follows:

Table 6.1. Diplexer Design Specifications

Specifications	Channel 1	Channel 2
Lower Isolation Frequency (f_{LI})	38.025 GHz	38.565 GHz
Lower Cutoff Frequency (f_{LC})	38.565 GHz	39.265 GHz
Upper Cutoff Frequency (f_{UC})	38.985 GHz	39.685 GHz
Upper Isolation Frequency (f_{UI})	39.265 GHz	40.225 GHz
Passband Return Loss (RL)	15.0 dB	15.0 dB
Isolation	40.0 dB	40.0 dB

In addition, the septum thickness is t=0.02".

The results of the rectangular waveguide H-plane diplexer design include the geometries for the channel filters and the T-junction. Table 6.2 shows the optimized dimensions of the diplexer channel filters, which require a 7-pole filter as shown in Figure 6.4.

Table 6.2. Optimized Diplexer Dimensions

Channel 1		Channel 2	
Septum Lengths	Section Lengths	Septum Lengths	Section Lengths
s1=0.0659"	r1=0.1252"	s1=0.0629"	r1=0.1196"
s2=0.2178"	r2=0.1247"	s2=0.2151"	r2=0.1188"
s3=0.2468"	r3=0.1246"	s3=0.2458"	r3=0.1187"
s4=0.2525"	r4=0.1246"	s4=0.2518"	r4=0.1187"
s5=0.2525"	r5=0.1246"	s5=0.2518"	r5=0.1187"
s6=0.2468"	r6=0.1247"	s6=0.2548"	r6=0.1188"
s7=0.2178"	r7=0.1252"	s7=0.2151"	r7=0.1196"
s8=0.0659"		s8=0.0629"	

The T-junction geometries as shown in Figure 6.8 are:

- Height of the central step in the T-junction, nw, is 0.0764"
- Length of the central step in the T-junction, nd, is 0.1046"
- Distance from the first filter to the T-junction, d_1, is 0.1045"
- Distance from the second filter to the T-junction, d_2, is 0.0596"

Figures 6.10 and 6.11 show the analyzed frequency response of the diplexer. Design and optimization of the diplexer required only 22 minutes on a Pentium III 600 MHz machine with 256 MB of RAM. Design and optimization of the same diplexer using the conventional approach described in Section 6.2 requires a couple of hours. Also, the conventional method may converge to a local minimum during optimization.

Both the insertion loss and the return loss shown in Figures 6.10 and 6.11 meet the design specifications thus validating the modified diplexer design procedure. In Figure 6.11 both channels have the same return loss so the lines are overlapping. The design procedure has also been successfully used by Dr. Pramanick at K&L Microwave Inc. to design and manufacture diplexers with an input channel that is a circular waveguide.

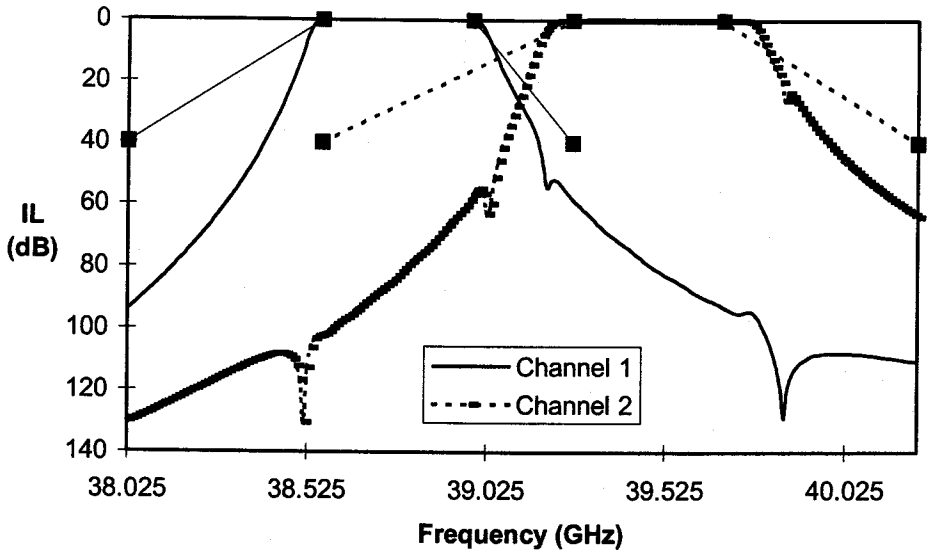

Figure 6.10. Diplexer Insertion Loss Frequency Response (black squares represent diplexer specification)

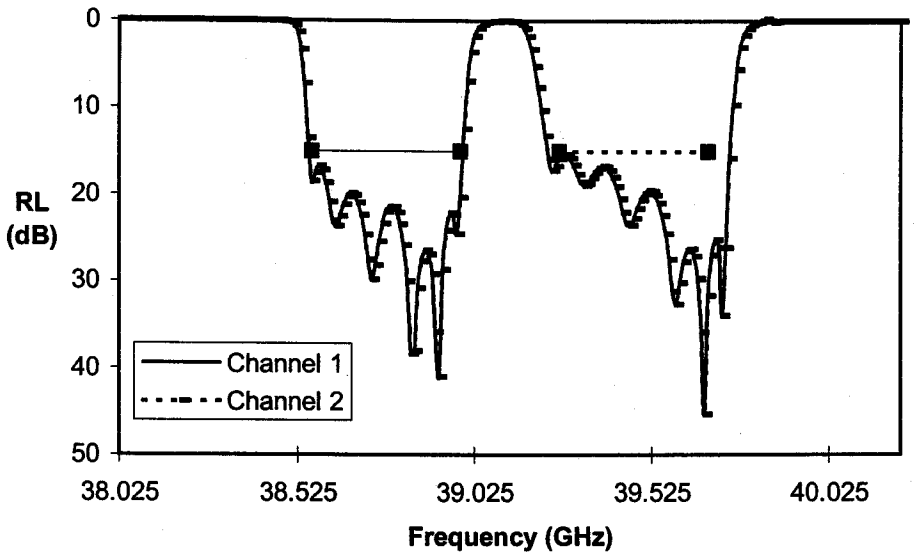

Figure 6.11. Diplexer Return Loss Frequency Response (black squares represent diplexer specification)

6.5 Summary

In this chapter the discontinuity analysis method, presented in the previous chapters, is used to design and analyze an entire rectangular waveguide H-plane diplexer. Specifically, the discontinuity analysis method is used to analyze a square notched T-junction during the modified diplexer design procedure and then to analyze the entire diplexer using only two-port networks. The modified diplexer design procedure is used to design a Ka-band diplexer, whose frequency response meets the diplexer specifications.

Chapter 7. Conclusion

The objective of this research, as previously stated in Chapter 1, is to develop a set of routines to accurately, quickly and efficiently analyze steps, right angle bends and T-junctions, which are the fundamental building blocks for microwave circuits, that can be used as a foundation for a microwave computer aided design (CAD) program. The routines will be developed to handle both rectangular waveguide H-plane and microstrip discontinuities. Since CAD of microwave circuits relies on accurate characterization of discontinuities, analyzing them is a logical first step towards the generation of a microwave CAD program.

In accordance with the above stated objective, the conclusions of the research is that routines have been developed to analyze rectangular waveguide H-plane and microstrip discontinuities using the port reduction method in conjunction with the mode matching method. Comparisons to published results for uncompensated steps, right angle bends and T-junctions show good agreement with the advantage of obtaining the solution much quicker than by use of other full-wave methods such as FDTD. The method can be implemented in a microwave CAD program to be used during the iterative design process, since it has good accuracy and significantly reduced computer time.

While the application of the method to compensated steps, right angle bends and T-junctions were obtained quickly, they did not provide good agreement with published results, particularly at higher frequencies. However, the lack of accuracy only means that a more rigorous numerical method is required for the analysis of the compensated discontinuities at higher frequencies. The port reduction method is still a valid approach for these structures, but the simple approach using the mode matching method is limited to more regular geometries, and specifically should be avoided when using stair-case approximations. The use of the port reduction method was successfully applied to the design and analysis of a rectangular waveguide H-plane diplexer, further validating the method and providing a practical application of the method to a real world problem.

7.1 Limitations

Some of the limitations of the microwave CAD method described in this thesis are as follows:

1. While the analysis method used to find the scattering parameters for the right angle bends and T-junctions described in Chapter 4, "Discontinuity Analysis Method" on page 36 uses a multi-mode scattering matrix approach, the resulting matrix from the analysis only contains the fundamental mode.
2. The analysis method may not be suitable for all compensated right angle bends and T-junctions. As an example consider the bend shown in Figure 7.1.

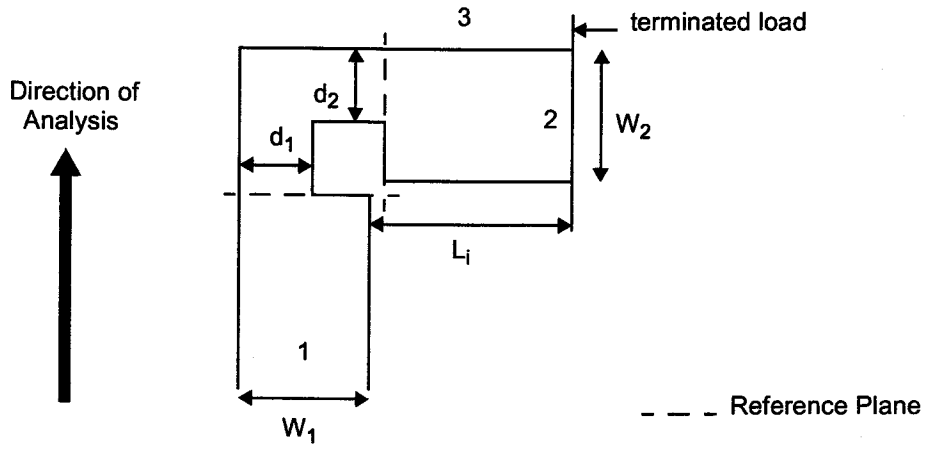

Figure 7.1. Inside Cut Right Angle Bend

The analysis method cannot directly handle the asymmetric step discontinuity d_2 to W_2 since this step discontinuity is in a plane perpendicular to the direction of the analysis. The structure can be analyzed by initially ignoring the asymmetric step discontinuity (assume $W_2 = d_2$) and separately analyze the asymmetric step discontinuity.

7.2 Future Research

Some of the future research that could be undertaken are as follows:

- Use the routines developed in this thesis as a foundation to produce a microwave CAD program that can be used to analyze microwave circuits.
- Use of another numerical method to analyze compensated discontinuities in conjunction with the port reduction method. The method should be validated with experimental results as there are limited published results for compensated structures. Research to find the optimum compensation for discontinuities would follow.

- Extend the routines developed in this thesis to handle rectangular waveguide E-plane discontinuities.
- Extend the routines developed in this thesis to handle discontinuities for additional planar transmission lines, such as stripline, suspended microstrip, shielded microstrip and inverted microstrip.
- Apply the discontinuity analysis method described in this thesis to other structures, such as power dividers, combline filters and patch antennas.
- Update the Fortran 90 implementation of the method to use the parallel computing features of High Performance Fortran to improve the numerical efficiency of the method.

List of References

[1] J. C. Maxwell, *A Treatise on Electricity and Magnetism*. Dover, New York, 1954.

[2] A. F. Peterson, S. L. Ray and R. Mittra, *Computational Methods for Electromagnetics*. IEEE Press, New York, 1998.

[3] D. M. Pozar, *Microwave Engineering*. Addison-Wesley Publishing Company, Inc., New York, 1990.

[4] S. C. Harsany, *Principles of Microwave Technology*. Prentice-Hall, Inc., New Jersey, 1997.

[5] G. Kompa and R. Mehran, "Planar waveguide model for calculating microstrip components," *Electronics Letters*, vol. 11, pp. 459-460, September 1975.

[6] I. Wolff, G. Kompa and R. Mehran, "Calculation method for microstrip discontinuities and T-junctions," *Electronics Letters*, vol. 8, pp. 177-179, April 1972.

[7] P. Pramanick and P. Bhartia, "Phase velocity dependence of frequency dependent characteristic impedance of microstrip," *Microwave Journal*, vol. 32, no. 6, pp. 180-184, June 1989.

[8] G. Wells and P. Pramanick, "An accurate dispersion expression for shielded microstrip lines," *International Journal of Microwave and Millimeter Wave Computer-Aided Engineering*, vol. 5, no. 4, pp. 287-295, July 1995.

[9] K.C. Gupta and M.D. Abouzahra, ed., *Analysis and Design of Planar Microwave Components*. IEEE Press, New York, 1994.

[10] R. J. P. Douville and D. S. James, "Experimental Study of Symmetric Microstrip Bends and Their Compensation," *IEEE Transactions on Microwave Theory and Techniques*, vol. MTT-26, no. 3, pp. 175-181, March 1978.

[11] S. S. Chang, W. X. Huang and T. Itoh, "Computer Aided Design for Planar Microstrip Circuits Analysis by Boundary-Integral Method," *19th European Microwave Conference Proceedings (1989)*, pp. 975-978.

[12] R. Chadha and K. C. Gupta, "Compensation of Discontinuities in Planar Transmission Lines", *IEEE Transactions on Microwave Theory and Techniques*, vol. MTT-30, no. 12, pp. 2151-2155, December 1982.

[13] P. Silvester and P. Benedek, "Microstrip discontinuities capacitances for right-angle bends, T-junctions and crossings," *IEEE Transactions on Microwave Theory and Techniques*, vol. MTT-21, no. 5, pp. 341-346, May 1973.

[14] A. Gopinath and B. Easter, "Moment method of calculating discontinuity inductance of microstrip right angled bends," *IEEE Transactions on Microwave Theory and Techniques*, vol. MTT-22, no. 10, pp. 880-883, October 1974.

[15] P. Stoyten, "Equivalent capacitances of T-junctions," *Electronics Letters*, vol. 9, pp. 552-553, November 1973.

[16] R. S. Pengelly, "RF and Microwave CAD: A Review of Present Status," *Microwave Journal*, vol. 36, no. 1, pp. 139 -146, January 1993.

[17] T. Quarles, A. R. Newton, D. O. Pederson and A. Sangiovanni-Vincentelli, *SPICE 3 Version 3F5 User's Manual*. Department of Electrical Engineering and Computer Sciences, University of California, Berkeley, California, March, 1994.

[18] Eagleware Corporation, *SuperStar Operation Manual*. Georgia, 1994.

[19] K. C. Gupta, R. Garg and R. Chadha, *Computer-Aided Design of Microwave Circuits*. Artech House, Inc., Massachusetts, 1981.

[20] J. A. Dobrowolski and W. Ostrowski, *Computer-Aided Analysis, Modeling, and Design of Microwave Networks*. Artech House, Inc., Massachusetts, 1996.

[21] J. A. Dobrowolski, *Introduction to Computer Methods for Microwave Circuit Analysis and Design*. Artech House, Inc., Massachusetts, 1991.

[22] T. Itoh, ed., *Numerical Techniques for Microwave and Millimeter-Wave Passive Structures*. John Wiley and Sons, Inc., New York, 1989.

[23] B. Veidt, "Selecting 3-D Electromagnetic Software," *Microwave Journal*, vol. 41, no. 9, pp. 126-137, September 1998.

[24] P. Perry and M. Soghomonian, "Microwave CAD review: a PC update," *Microwave Engineering Europe*, pp. 31-38, May 1993.

[25] G. A. Breed, "Caveats for Computer-Aided Design," *Applied Microwave & Wireless*, vol. 10, no. 7, p. 60, September 1998.

[26] M. Celuch-Marcysiak and W. K. Gwarek, "Formal Equivalence and Efficiency Comparison of the FD-TD, TLM and SN Methods in Application to Microwave CAD Programs," *21st European Microwave Conference Proceedings (1991)*, pp. 199-204.

[27] K. Kornbluh, "Technical Software," *IEEE Spectrum*, vol. 37, no. 1, pp. 59-62, January 2000.

[28] E. Wolff and R. Kaul, *Microwave Engineering and Systems Applications*. John Wiley & Sons, Inc., New York, 1988.

[29] K. C. Gupta, *Computer-Aided Microwave Circuit Design*. Department of Electrical and Computer Engineering, University of Colorado, Boulder, Fall 1995.

[30] W. J. R. Hoefer, "Time Domain Electromagnetic Simulation for Microwave CAD Applications," *IEEE Transactions on Microwave Theory and Techniques*, vol. MTT-40, no. 7, pp. 1517-1527, July 1992.

[31] J. Uher, J. Bornemann and U. Rosenberg, *Waveguide Components for Antenna Feed Systems: Theory and CAD*. Artech House, Inc., Massachusetts, 1993.

[32] A. D. Olver, P. J. B. Clarricoats, A. A. Kishk and L. Shafai, *Microwave Horns and Feeds*. IEEE Press, 1994.

[33] R. E. Collins, *Field Theory of Guided Waves*. IEEE Press, 1991.

[34] C. Christopoulos, *The Transmission-Line Modeling Method: TLM*. IEEE Press, 1995.

[35] Y. C. Shih and K. G. Gray, "Convergence of numerical solutions of step-type waveguide discontinuity problems by modal analysis," *1983 IEEE MTT-S International Microwave Symposium Digest*, pp. 233-235.

[36] T. S. Chu, T. Itoh and Y. C. Shih, "Comparative Study of Mode-Matching Formulations for Microstrip Discontinuity Problems," *IEEE Transactions on Microwave Theory and Techniques*, vol. MTT-33, no. 10, pp. 1018-1023, October 1985.

[37] M. Tong, *An Analytical Technique for the Design and Analysis of Waveguide Tapers*. Master of Science Thesis, University of Saskatchewan, 1995.

[38] K. C. Gupta, R. Garg, I. Bahl and P. Bhartia, *Microstrip Lines and Slotlines*. Artech House, Inc., Massachusetts, 1996.

[39] S. W. Lee, W. R. Jones and J. J. Campbell, "Convergence of numerical solutions of iris-type discontinuity problems," *IEEE Transactions on Microwave Theory and Techniques*, vol. MTT-19, no. 6, pp. 528-536, June 1971.

[40] T. Sieverding, U. Papziner and F. Arndt, "Mode-Matching CAD of Rectangular or Circular Multiaperture Narrow-Wall Couplers," *IEEE Transactions on Microwave Theory and Techniques*, vol. MTT-45, no. 7, pp. 1034-1040, July 1997.

[41] X. P. Liang and K. A. Zaki, "Characterizing Waveguide T-junctions by Three Plane Mode-Matching Techniques," *1991 IEEE MTT-S International Microwave Symposium Dig*est, pp. 849-852.

[42] J. F. Liang, H. C. Chang and K. A. Zaki, "Coaxial probe modeling in waveguides and cavities," *IEEE Transactions on Microwave Theory and Techniques*, vol. MTT-40, no. 12, pp. 2172-2180, December 1992.

[43] M. Davidovitz, "Reconstruction of the S-Matrix for a 3-Port Using Measurements at Only Two Ports," *IEEE Microwave and Guided Wave Letters*, vol. 5, no. 10. pp. 349-350, October 1995.

[44] Z. Ma and E. Yamashita, "Port Reflection Coefficient Method for Solving Multi-Port Microwave Network Problems," *IEEE Transactions on Microwave Theory and Techniques*, vol. MTT-43, no. 2, pp. 331-337, February 1995.

[45] G. Baoxin, Z. Jinsong, Z. Naiqian and L. Runsheng, "Simulation software for microwave integrated circuits and interconnections: Tsinghua microwave SPICE," *Journal of Tsinghua University*, vol. 36, iss. 9, pp. 28-34, September 1996.

[46] S. W. Haney, "Is C++ Fast Enough for Scientific Computing?" *Computers in Physics*, vol. 8, no. 6, pp. 690-694, November/December 1994.

[47] A. D. Robison, "C++ Gets Faster for Scientific Computing," *Computers in Physics*, vol. 10, no. 5, pp. 458-462, September/October 1996.

[48] J. E. Moreira, S. P. Midkiff and M. Gupta, "A Comparison of Java, C/C++, and FORTRAN for Numerical Computing," *IEEE Antennas and Propagation Magazine*, vol. 40, no. 5, pp. 102-105, October 1998.

[49] J. E. Moreira, S. P. Midkiff, M. Gupta, P. V. Artigas, M. Snir and R. D. Lawrence, "Java programming for high-performance numerical computing," *IBM Systems Journal*, vol. 39, no. 1, pp. 21-56, January 2000.

[50] D. B. Loveman, "High Performance Fortan," *IEEE Parallel & Distributed Technology*, vol. 1, no. 1, pp. 25-42, February 1993.

[51] L. R. Nyhoff and S. C. Leestma, *Fortran 90 for Engineers and Scientists*. Prentice-Hall, Inc., New Jersey, 1997.

[52] G. Kompa, "S-matrix computation of microstrip discontinuities with a planar waveguide model," *Archiv. Elektr. Übertr.*, vol. 30, pp. 58-64, 1976.

[53] T. Aguili, K. Grayaa, A. Bouallegue and H. Baudrand, "Application of a source method of modelling step discontinuities in microstrip circuit," *IEE-Proceedings-H-(Microwaves, Antennas-and-Propagation)*, vol. 143, no. 2, pp. 169-173, April 1996.

[54] N. Koster and R. Jansen, "The Microstrip Step Discontinuity: A Revised Description," *IEEE Transactions on Microwave Theory and Techniques*, vol. MTT-34, no. 2, pp. 213-223, February 1986.

[55] S. Nam, H. Ling and T. Itoh, "Time-Domain Method of Lines Applied to the Uniform Microstrip Line and its Step Discontinuity," *1989 IEEE MTT-S International Microwave Symposium Digest*, pp. 997-1000.

[56] X. Zhang and K. Mei, "Time-Domain Finite Difference Approach to the Calculation of the Frequency-Dependent Characteristics of Microstrip Discontinuities," *IEEE Transactions on Microwave Theory and Techniques*, vol. MTT-36, no. 12, pp. 1775-1787, December 1988.

[57] S. Worm, "Full-Wave Analysis of Discontinuities in Planar Waveguides by the Method of Lines Using a Source Approach," *IEEE Transactions on Microwave Theory and Techniques*, vol. MTT-38, no. 10, pp. 1510-1514, October 1990.

[58] N. Marcuvitz, *Waveguide Handbook*. Peter Peregrinus Ltd., London, UK, 1986.

[59] K. Chang, *Microwave Passive and Antenna Components*. John Wiley & Sons, Inc., New York, 1989.

[60] A. Weisshaar, M. Mongiardo and V. K. Tripathi, "CAD-Oriented Equivalent Circuit Modeling of Step Discontinuities in Rectangular Waveguides," *IEEE Microwave and Guided Wave Letters*, vol. 6, no. 4, pp. 171-173, April 1996.

[61] K. Naishadham and X. P. Lin, "A Study of Optimum Compensation of Open Microstrip Discontinuities Using the FDTD Method with Boundary Reflection Error Cancellation," *International Journal of Microwave and Millimeter Wave Computer-Aided Engineering*, vol. 6, no. 1, pp. 47-57, 1996.

[62] W. P. Harokopus and P. Katehi, "An Accurate Characterization of Open Microstrip Discontinuities Including Radiation Losses," *1989 IEEE MTT-S International Microwave Symposium Digest*, pp. 231-234.

[63] J. X. Zheng and D. C. Chang, "Numerical Modelling of Chamfered Bends and Other Microstrip Junctions of General Shap in MMICS," *1990 IEEE MTT-S International Microwave Symposium Digest*, pp. 709-712.

[64] A. Skrivervik and J. R. Mosig, "Equivalent Circuits of Microstrip Discontinuities Including Radiation Effects," *1989 IEEE MTT-S International Microwave Symposium Digest*, pp. 1147-1150.

[65] M. Koshiba and M. Suzuki, "Application of the Boundary-element Method to Waveguide Discontinuities," *IEEE Transactions on Microwave Theory and Techniques*, vol. MTT-34, no. 2, pp. 301-307, February 1986.

[66] M. S. Leong, P. S. Kooi and T. S. Yeo, "Application of Green's Theorem Approach to Symmetrical Right-Angled H-Plane Rectangular Waveguide Bend," *Microwave and Optical Technology Letters*, vol. 6, no. 6, pp. 363-370, May 1993.

[67] W. Menzel and I. Wolff, "A method for calculating the frequency dependent properties of microstrip discontinuities," *IEEE Transactions on Microwave Theory and Techniques*, vol. MTT-25, no. 2, pp. 107-112, February 1977.

[68] S. Wu, H. Yang, and N. Alexopoulos, "A Rigorous Dispersive Characterization of Microstrip Cross and Tee Junctions," *1990 IEEE MTT-S International Microwave Symposium Dig*est, pp. 1151-1154.

[69] T. Sieverding and F. Arndt, "Field Theoretic CAD of Open or Apeture Matched T-junction Coupled Rectangular Waveguide Structures," *IEEE Transactions on Microwave Theory and Techniques*, vol. MTT-40, no. 2, pp. 353-362, February 1992.

[70] E. A. Navarro, V. Such, B. Gimeno and J. L. Cruz, "Analysis of H-plane Waveguide Discontinuities With an Improved Finite-Difference Time Domain Algorithm, *IEE-Proceedings-H-(Microwaves, Antennas-and-Propagation)*, vol.139, no.2, pp.183-185, April 1992.

[71] G. Kompa, "Frequency-dependent Behaviour of Microstrip Offset Junctions," *Electronics Letters*, vol. 11, pp. 537-538, October 1975.

[72] T. S. Chu and T. Itoh, "Generalized Scattering Matrix Method for Analysis of Cascaded and Offset Microstrip Step Discontinuities," *IEEE Transactions on Microwave Theory and Techniques*, vol. MTT-34, no. 2, pp. 280-285, February 1986.

[73] B. E. Spielman and L. G. Chen, "A Full-wave Analysis for Microwave, Planar, Distributed Discontinuities," *1996 IEEE MTT-S International Microwave Symposium Dig*est, pp. 1055-1058.

[74] S. P. de Araujo, A. Gomes Neto, M. de S. Araujo Filho, "Analysis of Two-Dimensional Microstrip Discontinuity by the Step-segmentation Approach," *1993 SBMO International Microwave Conference/Brazil Proceedings*, pp. 105-110.

[75] C. H. Chan, H. Sangani, K. S. Yee and J. T. Elson, "A Finite-Difference Time-Domain Method Using Whitney Elements," *Microwave and Optical Technology Letters*, vol. 7, no. 14, pp. 673-676, October 1994.

[76] G. L. Matthaei, L. Young and E. M. T. Jones, *Microwave Filters, Impedance-matching Networks, and Coupling Structures*. McGraw-Hill, New York, 1964.

[77] R. E. Collin, *Foundations for Microwave Engineering*. McGraw-Hill, New York, 1966.

[78] R. Balasubramanian, *Computer Aided Design of Waveguide Filters Using the Mode Matching Method*. Master of Science Thesis, University of Saskatchewan, 1997.

[79] J. Hong, "Design of E-plane Filters Made Easy," *IEE-Proceedings-H-(Microwaves, Antennas-and-Propagation)*, vol.136, no.3, p.215-218, June 1989.

[80] F. Arndt, J. Bornemann, D. Grauerholz and R. Vahldieck, "Material and Circuit Evaluation for Millimetre-Wave Applications: High-Q Fin-Line Filters for Millimetre Waves," *European Space Agency Journal*, vol. 5, no. 1, pp. 33-42, 1981.

[81] J. Tucker, P. Bhartia and P. Pramanick, "A New Filter and Multiplexer Optimization Approach Using False Specifications," submitted for publication to *IEEE Transactions on Microwave Theory and Techniques*.

[82] A. Morini and T. Rozzi, "Design of Optimum Three-port Symmetrical Junctions for Diplexer Applications," *1994 IEEE MTT-S International Microwave Symposium Dig*est, pp. 739-742.

[83] X. Wen and P. Pramanick, "Optimization of Waveguide E-plane Filters," submitted to *International Journal of RF and Microwave Computer-Aided Engineering*.

[84] Ansoft Corporation, *Ansoft Harmonica Elements Library Version 8.7*. 2000.

[85] Agilent Technologies, *Agilent EEsof EDA Advanced Design System 1.3 Circuit Components*. January 2000.

[86] Eagleware Corporation, *Eagleware GENESYS Version 6 Simulation*. 1998.

[87] J. K. Prentice and A. K. Ameko, "Performance Benchmark Results for Selected Fortran 90 Compilers," *Fortran Journal*, vol. 6, no. 6, pp. 2-7, November/December, 1994.

[88] K. Dowd and C. R. Severance, *High Performance Computing*, O'Reilly & Associates, Inc., California, 1998.

Appendix A. Coupling Matrix Derivation

This appendix shows the mathematical derivation for the microstrip step discontinuity coupling matrix equation, which results in equation (3.35).

$$H_{ji} = \sqrt{\frac{\varepsilon_i \varepsilon_j}{a_1 a_2}} \int_{h_x}^{(h_x + a_2)} \cos\left(\frac{i\pi x}{a_1}\right) \cos\left(\frac{j\pi (x - h_x)}{a_2}\right) dx \tag{A.1}$$

There are five cases to consider for this equation.

1) $i = j = 0$

$$\therefore H_{ji} = \sqrt{\frac{\varepsilon_i \varepsilon_j}{a_1 a_2}} \int_{h_x}^{(h_x + a_2)} dx = \sqrt{\frac{\varepsilon_i \varepsilon_j}{a_1 a_2}} ((h_x + a_2) - h_x) = \sqrt{\frac{a_2}{a_1}} \tag{A.2}$$

2) $i = 0$ and $j \neq 0$

$$H_{ji} = \sqrt{\frac{\varepsilon_i \varepsilon_j}{a_1 a_2}} \int_{h_x}^{(h_x + a_2)} \cos\left(\frac{j\pi (x - h_x)}{a_2}\right) dx \tag{A.3}$$

let $w = x - h_x$

$$\therefore H_{ji} = \sqrt{\frac{\varepsilon_i \varepsilon_j}{a_1 a_2}} \int_0^{a_2} \cos\frac{j\pi w}{a_2} dw = 0 \tag{A.4}$$

3) $i \neq 0$ and $j = 0$

$$H_{ji} = \sqrt{\frac{\varepsilon_i \varepsilon_j}{a_1 a_2}} \int_{h_x}^{(h_x + a_2)} \cos\left(\frac{i\pi x}{a_1}\right) dx = \sqrt{\frac{\varepsilon_i \varepsilon_j}{a_1 a_2}} \frac{a_1}{i\pi} \sin\frac{i\pi x}{a_1} \Bigg|_{h_x}^{h_x + a_2} \tag{A.5}$$

$$\therefore H_{ji} = \sqrt{\frac{2a_1}{a_2}} \frac{1}{i\pi} \left\{ \sin\frac{i\pi (h_x + a_2)}{a_1} - \sin\frac{i\pi h_x}{a_1} \right\} \tag{A.6}$$

4) $i/a_1 = j/a_2$

$$H_{ji} = \sqrt{\frac{\varepsilon_i \varepsilon_j}{a_1 a_2}} \int_{h_x}^{(h_x + a_2)} \cos\left(\frac{i\pi x}{a_1}\right) \cos\left(\frac{j\pi (x - h_x)}{a_2}\right) dx \tag{A.7}$$

let $u = \frac{i\pi}{a_1}$, $v = \frac{j\pi}{a_2}$ and $w = x - h_x$

$$H_{ji} = \sqrt{\frac{\varepsilon_i \varepsilon_j}{a_1 a_2}} \int_0^{a_2} \cos u(w + h_x) \cos(vw) dw \tag{A.8}$$

$$H_{ji} = \sqrt{\frac{\varepsilon_i \varepsilon_j}{a_1 a_2}} \int_0^{a_2} (\cos uw \cos uh_x - \sin uw \sin uh_x) \cos vw dw \tag{A.9}$$

$$H_{ji} = \sqrt{\frac{\varepsilon_i \varepsilon_j}{a_1 a_2}}\left\{\cos uh_x \int_0^{a_2} \cos uw \cos vw dw - \sin uh_x \int_0^{a_2} \sin uw \cos vw dw\right\} \quad \text{(A.10)}$$

Using the relation $i/a_1 = j/a_2$

$$H_{ji} = \sqrt{\frac{\varepsilon_i \varepsilon_j}{a_1 a_2}}\left\{\cos uh_x \int_0^{a_2} \cos uw \cos uw dw - \frac{\sin uh_x}{2} \int_0^{a_2} \sin 2uw dw\right\} \quad \text{(A.11)}$$

let $\alpha = uw$ and $\beta = 2uw$

$$H_{ji} = \sqrt{\frac{\varepsilon_i \varepsilon_j}{a_1 a_2}}\left\{\frac{\cos uh_x}{u} \int_0^{ua_2} (\cos\alpha)^2 d\alpha - \frac{\sin uh_x}{2(2u)} \int_0^{2ua_2} \sin\beta d\beta\right\} \quad \text{(A.12)}$$

$$H_{ji} = \sqrt{\frac{\varepsilon_i \varepsilon_j}{a_1 a_2}}\left\{\frac{\cos uh_x}{u}\left(\frac{\alpha}{2} + \frac{\sin 2\alpha}{4}\right)\Big|_0^{ua_2} - \frac{\sin uh_x}{2(2u)}(-\cos\beta)\Big|_o^{2ua_2}\right\} \quad \text{(A.13)}$$

$$H_{ji} = \sqrt{\frac{\varepsilon_i \varepsilon_j}{a_1 a_2}}\left\{\frac{\cos uh_x}{u}\left(\frac{ua_2}{2} + \frac{\sin 2ua_2}{4}\right) - \frac{\sin uh_x}{2(2u)}(-\cos 2ua_2 + 1)\right\} \quad \text{(A.14)}$$

now $\sin 2ua_2 = \sin\frac{2j\pi a_2}{a_2} = 0$ and $\cos 2ua_2 = \cos\frac{2j\pi a_2}{a_2} = 1$

$$\therefore H_{ji} = \sqrt{\frac{\varepsilon_i \varepsilon_j}{a_1 a_2}}\left\{\frac{\cos uh_x}{u}\left(\frac{ua_2}{2}\right)\right\} = \frac{1}{2}\sqrt{\frac{(\varepsilon_i \varepsilon_j) a_2}{a_1}} \cos\frac{j\pi h_x}{a_2} = \sqrt{\frac{a_2}{a_1}} \cos\frac{j\pi h_x}{a_2} \quad \text{(A.15)}$$

Note that when $i = j = 0$, equation (A.15) simplifies to equation (A.2).

5) otherwise: Beginning with equation (A.10)

$$H_{ji} = \sqrt{\frac{\varepsilon_i \varepsilon_j}{a_1 a_2}}\left\{\frac{\cos uh_x}{u^2 - v^2}(u\sin uw\cos vw - v\cos uw\sin vw)\Big|_0^{a2} - \right. \quad \text{(A.16)}$$

$$\left. \sin uh_x\left(-\frac{\cos(u-v)w}{2(u-v)} - \frac{\cos(u+v)w}{2(u+v)}\right)\Big|_0^{a2}\right\}$$

$$H_{ji} = \sqrt{\frac{\varepsilon_i \varepsilon_j}{a_1 a_2}}\left\{\frac{\cos uh_x}{u^2 - v^2}(u\sin ua_2\cos va_2 - v\cos ua_2\sin va_2) + \right. \quad \text{(A.17)}$$

$$\sin uh_x\left(\frac{\cos ua_2\cos va_2 + \sin ua_2\sin va_2 - 1}{2(u-v)} + \right.$$

$$\left.\left.\frac{\cos ua_2\cos va_2 - \sin ua_2\sin va_2 - 1}{2(u+v)}\right)\right\}$$

but $\sin va_2 = \sin\frac{j\pi a_2}{a_2} = \sin j\pi = 0$

$$H_{ji} = \sqrt{\frac{\varepsilon_i \varepsilon_j}{a_1 a_2}}\left\{\frac{\cos uh_x}{u^2 - v^2}(u\sin ua_2 \cos va_2) + \frac{\sin uh_x}{u^2 - v^2}(u\cos ua_2 \cos va_2 - u)\right\} \quad \text{(A.18)}$$

$$H_{ji} = \sqrt{\frac{\varepsilon_i \varepsilon_j}{a_1 a_2}}\frac{u}{u^2 - v^2}\{\cos va_2(\cos uh_x \sin ua_2 + \sin uh_x \cos ua_2) - \sin uh_x\} \quad \text{(A.19)}$$

$$H_{ji} = \sqrt{\frac{\varepsilon_i \varepsilon_j}{a_1 a_2}}\frac{u}{u^2 - v^2}\{\cos va_2(\sin u(h_x + a_2)) - \sin uh_x\} \quad \text{(A.20)}$$

and $\cos va_2 = \cos\frac{j\pi a_2}{a_2} = \cos j\pi = (-1)^j$

$$\therefore H_{ji} = \frac{2}{\sqrt{a_1 a_2}}\frac{\frac{i\pi}{a_1}}{\left(\frac{i\pi}{a_1}\right)^2 - \left(\frac{j\pi}{a_2}\right)^2}\left\{(-1)^j \sin\left(\frac{i\pi(h_x + a_2)}{a_1}\right) - \sin\left(\frac{i\pi h_x}{a_x}\right)\right\} \quad \text{(A.21)}$$

Appendix B. Discontinuity Elements Available with Commercial Microwave CAD Programs

This appendix contains some of the microstrip discontinuity elements available with some commercial microwave CAD programs.

B.1 Ansoft Harmonica

Ansoft's microwave CAD program Harmonica contains numerous microstrip elements in its element catalog [84]. As a reference to the right angle bends, T-junctions and step junctions presented in Chapter 4, the corresponding Harmonica microstrip discontinuities are briefly presented in this section.

B.1.1 Right Angle Bends

BEND is the Harmonica element that is used to represent microstrip right angle bends. The BEND includes support for the following types of bends (among others):

1) Uncompensated right angle bend that has the same width for both microstrip lines.
2) Uncompensated right angle bend that has different widths for both microstrip lines.
3) Mitered right angle bend that can have either the same or different widths for both microstrip lines, and whose mitering is shown in Figure 4.9 (a) on page 49.
4) Optimally mitered right angle bend that has the same width for both microstrip lines.

B.1.2 T-Junctions

The following Harmonica element can be used to represent microstrip T-junctions of arbitrary widths whose center lines of transmission lines 1 and 2 are aligned (see Figure 2.7 on page 19):

1) TEE is an uncompensated T-junction.

B.1.3 Step Junctions

The following Harmonica elements can be used to represent microstrip step junctions:

1) STEP is an uncompensated step junction whose lines may be offset.
2) TAP is a linear or exponential taper step junction whose center lines of the two transmission lines are aligned. The model is based on the discretization of the transmission line.

B.2 Agilent EEsof

Agilent's microwave CAD program EEsof contains numerous microstrip elements in its component catalog [85]. As a reference to the right angle bends, T-junctions and step junctions presented in Chapter 4, the corresponding EEsof microstrip discontinuities are briefly presented in this section.

B.2.1 Right Angle Bends

The following EEsof elements can be used to represent microstrip right angle bends that have the same width for both microstrip lines:

1) MCORN is an uncompensated right angle bend. The model is an empirically based, analytical model which consists of a static, lumped, equivalent circuit.

2) MBEND is an arbitrary angle bend that can support mitering. When the angle is 90° it is equivalent to a right angle bend that can support mitering. However, the catalog recommends the use of MCORN, MBEND2 or MBEND3 for right angle bends.

3) MBEND2 is a mitered right angle bend that corresponds to the mitering shown in Figure 4.9 (a) on page 49. The model is an empirically based, analytical model which consists of a static, lumped, equivalent circuit.

4) MBEND3 is an optimally mitered right angle bend. The optimal mitering is based on the expression developed in reference [10]. The model is an empirically based, analytical model.

B.2.2 T-Junctions

The following EEsof element can be used to represent microstrip T-junctions of arbitrary widths whose center lines of transmission lines 1 and 2 are aligned (see Figure 2.7 on page 19):

1) MTEE is an uncompensated T-junction. The model is an empirically based, analytical model which consists of a static, lumped, equivalent circuit.

B.2.3 Step Junctions

The following EEsof elements can be used to represent microstrip step junctions whose center lines of the two transmission lines are aligned:

1) MSTEP is an uncompensated step junction. The model is derived from a TEM (fundamental mode) planar waveguide model of the discontinuity.

2) MTAPER is a linear taper symmetrical step junction. The model is a microstrip line macro-model developed by EEsof. The taper is constructed from a series of straight sections of various widths that are cascaded together.

B.3 Eagleware GENESYS

Eagleware's microwave CAD program GENESYS contains numerous microstrip elements in its simulation manual [86]. As a reference to the right angle bends, T-junctions and step junctions presented in Chapter 4, the corresponding GENESYS microstrip discontinuities are briefly presented in this section.

B.3.1 Right Angle Bends

The following GENESYS element can be used to represent microstrip right angle bends that have the same width for both microstrip lines:

1) MBN is a right angle bend that can be either uncompensated or mitered as shown in Figure 4.9 (a) on page 49. The model is an based on a lumped, equivalent circuit.

B.3.2 T-Junctions

The following GENESYS element can be used to represent microstrip T-junctions whose widths of transmission lines 1 and 2 are the same (see Figure 2.7 on page 19):

1) MTE is an uncompensated T-junction. The model was developed by Eagleware and verified with field simulations.

B.3.3 Step Junctions

The following GENESYS elements can be used to represent microstrip step junctions:

1) MSTE is an uncompensated step junction that can be either symmetric or asymmetric. The model is an based on a lumped, equivalent circuit.

2) MTAPER is a linear taper symmetrical step junction. The taper is modelled as a cascade of 10 equal length microstrip lines that have widths varying linearly from the width of transmission line 1 to the width of transmission line 2.

Appendix C. Sample Source Code

This appendix contains some segments of the source code for the discontinuity analysis routines developed in this thesis.

C.1 STEP Routine

```
C* STEP ROUTINES *
C*************************************************************************
C*      COMPUTE THE S PARAMETERS OF A STEP DISCONTINUITY
C*      NOTE: FOR MICROSTRIP A1 AND A2 ARE THE WIDTH OF THE
C*            LINE AS OPPOSED TO THE EFFECTIVE VALUES SINCE
C*            DISPERSION HAS TO BE TAKEN INTO ACCOUNT.
C*************************************************************************
      INTEGER FUNCTION STEP(ER,ER1,ER2,H,A1,A2,STYPE,OFFSET,
     +      ISTART,ISTOP,ISTEP,ISCALE,S)
      USE CONSTANT
      IMPLICIT NONE
      COMPLEX S(2,2),CS11(NR,NC),CS12(NR,NC),CS21(NR,NC),CS22(NR,NC)
      COMPLEX BS11(NR,NC),BS12(NR,NC),BS21(NR,NC),BS22(NR,NC)
      COMPLEX TS11(NR,NC),TS12(NR,NC),TS21(NR,NC),TS22(NR,NC)
      COMPLEX TL(NR,NC)

      REAL    A1,A2,AW,F,AM11,AM22,ASMALL,ABIG,OFFSET
      REAL    H,ER,ER1,ER2,ERW,W,W1,W2,AM21,SWR,SOUT,LAMBDAG
      INTEGER IM,N1,N2,NW,CESTEP,STYPE,ISTART,ISTOP,ISTEP,ISCALE

      W1 = A1; W2 = A2;
      WRITE(*,*) '    F       S11        S12'
      STEP=0
      DO 100 IM=ISTART,ISTOP,ISTEP
       F=1.0E9*REAL(IM)/REAL(ISCALE)
       WRITE(*,*) 'FREQUENCY = F', F
       IF (STYPE.EQ.STMICRO) THEN
         CALL MICROEFF(ER,W1,H,F,ER1,A1)
         CALL MICROEFF(ER,W2,H,F,ER2,A2
       END IF

C* TO ACCOUNT FOR DISPERSION WITH MICROSTRIP USE ORIGINAL WIDTHS
       IF (W1.GE.W2) THEN
         ABIG = W1; ASMALL = W2;
       ELSE
         ABIG = W2; ASMALL = W1;
       ENDIF

C* CONSIDER THE VARIOUS TYPES OF STEPS
C*************************************************************************
C* SYMMETRICAL: DIVIDE STRUCTURE IN HALF AND USE CESTEP.
C*************************************************************************
       IF ((OFFSET.EQ.0.0).AND.(STYPE.EQ.STMICRO)) THEN
         IF (ABIG.EQ.W2) THEN
           N2 = MAXMODE
           STEP = CESTEP(STYPE,N1,N2,F,ER1,ER2,A1/2.0,A2/2.0,
     +          CS11,CS12,CS21,CS22)
```

```
            ELSE
              N1 = MAXMODE
              STEP = CESTEP(STYPE,N2,N1,F,ER2,ER1,A2/2.0,A1/2.0,
     +            CS22,CS21,CS12,CS11)
            ENDIF
C*********************************************************************
C* A COMMON EDGE STEP
C*********************************************************************
          ELSE IF ((ASMALL/2.0+OFFSET).EQ.(ABIG/2.0)) THEN
            IF (ABIG.EQ.W2) THEN
              N2 = MAXMODE
              STEP = CESTEP(STYPE,N1,N2,F,ER1,ER2,A1,A2,
     +            CS11,CS12,CS21,CS22)
            ELSE
              N1 = MAXMODE
              STEP = CESTEP(STYPE,N2,N1,F,ER2,ER1,A2,A1,
     +            CS22,CS21,CS12,CS11)
            ENDIF
          ELSE
            .
            .  OTHER STEP LOGIC
            .
          ENDIF

          S(1,1)=CS11(1,1); S(2,2)=CS22(1,1)
          S(1,2)=CS12(1,1); S(2,1)=CS21(1,1)

          AM11=CABS(S(1,1))
          AM21=CABS(S(2,1))
          AM22=CABS(S(2,2))
          SWR =(1.0+AM11)/(1.0-AM11)
          SOUT= AM11**2.0+AM21**2.0

100       WRITE(*,101) FLOAT(IM)/REAL(ISCALE),AM11,AM21,AM22,SWR,SOUT
101       FORMAT(1X,F5.2,1X,F15.10,1X,F15.10,1X,F15.10,1X,F15.10,1X,F15.10)

          RETURN
          END
```

C.2 SCAS Routine

```
C*********************************************************************
C*       CASCADES TWO S MATRICES
C*        THE LEFT  MATRIX IS CHARACTERIZED BY N X M MODES
C*        THE RIGHT MATRIX IS CHARACTERIZED BY M X P MODES
C*        THE TOTAL MATRIX IS CHARACTERIZED BY N X P MODES
C*********************************************************************
          INTEGER FUNCTION S_CAS_S(N, M, P, SL11, SL12, SL21, SL22, SR11,
     +    SR12, SR21, SR22, ST11, ST12, ST21, ST22, NR, NC)
          IMPLICIT NONE
          INTEGER N, M, P, K, J, NR, NC, MINVS
          COMPLEX SL11(NR,NC),SL12(NR,NC),SL21(NR,NC),SL22(NR,NC),
     +            SR11(NR,NC),SR12(NR,NC),SR21(NR,NC),SR22(NR,NC),
     +            ST11(NR,NC),ST12(NR,NC),ST21(NR,NC),ST22(NR,NC)
          COMPLEX W(NR,NC),I(NR,NC)

C******* SET UP IDENTITY MATRIX
```

```
        DO 80 K=1,M
         DO 60 J=1,M
60        I(K,J)=(0.0,0.0)
80       I(K,K)=(1.0,0.0)

C******* SET UP W MATRIX
        CALL MMULT(SL22, SR11, M, M, M, ST11, NR, NC)
        CALL MSUB(I, ST11, M, M, W, NR, NC)
        S_CAS_S = MINVS(W, M, NR, NC)
        IF (S_CAS_S.NE.0) RETURN
C******* BEGINNING CASCADING... USE EXISTING MATRICES TO HOLD
C*******  INTERMEDIATE RESULTS (IE. WILL REUSE I AND W)
        CALL MMULT(SR11, W, M, M, M, ST22, NR, NC)
        CALL MMULT(SL12, ST22, N, M, M, ST21, NR, NC)
        CALL MMULT(ST21, SL21, N, M, N, ST12, NR, NC)
C******* ST11 RESULT
        CALL MADD(SL11, ST12, N, N, ST11, NR, NC)
        CALL MMULT(ST22, SL22, M, M, M, ST21, NR, NC)
        CALL MADD(I, ST21, M, M, ST22, NR, NC)
        CALL MMULT(SL12, ST22, N, M, M, ST21, NR, NC)
C******* ST12 RESULT
        CALL MMULT(ST21, SR12, N, M, P, ST12 , NR, NC)
        CALL MMULT(SR21, W, P, M, M, I, NR, NC)
C******* ST21 RESULT
        CALL MMULT(I, SL21, P, M, N, ST21, NR, NC)
        CALL MMULT(I, SL22, P, M, M, W, NR, NC)
        CALL MMULT(W, SR12, P, M, P, I, NR, NC)
C******* ST22 RESULT
        CALL MADD(SR22, I, P, P, ST22, NR, NC)

        RETURN
        END

C*************************************************************************
C*      CASCADE AN S MATRIX WITH A TRANSMISSION LINE
C*       THE LEFT  MATRIX IS CHARACTERIZED BY N X M MODES
C*       THE RIGHT MATRIX IS CHARACTERIZED BY M X M MODES (TLINE)
C*       THE TOTAL MATRIX IS CHARACTERIZED BY N X M MODES
C*
C*      SPECIAL CASE OF ABOVE ROUTINE AS SR11=SR22=0 & SR12=SR21=T
C*       SO W=I AND AN INVERSE IS NOT REQUIRED
C*************************************************************************
        SUBROUTINE S_CAS_T(N, M, SL11, SL12, SL21, SL22, T,
     +   ST11, ST12, ST21, ST22, NR, NC)
        IMPLICIT NONE
        INTEGER N, M, I, J, NR, NC
        COMPLEX SL11(NR,NC),SL12(NR,NC),SL21(NR,NC),SL22(NR,NC),
     +  T(NR,NC),ST11(NR,NC),ST12(NR,NC),ST21(NR,NC),ST22(NR,NC)

C******* ST11=SL11
        DO 60 I=1,N
         DO 60 J=1,N
60        ST11(I,J)=SL11(I,J)

C******* ST22 = T*SL22*T
        CALL MMULT(T, SL22, M, M, M, ST12, NR, NC)
```

```
        CALL MMULT(ST12, T, M, M, M, ST22, NR, NC)

C******* ST12= SL12*T
        CALL MMULT(SL12, T, N, M, M, ST12, NR, NC)

C******* ST21= T*SL21
        CALL MMULT(T, SL21, M, M, N, ST21, NR, NC)
        END
```

C.3 COUPLING Routine

```
C* COUPLING ROUTINES *
C*********************************************************************
C*      COMPUTE THE S PARAMETERS FOR A COMMON EDGE STEP DISCONTINUITY
C*      --------------------------
C*
C*      A1
C*                              A2
C*      -----------------
C*                      |
C*                      |
C*                      -----------
C*
C*       THE ROUTINE CAN HANDLE A1 < A2 AND A1 > A2 (MORE EFFICENT
C*       IF A2 > A1)
C*********************************************************************
        INTEGER FUNCTION CESTEP(STYPE, NM1, NM2, F, ER1, ER2, A1, A2,
     +   S11, S12, S21, S22)
        USE CONSTANT
        IMPLICIT NONE
        REAL    F, ER1, ER2, A1, A2, AK0
        INTEGER NM1,NM2,I,J,MINVS,NMS,NMB,STYPE
        COMPLEX S11(NR,NC),S12(NR,NC),S21(NR,NC),S22(NR,NC),
     +          AI(NR,NC),LE(NR,NC),LH(NR,NC),LEH(NR,NC),
     +          ZB(NR,NC),YS(NR,NC),ZS(NR,NC),YB(NR,NC),TEMP

        AK0=2.0*PI*F*SQRT(E0*U0)

        IF (A2.GE.A1) THEN
              NM1 = NINT(FLOAT(NM2)*A1/A2)
              IF (NM1.LT.MINMODE) THEN
                NM1 = MINMODE
                NM2 = NINT(FLOAT(NM1)*A2/A1)
                IF (NM2.GT.NR.OR.NM2.GT.NC) THEN
                  WRITE(*,*) 'NUMBER OF MODES NEEDED > THAN AVAILABLE'
                  WRITE(*,*) 'WANT ', NM2, ' HAVE ', NR, ' OR ', NC
                  CESTEP = 2
                  NM2 = NR
                ENDIF
              ENDIF
              CALL COUPCESTEP(STYPE,F,ER1,ER2,A1,A2,NM1,NM2,LE)
              IF (STYPE.EQ.STMICRO) THEN
                CALL ADMITT(STYPE, NM1, ER1, A1, AK0, YS)
                CALL IMPED(STYPE, NM2, ER2, A2, AK0, ZB)
              ELSE
                CALL ADMITT(STYPE, NM2, ER2, A2, AK0, YB)
                CALL IMPED(STYPE, NM1, ER1, A1, AK0, ZS)
```

```
            ENDIF
            NMB = NM2
            NMS = NM1
          ELSE
C*          LOGIC FOR A1>A2
          ENDIF

C*        LE HAS DIMENSIONS NMS X NMB, LH=TRANSPOSE(LE)
C*         WHERE NMB > NMS
          CALL MTRAN(NMS,NMB,LE,LH,NR,NC)

          DO 61 I=1,NMB
           DO 60 J=1,NMB
60          AI(I,J)=CMPLX(0.0,0.0)
61         AI(I,I)=CMPLX(1.0,0.0)

          IF (STYPE.EQ.STMICRO) THEN
C*         COMPUTE COMMONLY USED MATRIX GROUPINGS
           CALL MMULT(ZB,LH,NMB,NMB,NMS,S11,NR,NC)
           CALL MMULT(S11,YS,NMB,NMS,NMS,S22,NR,NC)
           CALL MMULT(LE,S22,NMS,NMB,NMS,S21,NR,NC)
           CALL MADD(AI,S21,NMS,NMS,S12,NR,NC)
           CESTEP = MINVS(S12,NMS,NR,NC)
           IF (CESTEP.NE.0) RETURN
C*         COMPUTE S11
           CALL MSUB(S21,AI,NMS,NMS,LEH,NR,NC)
           CALL MMULT(S12,LEH,NMS,NMS,NMS,S11,NR,NC)
C*         COMPUTE S12
           CALL MMULT(S12,LE,NMS,NMS,NMB,S21,NR,NC)
           DO 99 I=1,NMS
            DO 99 J=1,NMB
99            S12(I,J)=CMPLX(2.0,0.0)*S21(I,J)
C*         COMPUTE S21
           CALL MSUB(AI,S11,NMS,NMS,LEH,NR,NC)
           CALL MMULT(S22,LEH,NMB,NMS,NMS,S21,NR,NC)
C*         COMPUTE S22
           CALL MMULT(S22,S12,NMB,NMS,NMB,LEH,NR,NC)
           CALL MSUB(AI,LEH,NMB,NMB,S22,NR,NC)
          ELSE
C*         COMPUTE COMMONLY USED MATRIX GROUPINGS
           CALL MMULT(ZS,LE,NMS,NMS,NMB,S11,NR,NC)
           CALL MMULT(S11,YB,NMS,NMB,NMB,S22,NR,NC)
           CALL MMULT(S22,LH,NMS,NMB,NMS,S21,NR,NC)
           CALL MADD(AI,S21,NMS,NMS,S12,NR,NC)
           CESTEP = MINVS(S12,NMS,NR,NC)
           IF (CESTEP.NE.0) RETURN
C*         COMPUTE S11
           CALL MSUB(AI,S21,NMS,NMS,LEH,NR,NC)
           CALL MMULT(S12,LEH,NMS,NMS,NMS,S11,NR,NC)
C*         COMPUTE S12
           CALL MMULT(S12,ZS,NMS,NMS,NMS,S21,NR,NC)
           CALL MMULT(S21,LE,NMS,NMS,NMB,S12,NR,NC)
           CALL MMULT(S12,YB,NMS,NMB,NMB,S21,NR,NC)
           DO 199 I=1,NMS
            DO 199 J=1,NMB
199           S12(I,J)=CMPLX(2.0,0.0)*S21(I,J)
```

```
C*       COMPUTE S21
         CALL MADD(AI,S11,NMS,NMS,LEH,NR,NC)
         CALL MMULT(LH,LEH,NMB,NMS,NMS,S21,NR,NC)
C*       COMPUTE S22
         CALL MMULT(LH,S12,NMB,NMS,NMB,LEH,NR,NC)
         CALL MSUB(LEH,AI,NMB,NMB,S22,NR,NC)
        ENDIF

        IF (A2.LT.A1) THEN
               DO 101 I=1,NMB
                DO 101 J=1,NMB
                 IF ((I.LE.NMS).AND.(J.LE.NMS)) THEN
                       TEMP=S22(I,J)
                       S22(I,J)=S11(I,J)
                       S11(I,J)=TEMP
                       TEMP=S12(I,J)
                       S12(I,J)=S21(I,J)
                       S21(I,J)=TEMP
                 ELSE
                       S11(I,J)=S22(I,J)
                       IF (J.LE.NMS) S12(I,J)=S21(I,J)
                       IF (I.LE.NMS) S21(I,J)=S12(I,J)
                 ENDIF
101             CONTINUE
        ENDIF

        WRITE(*,*) 'UNNORMALIZED S11(1,1)=',S11(1,1)
        WRITE(*,*) 'UNNORMALIZED S12(1,1)=',S12(1,1)
        WRITE(*,*) 'UNNORMALIZED S21(1,1)=',S21(1,1)
        WRITE(*,*) 'UNNORMALIZED S22(1,1)=',S22(1,1)
        RETURN
        END

C*********************************************************************
C*      COMPUTE THE COUPLING MATRIX FOR A COMMON EDGE STEP
C*      NOTE: ROUTINE SETUP TO INTEGRATE OVER THE SMALLER WIDTH (IE. A)
C*      -------------------------  <-- COMMON EDGE
C*
C*      A
C*                               B
C*      -----------------
C*                      |
C*                      |
C*                      -----------
C*      LE HAS DIMENSIONS NMA X NMB (NMB IS LARGER)
C*********************************************************************
        SUBROUTINE COUPCESTEP(STYPE,F,ERA,ERB,A,B,NMA,NMB,LE)
        USE CONSTANT
        IMPLICIT NONE
        INTEGER P,M,NMA,NMB,STYPE
        REAL    A,B,AKM,AKP,ERA,ERB,F
        COMPLEX LE(NR,NC)
C*      AK02=4.0*PI*PI*F*F*E0*U0

        F=F; ERA=ERA; ERB=ERB;
```

```
      SELECT CASE(STYPE)
      CASE(STMICRO)
       DO 10 M=0,NMA-1
        AKM=REAL(M)*PI/A
        DO 10 P=0,NMB-1
         AKP=REAL(P)*PI/B
         IF((M.EQ.0).AND.(P.EQ.0)) THEN
          LE(M+1,P+1)=CMPLX(SQRT(A/B),0.0)
         ELSEIF((M.NE.0).AND.(P.EQ.0)) THEN
          LE(M+1,P+1)=CMPLX(0.0,0.0)
         ELSEIF((M.EQ.0).AND.(P.NE.0)) THEN
          LE(M+1,P+1)=CMPLX((SQRT(2.0/A/B)/AKP)*SIN(AKP*A),0.0)
         ELSEIF((M*B-P*A).LE.0.001) THEN
          LE(M+1,P+1)=CMPLX(SQRT(A/B),0.0)
         ELSE
          LE(M+1,P+1)=CMPLX((2.0*AKP/SQRT(A*B)/(AKP*AKP-AKM*AKM))*
     +      ((-1.0)**M*SIN(AKP*A)),0.0)
         ENDIF
10      CONTINUE

      CASE (STHPLANE)
       DO 20 M=1,NMA
         AKM=FLOAT(M)*PI/A
         DO 20 P=1,NMB
          AKP=FLOAT(P)*PI/B
          IF((M*B-P*A).LE.0.001) THEN
           LE(M,P)=CMPLX(SQRT(A/B),0.0)
          ELSE
           LE(M,P)=CMPLX(2.0*((-1.0)**M)*SIN(AKP*A)*AKM/
     +       (AKP*AKP-AKM*AKM)/SQRT(A*B),0.0)
          ENDIF
20      CONTINUE
      END SELECT
      END
```

Appendix D. FORTRAN 77 versus Fortran 90 Performance Comparison

Before upgrading from FORTRAN 77 to Fortran 90, to take advantage of the newer language features, some performance results were analyzed to determine if there were any severe performance penalties in upgrading to the newer Fortran standard.

D.1 Discontinuity Analysis Routines

The first performance test to evaluate the performance of a Fortran 90 compiler relative to a FORTRAN 77 compiler was the discontinuity analysis routines developed for this thesis. The program was compiled using both the Watcom FORTRAN 77 compiler and the Microsoft Fortran PowerStation Fortran 90 compiler (now the Digital Visual Fortran compiler). The program took 19.3 seconds to run compiled with the FORTRAN 77 compiler and 17.7 seconds to run compiled with the Fortran 90 compiler. So the improved performance of Fortran 90 relative to FORTRAN 77 for the discontinuity analysis routines is obviously acceptable.

D.2 SPEC CFP95

The Standard Performance Evaluation Corporation (SPEC) web site, http://www.spec.org/, has performance results for the Fortran benchmark suite CFP95. CFP95 is a benchmark suite that evaluates compute-intensive floating point Fortran programs in order to measure the performance of the computer's processor, memory architecture and compiler. Among the submitted results was data for Digital's Personal Workstation with a 433 MHz CPU for a FORTRAN 77 compiler, kf77 (Fortran 77 X4) running on the Digital UNIX V4.0C operating system, and a Fortran 90 compiler, f90 (Visual Fortran V5) on the Windows NT V4.0 operating system. The real time in seconds to run each of the benchmarks for both of these compilers are summarized in Table D.1.

Table D.1. Fortran SPEC CFP95 Results

Benchmark Number and Name	FORTRAN 77 (seconds)	Fortran 90 (seconds)
101.tomcatv	169	190
102.swim	353	358
103.su2cor	147	151
104.hydro2d	280	292
110.applu	261	258
125.turb3d	213	239

Benchmark Number and Name	FORTRAN 77 (seconds)	Fortran 90 (seconds)
141.apsi	100	119
145.fpppp	274	246
146.wave5	130	143

The FORTRAN 77 results are generally better than Fortran 90 and the geometric mean shows only a 5% degradation for Fortran 90. Since the benchmarks were executed on different operating systems this could account for the difference in performance. Overall, 5% is not a very significant degradation, so the performance of Fortran 90 relative to FORTRAN 77 for these benchmarks is acceptable.

D.3 Fortran Journal Benchmarks

The Fortran Journal has also published some performance comparisons of Fortran 90 and the information is available at the Fortran web site, http://www.fortran.com. There are two studies of interest at this web site: SPARC Fortran Compiler Comparison, which includes a FORTRAN 77 comparison, and the Microsoft Windows NT Fortran Compiler Comparison. Summarizes of these studies are in the following sections.

D.3.1 SPARC Fortran Compiler Comparison

This study compares the speed of Fortran 90 programs compiled with various commercially available FORTAN 77 and Fortran 90 compilers on a Sun SPARC 10 with 64 MB of memory running on a Solaris Version 1.1 operating system. The compilers used were Sun Fortran 77 version 2.0.1, Pacific-Sierra Research VAST/f90 version 1.06G6, and Edinburgh Portable Compilers F90 version 1.0.8. The data is from the web site http://www.fortran.com/bench.html and is also available in reference [87]. The CPU time to run each of the benchmarks for each of these compilers is summarized in Table D.2.

Table D.2. SPARC Fortran Compiler Comparison

Benchmark	Sun F77	PSRVAST90 (CPU seconds)	EDC F90 (CPU seconds)
kepler	41.5	50.9	42.9
gas dynamics	66.6	61.6	60.6
overlap	16.9	16.4	20.5
scattering	803.5	808.8	580.5
channel	1523.2	1031.4	1438.2

With these benchmarks, the performance of the Fortran 90 compilers is generally superior to the FORTAN 77 compiler as both Fortran 90 compilers have a geometric mean

that shows a 5% improvement over the FORTRAN 77 compiler, so the performance of Fortran 90 relative to FORTRAN 77 for these benchmarks is also acceptable.

D.3.2 Microsoft Windows NT Fortran Compiler Comparison

This study compares the speed of Fortran 90 programs compiled with various commercially available Fortran 90 compilers on a Dual Processor, 200MHz Pentium Pro workstation with 128 MB of memory running on a Microsoft Windows NT V4.0 operating system. The compilers evaluated include the Fujitsu Fortran Version 1.3 beta 2, Lahey Fortran 90 LF90 Version 3.50 patch 3. 50f, and the Digital Visual Fortran Optimizing Compiler V5. The data is taken from the web site http://www.fortran.com/quetzal_pc_benchmarks.html. The CPU time in seconds to run each of the benchmarks for each of these compilers are summarized in Table D.3.

Table D.3. Microsoft Windows NT Fortran Compiler Comparison

Benchmark	Fujitsu (CPU Seconds)	Digital (CPU Seconds)	Lahey (CPU Seconds)
channel	467	482	529
fatigue	429	790	1346
gas dynamics	252	304	279
inductance	13	27	189
kepler	112	71	160
protein	86	68	973
rnflow	115	103	99
scattering	376	222	140

With these benchmarks, the performance of the Fujitsu and Digital Fortran 90 compilers are very similar, as the Fujitsu compiler has a geometric mean that shows less than 3% improvement over the Digital compiler. So the performance of the Digital Visual Fortran 90 compiler, which was used to develop the discontinuity analysis routines in this thesis, is acceptable.

D.4 Summary

From analyzing the performance results of the FORTAN 77 versus Fortran 90 performance comparisons in this appendix it is clear that the Fortran 90 compilers have similar performance characteristics to FORTAN 77 compilers, so upgrading should not introduce any severe performance penalties. Also, the Digital Visual Fortran 90 compiler used to develop the discontinuity analysis routines in this thesis is one of the better compilers available for Microsoft Windows.

Appendix E. Computer Comparisons

In Chapter 5 data is presented comparing the time to generate results for various transmission line discontinuities using the method described in this thesis and other published results. Comparing different programs running on different computers can be an exceptionally difficult task. The SPEC group, described in Appendix D.2, attempts to solve this problem by evaluating a set of compute-intensive benchmark suites in order to measure the performance of the computer's processor, memory architecture and compiler. When the same benchmarks are run on each computer the differences in the results can be attributed to the differences between computers. When the clock speed of the two systems are not the same the SPEC results are frequently normalized to the clock speed for one of the machines (either scale up the slower machine or scale down the faster machine) to determine the true difference between the machines.

Unfortunately SPEC results are not available for the computers referenced in Chapter 5, so this appendix will provide the data that was found for the computers and attempt to characterize the speed of these computers relative to the Pentium 166 MHz used to develop the discontinuity analysis method described in this thesis.

- Cray YMP supercomputer
    - The web site, http://www.cray.com/company/history.html states:

      In 1988, Cray Research introduced the Cray YMP, the world's first supercomputer to sustain over 1 giga-flop on many applications. Multiple 333 MFLOPS processors powered the system to record a sustained speed of 2.3 gigaflops.
- IBM 6000/520
    - This machine was manufactured in the early 1990's as a desktop computer. The clock speed was 20 MHz.
- SUN SPARC Model 10
    - This machine was manufactured in the late 1980s until 1997 as a desktop computer. The clock speed varied from 50 to 150 MHz depending on what year it was manufactured (the 150 MHz was available in 1997). Since the paper was submitted in 1996 it has a clock speed ranging from 50 to 125 MHz. The maximum amount of memory available was 512 MB.
- Pentium 166
    - This is the machine used to develop the discontinuity analysis method described in this thesis. It is an IBM ThinkPad 380ED (part number 26357AU) which was manufactured in 1997. It has a 166 MHz Pentium MMX processor with 80 MB of memory. The L1 cache is 32 KB and the L2 cache is 256 KB. As stated in Chapter 4, the Fortran 90 Microsoft PowerStation compiler was used to develop the software routines.

The easy comparison is between the Cray YMP supercomputer and the Pentium 166. The Cray is a multi-processor machine designed for floating-point intensive workloads and is capable of giga-flop processing speed. The Pentium is a single processor machine so its peak megaflop value will be the same as the clock speed [88], which is 166 MHz or 166 mega-flops. Thus the Cray YMP supercomputer is faster by at least a factor of 6.

Comparing the IBM 6000/520 and the SUN SPARC Model 10 to the Pentium 166 is not as easy since there is very limited data available for these machines. An estimate will be used since the exact overall improvement between machines is a non-linear factor that can only be accurately determined by actually running the same workload on each machine. The estimate will be primarily based upon scaling the computer speed to account for the difference in clock speeds between machines, since over the past few years the majority of the improvements have been in processor speed. The difficulty comes in determining the improvements in memory, superscalar architecture and compiler optimization, which have all been minor and at significantly smaller growth rate than the improvements in processor speed. From first hand experience in compiler technologies, improvements of more than 3% are very rare. As an overly optimistic estimate, a factor of two will be used to account for the improvements in memory, superscalar architecture and compiler optimization. Thus the IBM 6000/520 is approximately $(166/20) \times 2 \approx 9 \times 2 = 18$ times slower than the Pentium 166. Similarly, the SUN SPARC Model 10 is approximately $(166/50) \times 2 \approx 4 \times 2 = 8$ times slower than the Pentium 166 (assuming the slowest SUN SPARC clock speed).